

UC Berkeley

UC Berkeley Electronic Theses and Dissertations

Title

Investigation of Passive NO_x Storage on Pd/H-CHA: Effect of Water and Other Co-Adsorbates

Permalink

<https://escholarship.org/uc/item/62459577>

Author

Kim, Paul

Publication Date

2023

Peer reviewed|Thesis/dissertation

Investigation of Passive NO_x Storage on Pd/H-CHA: Effect of Water and Other Co-Adsorbates

By

Paul Kim

A dissertation submitted in partial satisfaction of the

requirements for the degree of

Doctor of Philosophy

in

Chemical Engineering

in the

Graduate Division

of the

University of California, Berkeley

Committee in charge:

Professor Alexis T. Bell, Chair

Professor Enrique Iglesias

Professor T. Don Tilley

Spring 2023

Investigation of Passive NO_x Storage on Pd/H-CHA: Effect of Water and Other Co-Adsorbates

© Copyright 2023

Paul Kim

Abstract

Investigation of Passive NO_x Storage on Pd/H-CHA: Effect of Water and Other Co-Adsorbates

by

Paul Kim

Doctor of Philosophy in Chemical Engineering

University of California, Berkeley

Professor Alexis T. Bell, Chair

Automotive exhaust contributes to air pollution through the emission of NO_x, CO, and hydrocarbons (HCs). Since the 1970s, catalytic converters, installed downstream of the engine, have significantly reduced the emissions of these harmful pollutants by converting toxic gases such as NO_x to N₂. However, to do so, catalytic converters need to reach a high enough temperature to efficiently convert a high fraction of the NO_x in the engine exhaust, which occurs during a “cold start” of the engine. One way of handling this issue is to install a passive NO_x adsorber (PNA), between the catalytic converter and engine. The purpose of the PNA is to adsorb NO at lower temperatures and release it once the catalytic converter is at a sufficiently high temperature. Pd/H-CHA has attracted attention as a possible PNA because of its ability to adsorb NO strongly and its hydrothermal stability. Despite the attention Pd/H-CHA has received, the mechanism by which NO adsorption on this adsorbent occurs has been heavily debated in the literature; most of the discussion focuses on the formation of Pd⁺ cations, believed to be responsible for storing NO and releasing at appropriately high temperatures. A second issue has centered on the interpretation of peaks observed in infrared spectra of adsorbed NO and their assignment to NO adsorbed on Pd⁺ vs Pd²⁺. The roles of CO and ethene in the stabilization of NO adsorption have also been a subject of debate.

This dissertation is focused on uncovering the mechanism of NO adsorption on Pd-based zeolites, specifically Pd/H-CHA. The emphasis is on investigating the influence of the various components of exhaust gas (i.e. water, CO, ethene, air, and NO) to see how they affect the NO release temperatures and the infrared spectrum of adsorbed NO. From observing the impact of co-adsorbates, insights into the adsorption mechanism were obtained and used to propose elementary processes by which NO adsorbs and desorbs from Pd/H-CHA. This understanding is essential for determining the effectiveness of this adsorbent as a PNA material in terms of its ability to adsorb NO and desorb it at temperatures above 573 K.

Chapter 1 gives an overview of the literature concerning Pd/H-CHA and details what is known and what is still controversial regarding the modes of NO adsorption, the oxidation state of Pd, how Pd⁺ is formed, and the interactions of CO and ethene with adsorbed NO. Pd/H-CHA is well-suited for use in PNAs due to its combination of high capacity for NO storage and its durability to hydrothermal aging and poisoning from other exhaust gas components. Theoretical calculations have proposed that Pd⁺ binds NO more strongly than other Pd states, such as Pd²⁺, PdO, and Pd nanoparticles. But observation of this oxidation state has eluded the field, and most

evidence of this material is founded on indirect observation through theoretical calculations and, for example, the production of NO_2 during the adsorption step. Electron paramagnetic resonance spectroscopy has only identified Pd^+ in very restricted conditions outside the operating range of PNAs. Another important factor to consider when studying NO storage on Pd is the impact other co-adsorbates in the exhaust gas will have on total storage capacity. CO , H_2O , and C_2H_4 are of particular interest due to their proposed abilities to increase total NO storage capacity. The mechanism by which these co-adsorbates increase storage is also debated, ranging from partial reduction of Pd^{2+} to Pd^+ to the production of yet to be identified co-adsorbed complexes. The literature surrounding NO adsorption on Pd-based zeolites has a wide variety of hypotheses. To better understand the adsorption mechanism, this study seeks to reduce the complexity of the feed conditions and propose reaction mechanisms, examining the effect of one adsorbate gas at a time.

Chapter 2 explores how NO adsorbs on Pd/H-CHA and the support zeolite, H-CHA. It was determined that Pd improves the total adsorption capacity of the base zeolite, and is necessary for high-temperature NO storage. The composition of the feed plays an important role in the adsorption capabilities of Pd/H-CHA: in the presence of air, all of the adsorbed NO is released at low temperatures (<573 K). A similar behavior in the temperature-programmed desorption (TPD) spectra is also seen when NO is adsorbed from He. Water is found to be essential to produce the sites that desorb NO at temperature >573 K. Pretreating Pd/H-CHA in water results in two NO desorption peaks during TPD, one of which is observed at higher temperatures suitable for PNA applications. Based on a combination of theoretical calculations and experimental results, it is hypothesized that water reacts with NO and Pd^{2+} cations to produce the Pd^+ cations, and these sites are found to be responsible for high-temperature NO desorption. IR spectroscopy was used to observe the frequency of N-O stretching vibrations. Evidence of NO bound on Pd can be found at 1860 cm^{-1} and 1810 cm^{-1} . Further calculations revealed multiple possible Pd cation species depending on their location in the CHA, that have overlapping, expected IR stretching frequencies. In contrast to the literature, both experiments and theoretical calculations indicate that the two bands observed cannot be assigned unambiguously to NO adsorbed on Pd^{2+} and Pd^+ cations. Multiple NO- Pd^{2+} and NO- Pd^+ species exist, differentiated by their location within the CHA, and a mix of these complexes makeup the TPD peaks and the IR bands. However, experiments designed to target Pd oxidation states could be used to support the formation of the Pd^+ cation. For example, water can be introduced to Pd/H-CHA saturated with NO and used to selectively displace NO that was stored on Pd^{2+} : the remaining NO is bound to only Pd^+ cations.

Chapter 3 complements the findings from the previous chapter and examines the influence of carbon monoxide on the adsorption of NO. The impact of CO on the NO adsorption abilities of Pd has been heavily debated in the literature. This co-adsorbate was of particular interest because of one popular hypothesis that suggests that CO performs a similar function to that of NO by partially reducing Pd^{2+} to Pd^+ . TPD experiments revealed that CO increases the amount of NO desorbing at higher temperatures and decreases the amount of NO desorbing at lower temperatures. The total NO stored during these tests does not change as a function of how CO is introduced, demonstrating that CO does not increase the NO storage capacity, but redistributes the available Pd cations between the two oxidation states. In addition, the lack of CO observed during TPD indicates that CO does not form co-adsorbed complexes and bolsters NO storage by reacting with Pd alone. Repeated NO storage cycles on Pd/H-CHA without any pretreatment or regenerative steps were also studied. It is shown that without water in the pretreatment gas stream, the high-temperature adsorption site, Pd^+ is lost after releasing NO. Theoretical calculations were used to hypothesize that traces amounts of O_2 were sufficient to re-oxidize Pd^+ to Pd^{2+} without the presence

of water. As a result, Pd/H-CHA cannot be used in successive storage cycles without the aid of a pretreatment step to enable partial reduction of Pd²⁺. This phenomenon also impacts efforts undertaken to identify Pd⁺ via electron paramagnetic resonance spectroscopy. Since only a minute amount of O₂ is necessary to re-oxidize it to Pd²⁺, it is very difficult to detect Pd⁺.

Chapter 4 focuses on the effect of ethene, as a co-adsorbate. Ethene has been reported to perform a similar function as CO and improve the NO storage capacity of Pd-exchanged zeolites. In contrast to literature, TPD experiments show that ethene actually inhibits NO adsorption, particularly the desorption at high-temperatures. Ethene competes with NO for low-temperature adsorption sites (i.e. Pd²⁺ sites), and reacts with NO to produce CO and methane. Ethene does not adsorb on Brønsted acid sites to a significant extent. Investigation of ethene storage on Pd/H-CHA shows that ethene is primarily adsorbed but reacts during desorption to form CO. In addition, exposure of the Pd/H-CHA to ethene results in the formation of coke, which inhibits NO storage in subsequent adsorption cycles. Other adsorption methodologies, such as co-adsorption of NO and ethene or sequential adsorption of ethene and NO leads to a reduction in the NO storage capacity. The NO helps oxidize ethene to CO and CO₂. IR spectroscopy was used to identify the adsorbed species. Though no CO-Pd bands were observed, bands attributed to ethene adsorbed on Pd are observed. However, Pd/H-CHA suffers from coking due to exposure to ethene that hurts its ability to store NO over several adsorption cycles; therefore, Pd/H-CHA functions as an effective HC trap but at the expense of diminished NO storage.

Dedication

To my family, who have supported me throughout my education.

Table of Contents

Abstract.....	1
Dedication.....	i
Table of Contents.....	ii
List of Figures.....	v
List of Tables.....	xi
Acknowledgements.....	xiii
1 Introduction.....	1
1.1 Pd-based catalysts for passive NO _x storage.....	1
1.2 Zeolite supports for PNA.....	2
1.3 Influence of co-adsorbates on NO storage.....	3
2 Investigation of the Modes of NO Adsorption in Pd/H-CHA ZnCl ₂	5
2.1 Abstract.....	5
2.2 Introduction.....	5
2.3 Experimental Methods.....	7
2.3.1 Adsorbent synthesis and characterization.....	7
2.3.2 Temperature-programmed desorption (TPD) studies.....	8
2.3.3 IR spectroscopy.....	8
2.3.4 Theoretical calculations.....	9
2.4 Results and Discussion.....	10
2.4.1 NO adsorption on H-CHA.....	10
2.4.2 NO adsorption on Pd/H-CHA.....	13
2.4.3 Effect of water on NO adsorption.....	15
2.4.4 Effect of air on the adsorption of NO on Pd/H-CHA.....	17
2.5 Theoretical Interpretation.....	19
2.5.1 NO adsorption in Pd/H-CHA.....	19
2.5.2 Effect of water on NO adsorption on Pd ⁺ and Pd ²⁺ sites.....	25
2.5.3 Effects of O ₂ on the adsorption of NO on Pd ⁺ and Pd ²⁺ sites.....	26
2.6 Conclusions.....	27
2.7 Acknowledgements.....	28
2.8 Supporting Information.....	29
2.8.1 X-ray diffraction.....	29
2.8.2 Synthesis of H-CHA and Pd/H-CHA.....	30
2.8.3 Effect of water on NO adsorption on H-CHA.....	30

2.8.4	Effect of water in pretreatment on Pd/H-CHA	32
2.8.5	Effect of increasing ion-exchanged Pd on NO adsorption.....	33
2.8.6	Details of experiments reported in the manuscript	34
2.8.7	Calculated peak desorption temperatures	35
2.8.8	Al pairs considered in QMMM study	36
2.8.9	Calculated vibrational frequencies for NO adsorbed on Pd ⁺ and Pd ²⁺ sites	37
2.8.10	XYZ coordinates of optimized structures	38
3	Experimental and Theoretical Studies of Pd Cation Reduction and Oxidation During NO Adsorption on and Desorption from Pd/H-CHA.....	40
3.1	Abstract	40
3.2	Introduction	40
3.3	Experimental Methods	42
3.3.1	Adsorbent synthesis and characterization	42
3.3.2	Temperature-programmed desorption studies	43
3.3.3	IR spectroscopy.....	43
3.3.4	Theoretical calculations	44
3.3.5	EPR spectroscopy	45
3.4	Results and Discussion.....	45
3.4.1	NO adsorption on Pd/H-CHA.....	45
3.4.2	Effect of CO on NO adsorption on Pd/H-CHA	47
3.4.3	Electron paramagnetic resonance experiments on NO adsorbed Pd/H-CHA.....	51
3.4.4	Retention of Pd ⁺ sites following NO TPD	53
3.5	Conclusions.....	55
3.6	Acknowledgements.....	56
3.7	Supporting Information.....	56
4	Investigation on the Impact of Ethene on the NO Adsorption Abilities of Pd/H-CHA	64
4.1	Abstract	64
4.2	Introduction	64
4.3	Experimental Methods	65
4.3.1	Adsorbent synthesis	65
4.3.2	Temperature-programmed desorption studies	65
4.3.3	IR spectroscopy.....	66
4.4	Results and Discussion.....	66
4.4.1	NO and C ₂ H ₄ storage on H-CHA.....	66
4.4.2	NO and C ₂ H ₄ storage on Pd/H-CHA	67

4.4.3	IR spectroscopy of NO and C ₂ H ₄ on Pd/H-CHA.....	74
4.4.4	Effect of NO on C ₂ H ₄ oxidation on Pd/H-CHA.....	76
4.5	Conclusions.....	77
4.6	Acknowledgements.....	78
5	Conclusions.....	79
6	References.....	81

List of Figures

Figure 2.1: Left: T696 cluster model for CHA used in QM/MM calculations. Si atoms are represented in cyan, Al in pink, O in red, H in white. The central CHA cage containing the adsorption sites is shown in bold lines. Right: 6-, 8- and 4-rings in *cha* cage.10

Figure 2.2: NO/NO₂ TPD profiles (a) and TPD IR spectra (b) for NO adsorbed on H-CHA. H-CHA was heated in air from 348 K to 773 K at 2 K/min and held at 773 K for 1 h. The sample was then cooled in air from 773 K to 348 K. Adsorption was from a flow of He (250 mL/min) containing 200 ppm of NO at 348 K. During TPD, the temperature was ramped from 348 K to 773 K at 10 K/min and then held at 773 K for 20 min in He. The dashed line corresponds to the maximum temperature of 773 K; the TPD profile beyond this line represents the continued temporal evolution of the system at constant temperature. Nearly identical results were obtained over four adsorption-desorption cycles. For the IR spectra, a reference spectrum was taken of H-CHA before NO adsorption, and then subtracted from the spectrum taken after NO adsorption. Scans were taken every 100 K during which the temperature was ramped at 2.5 K/min in He.10

Figure 2.3: NO/NO₂ TPD profiles (a) and TPD IR spectra (b) for NO adsorbed on H-CHA. H-CHA was heated in air 348 K to 773 K at 2 K/min and held at 773 K for 1 h. The sample was then cooled in air from 773 K to 348 K. Adsorption was from a flow of air (250 mL/min) containing 200 ppm of NO at 348 K. During TPD, the temperature was ramped from 348 K to 773 K at 10 K/min and then held at 773 K for 20 min in air. The dashed line corresponds to the maximum temperature of 773 K; the TPD profile beyond this line represents the continued temporal evolution of the system at constant temperature. Nearly identical results were obtained over four adsorption-desorption cycles. For the IR spectra, a reference spectrum was taken of H-CHA before NO adsorption, and then subtracted from the spectrum taken after NO adsorption. Scans were taken every 100 K during which the temperature was ramped at 2.5 K/min.13

Figure 2.4: The NO TPD profile (a) and the TPD IR spectra (b) for NO adsorbed on Pd/H-CHA. Pd/H-CHA was heated in air and 5% H₂O from 348 K to 773 K at 2 K/min and held at 773 K for 5 h. The sample was the cooled in He and 5% H₂O from 773 K to 348 K. NO adsorption was from a flow of He (250 mL/min) containing 200 ppm of NO at 348 K. During TPD, the temperature was ramped from 348 K to 773 K at 10 K/min and then held at 773 K for 20 min in He. The dashed line corresponds to the maximum temperature of 773 K; the TPD profile beyond this line represents the continued temporal evolution of the system at constant temperature. Nearly identical results were obtained over four adsorption-desorption cycles. For the IR spectra, a reference spectrum was taken of Pd/H-CHA before NO adsorption, and then subtracted from the spectrum taken after NO adsorption. Scans were taken every 100 K during which the temperature was ramped at 2.5 K/min.....14

Figure 2.5: (a) NO TPD profile for Pd/H-CHA without and with exposure of adsorbed NO to water vapor prior to the onset of TPD. (b) The desorption of NO caused by exposure of NO adsorbed on Pd/H-CHA prior to the onset of TPD. Pd/H-CHA was heated in air and 5% H₂O from 348 K to 773 K at 2 K/min and held at 773 K for 5 h. After heating, the sample was cooled in He and 5% H₂O from 773 K to 348 K. NO adsorption was from

a flow of He (250 mL/min) containing 200 ppm of NO at 348 K. To observe the effects of water vapor on adsorbed NO on Pd/H-CHA, the flow of NO in He was stopped and replaced by a He flow constraining 5% H₂O at 348 K. The water exposure was held for 20 min, after which the water flow was stopped and TPD started. During TPD, the temperature was ramped from 348 K to 773 K at 10 K/min and then held at 773 K for 20 min in He. The dashed line corresponds to the maximum temperature of 773 K; the TPD profile beyond this line represents the continued temporal evolution of the system at constant temperature.16

Figure 2.6: IR spectra (a) and TPD IR profiles (b) for NO adsorbed on Pd/H-CHA. Pd/H-CHA was heated in air and 5% H₂O 348 K to 773 K at 2 K/min and then held at 773 K for 5 h. After heating, the sample was cooled in He and 5% H₂O from 773 K to 348 K. NO adsorption was from a flow of He (250 mL/min) containing 200 ppm of NO at 348 K. To observe the effects of water vapor on adsorbed NO on Pd/H-CHA, the flow of NO in He was stopped and replaced by a He flow constraining 5% H₂O at 348 K. The water exposure was held for 20 min, after which the water flow was stopped and the acquisition of TPD IR spectra was initiated. During TPD IR, the temperature was ramped from 348 K to 773 K at 10 K/min and then held at 773 K for 20 min in He. .16

Figure 2.7: Comparison of NO and NO₂ TPD profiles for NO adsorbed from air on Pd/H-CHA (a) and for NO adsorbed from air on H-CHA (b) Pd/H-CHA was heated in air and 5% H₂O from 348 K to 773 K at 2 K/min and then held at 773 K for 5 h. H-CHA was heated in air from 348 K to 773 K at 2 K/min and then held at 773 K for 1 h. Following initial heating, both samples were cooled in air from 773 K to 348 K. Adsorption was from a flow of air (250 mL/min) containing 200 ppm of NO at 348 K. During TPD, the temperature was ramped from 348 K to 773 K at 10 K/min and then held at 773 K for 20 min in air. The dashed line corresponds to the maximum temperature of 773 K; the TPD profile beyond this line represents the continued temporal evolution of the system at constant temperature.17

Figure 2.8: (a) IR spectra of NO adsorbed from He or air on Pd/H-CHA. For the case of NO adsorption from He. Pd/H-CHA was heated in air and 5% H₂O from 348 K to 773 K at 2 K/min and held at 773 K for 5 h. In 8a, for the NO adsorption from He, the sample was cooled in He and 5% H₂O from 773 K to 348 K. For the NO adsorption from air, the sample was cooled in air from 773 K to 348 K. Adsorption occurred at 348 K from a flow (250 mL/min) containing 200 ppm NO in He or air. A reference spectrum was taken of Pd/H-CHA before NO adsorption and then subtracted from the spectrum taken after NO adsorption. (b) TPD IR spectra taken during heating at a rate of 2.5 K/min in flowing air (250 mL/min).18

Figure 2.9: [P_{H₂O}, T] phase diagrams showing the thermodynamically preferred Pd species at isolated Al and next-nearest neighbor (NNN), next-next-nearest (NNNN) neighbor and next-next-next-nearest neighbor NNNNN) Al pair in the 6- and 8-rings of CHA under flowing air (P_{O₂} = 20 kPa). Reprinted with permission from ref.¹⁹20

Figure 2.10: Theoretical estimates of IR stretching frequencies for NO ($\Delta_{\text{NO, est}}$) adsorbed on Pd⁺ and Pd²⁺ sites in Pd/H-CHA vs. calculated temperatures of maximum desorption (T_{max}) from the respective sites. Experimental IR spectra collected at 348K, 373K, 473K, 573K, 673K and 773K are shown as solid black lines. The corresponding TPD profile

is shown above the graph. During TPD, the temperature was ramped from 348 K to 773 K at 10 K/min and then held at 773 K for 20 min in He. The dashed line corresponds to the maximum temperature of 773 K; the TPD profile beyond this line represents the continued temporal evolution of the system at constant temperature.23

Figure 2.11: Calculated temperatures of maximum desorption (T_{\max}) from Pd^+ and Pd^{2+} sites in Pd/H-CHA vs. corresponding experimental desorption profiles for NO (blue) and NO_2 (red) after NO adsorption from air. The blue and red curves in this graph represent the difference between the TPD profiles on Pd/H-CHA and H-CHA (see Figures 7a and 7b) in order to isolate NO adsorption associated with the Pd sites. The dashed line corresponds to the maximum temperature of 773 K; the TPD profile beyond this line represents the continued temporal evolution of the system at constant temperature. The Pd^+ sites that may be re-oxidized to Pd^{2+} sites by air exposure are represented by open symbols with black outlines. The corresponding Pd^{2+} sites at the same Al pairs, which may become more abundant by the oxidation of these Pd^+ sites, are represented by enlarged symbols.27

Figure S2.1: Ex-situ X-ray diffraction patterns of a (a) reference purely siliceous CHA, (b) H-CHA (Si/Al = 12), and (c) H-CHA (Si/Al = 14).29

Figure S2.2: Effects of water vapor on the NO TPD. H-CHA (Si/Al = 12) was heated from in air 348 K to 773 K at 2 K/min and held at 773 K for 1 h. The sample was then cooled in air from 773 K to 348 K. H-CHA adsorption was from a flow of He (250 mL/min) containing 200 ppm of NO at 348 K. After saturating with NO, the flow of NO in He was stopped and replaced by He flow constraining 5% H_2O . During TPD, the temperature was ramped from 348 K to 773 K at 10 K/min. It was then held at 773 K for 20 min. The dashed line corresponds to 773 K; beyond this line, the temperature was held at 773 K for 20 min.31

Figure S2.3: Desorption curves that result from the different pretreatment conditions on Pd/H-CHA (Si/Al = 14). Pd/H-CHA was heated in air and 5% H_2O from 348 K to 773 K at 2 K/min and held at 773 K for 5 h. The sample was the cooled in He and 5% H_2O from 773 K to 348 K. These TPD profile result from flowing about 200 ppm of NO with CH_4 tracer in He or air at a flow rate of about 250 mL/min. Adsorption occurred at 348 K. During TPD, the temperature is ramped from 348 K to 773 K at 10 K/min. It was then held at 773 K for 20 min. The dashed line corresponds to 773 K; beyond this line, the temperature was held at 773 K. Each pretreatment condition was performed on the same sample of Pd/H-CHA (Si/Al = 14).32

Figure S2.4: The TPD profiles for NO desorption from Pd/H-CHA (Si/Al = 12) and Pd/H-CHA (Si/Al = 14). The peak concentration values were adjusted for the weight of CHA zeolite. Both Pd/H-CHA samples were heated in air and 5% H_2O from 348 K to 773 K at 2 K/min and held at 773 K for 5 h. The samples were then cooled in He and 5% H_2O from 773 K to 348 K. About 200 ppm NO, 20% O_2 , and CH_4 tracer were flowed in a He at a flow rate of about 250 mL/min. Adsorption occurred at 348 K. During TPD, the temperature was ramped from 348 K to 773 K at 10 K/min. It was then held at 773 K for 20 min. The dashed line corresponds to 773 K; beyond this line, the temperature was held at 773 K.33

Figure S2.5: Schematic representation of the different NNN, NNNN and NNNNN Al pairs considered in the QMMM study. The difference in formation energy ($\Delta\Delta E_{\text{form}}$) in kJ/mol between Pd^{2+} and Pd^+H^+ at each Al pair is shown in blue. Schematic representations of the corresponding $\text{P}_{\text{H}_2\text{O},\text{T}}$ phase diagrams are also shown (purple square: Pd^{2+} most favorable over entire range of conditions; green square: Pd^+H^+ most favorable over entire range of conditions; split green and purple square: Pd^{2+} or Pd^+H^+ most favorable, depending on $\text{P}_{\text{H}_2\text{O},\text{T}}$). * = inferred on the basis of $\Delta\Delta E_{\text{form}}$36

Figure 3.1. Left: T696 cluster model for CHA used in QM/MM calculations. Si atoms are represented in cyan, Al in pink, O in red, H in white. The central CHA cage containing the adsorption sites is shown in bold lines. Center: 6-ring and 8-ring in the *cha* cage. Right: Al pairs in next-nearest neighbor (NNN), next-next-nearest neighbor (NNNN) and next-next-next-nearest neighbor (NNNNN) configurations in the 6-ring (6R) and 8-ring (8R). Adapted with permission from [19]44

Figure 3.2. a) NO/ NO_2 profile for NO adsorbed on Pd/H-CHA during the adsorption step. NO adsorption was from a flow of He (250 mL/min). (b) NO TPD profile for NO adsorbed on Pd/H-CHA. Nearly identical results were obtained over four adsorption-desorption cycles.45

Figure 3.3. TPD IR spectra for NO adsorbed on Pd/H-CHA. A reference spectrum was taken of Pd/H-CHA before NO adsorption, and then subtracted from the spectrum taken after NO adsorption. Scans were taken every 100 K during which the temperature was ramped at 2.5 K/min.47

Figure 3.4. NO TPD profiles for NO adsorbed on Pd/H-CHA. Additional gas feeds were tested: NO and CO were co-adsorbed in one case, and the Pd/H-CHA was pre-saturated with CO prior to NO adsorption in the other.48

Figure 3.5. TPD IR spectra for NO adsorbed on Pd/H-CHA. In (a), additional gas feeds were tested: NO and CO were co-adsorbed in one case, and the Pd/H-CHA was pre-saturated with CO prior to NO adsorption in the other. In (b) the sample was first pre-saturated with CO from a flow of He (250 mL/min) at 348 K. A scan was taken after CO adsorption and prior to NO adsorption. This scan is then compared to a scan taken after NO adsorption.48

Figure 3.6. NO/CO/ CO_2 profiles during adsorption for CO and NO adsorbed on Pd/H-CHA. The profiles for NO, CO, and CO_2 were recorded during the adsorption step for Pd/H-CHA that was pre-saturated with CO prior to NO adsorption.49

Figure 3.7. EPR spectra of Pd/H-CHA and H-CHA samples. Samples were pretreated in He and 5% H_2O . Samples were removed from the quartz reactor and transferred to quartz EPR tubes. They were then moved to a Schlenk line to put under vacuum. A stopcock was used to separate the vacuum sealed EPR tube from the Schlenk line. Samples were then flame sealed. The Pd_zeolite sample was removed immediately after pretreatment. The NO_zeolite sample was the H-CHA sample that was saturated with NO after pretreatment. The Pd_zeolite_NO sample was the Pd/H-CHA sample that was saturated with NO after pretreatment.51

Figure 3.8. EPR spectra of Pd/H-CHA samples taken using two different methodologies. In Fig. 3.8a, a Pd/H-CHA sample was saturated with NO. Afterwards, two valves installed

around the reactor were closed to seal the sample from the air, and then the reactor was transferred to a glove box. In the glove box, the sample was transferred to a EPR quartz tube before being sealed with a stopcock and connected to a Schlenk line to be put under vacuum. In Fig. 3.8b, a Pd/H-CHA sample was pretreated in a quartz reactor, and then transferred to an EPR quartz tube. Once connected to a Schlenk line, the sample was exposed to NO before being put under vacuum for flame sealing.52

Figure 3.9. NO/NO₂ TPD profile for NO adsorbed on Pd/H-CHA. The spectra above were collected after degreening the Pd/H-CHA in air and H₂O, adsorbing NO, and then doing TPD. Afterwards, the sample was cooled in He from 773 K to 348 K, NO was adsorbed again at 348 K, and then the TPD was done again, resulting in the spectrum presented above.....53

Figure 3.10. a) The NO/NO₂ profile for NO adsorbed on Pd/H-CHA during the adsorption step. NO adsorption was from a flow of He (250 mL/min) containing 200 ppm of NO at 348 K. b) The CO/CO₂ profile for CO adsorbed on Pd/H-CHA during the adsorption step. CO adsorption was from a flow of He (250 mL/min) containing 100 ppm of CO at 348 K.54

Figure 4.1. NO and NO₂ TPD profiles for NO adsorbed on H-CHA. H-CHA was de-greened in air and NO was adsorbed in He balance.66

Figure 4.2. CO and C₂H₄ TPD profiles for C₂H₄ adsorbed on H-CHA. H-CHA was de-greened in He and C₂H₄ was adsorbed in He balance.....67

Figure 4.3. NO and NO₂ TPD profiles for NO adsorbed on Pd/H-CHA. Pd/H-CHA was de-greened in air and NO was adsorbed in He balance.....67

Figure 4.4. CO and C₂H₄ TPD profiles for C₂H₄ adsorbed on Pd/H-CHA. Pd/H-CHA was first de-greened in He, and C₂H₄ was adsorbed in He balance..68

Figure 4.5. C₂H₄ and CO TPR profiles for Pd/H-CHA (left axis) and the temperature (right axis). Samples were cooled in He from 773 K to 348 K, and then C₂H₄ was fed in He balance while increasing the temperature at 10 K/min to 773 K. It was held at 773 K for an hour. At high temperatures, CO begins to be produced before falling to a steady ~4 ppm, while C₂H₄ fell with the peak of CO before returning and holding at around 250 ppm69

Figure 4.6. TPD profiles for C₂H₄ adsorbed on Pd/H-CHA. Pd/H-CHA was first pretreated in He and 5% H₂O, and C₂H₄ was adsorbed in He balance.69

Figure 4.7. TPD profiles for C₂H₄ adsorbed on Pd/H-CHA. Pd/H-CHA was first pretreated in He, and then saturated with air for 20 min. After stopping air flow and purging for 1 h in He, C₂H₄ was adsorbed in He balance.....70

Figure 4.8. In Fig. 4.8a, the CO₂ profile is shown during a high-temperature air treatment for a Pd/H-CHA sample that recently underwent C₂H₄ TPR. Exposure to C₂H₄ at high temperatures results in build up of coke on the sample: the Pd/H-CHA was then exposed to a feed of air at 773 K for about 20-30 min to burn off coke. As a result, a peak of CO₂ is observed. In Fig. 4.8b, the NO_x TPD profile is shown for a sample that did not undergo a high-temperature air treatment. Without this air treatment, the coke leftover

- from C₂H₄ TPR will remain and block NO adsorption from occurring in subsequent cycles.71
- Figure 4.9. TPD spectra for NO and C₂H₄ adsorption on Pd/H-CHA. Pd/H-CHA was pretreated in air and H₂O and NO and C₂H₄ were adsorbed in He balance. NO and C₂H₄ react with one another resulting in additional byproducts like CO and small amounts of CH₄....71
- Figure 4.10. NO and NO₂ TPD profiles for Pd/H-CHA after adsorbing NO in He balance. First, Pd/H-CHA pretreated in air and H₂O was exposed to NO and C₂H₄ in He balance. Then, a TPD experiment was conducted, resulting in the desorption profiles seen in Fig. 4.6. Afterwards, the sample was then pretreated in He and H₂O from 773 K to 348 K. The sample was exposed to NO in He balance, and then TPD was conducted again, resulting in the TPD profile above. Due to the ethene exposure in the previous cycle, high-temperature NO desorption sites were blocked.72
- Figure 4.11. TPD spectra for C₂H₄ then NO adsorption on Pd/H-CHA. Pd/H-CHA was pretreated in air and H₂O. The catalyst was first saturated with C₂H₄ in He balance for about 20 min, then the C₂H₄ flow was stopped, and the sample was exposed to NO in He balance.73
- Figure 4.12. TPD IR spectrum for NO adsorbed on Pd/H-CHA taken at 348 K. A reference spectrum was taken of Pd/H-CHA before NO adsorption, and then subtracted from the spectrum taken after NO adsorption.74
- Figure 4.13. TPD IR spectrum for C₂H₄ adsorbed on Pd/H-CHA taken at 348 K. A reference spectrum was taken of Pd/H-CHA before C₂H₄ adsorption, and then subtracted from the spectrum taken after C₂H₄ adsorption..75
- Figure 4.14. TPD IR spectrum for NO and C₂H₄ adsorbed on Pd/H-CHA taken at 348 K. A reference spectrum was taken of Pd/H-CHA before NO and C₂H₄ adsorption, and then subtracted from the spectrum taken after NO and C₂H₄ adsorption.76

List of Tables

Table 2.1. Formation energies (ΔE_{form}) in kJ/mol for Pd ⁺ and Pd ²⁺ sites relative to the Brønsted acid protons at the same Al pair reported in ref. [19] (†) and ref. [81] (‡).	21
Table 2.2. Adsorption free energies (ΔG_{ads}) in kJ/mol for 200 ppm NO ($P_{\text{NO}} = 20$ Pa) and 5% water ($P_{\text{H}_2\text{O}} = 5$ kPa) at 348.15 K on Pd ²⁺ sites at NNN Al pairs, Pd ⁺ and Pd ²⁺ sites at NNN Al pairs in the 6-ring and 8-ring and Brønsted acid sites in CHA.	25
Table S2.1. Table comparing the characteristics of the Pd/H-CHA samples analyzed in this paper and supplemental material. Note that the main manuscript only examines Pd/H-CHA (Si/Al = 12). Percentage of isolated Pd was determined by temperature programmed reduction (TPR) in H ₂ : the Pd/H-CHA samples were pretreated in air to 773 K prior to TPR. ¹	30
Table S2.2. Table comparing the NO/Pd ratios resulting from applying different pretreatments (cooling from 773 K to 348 K) to Pd/H-CHA (Si/Al = 14) adsorbent before adsorption and TPD.	32
Table S2.3. List of pretreatment conditions, adsorption composition, carrier gas used for TPD, and the amounts of NO adsorbed for different experiments reported in the manuscript. The table is split into two for easier viewing.	34
Table S2.4. Calculated maximum desorption temperatures in K and vibrational frequencies in cm ⁻¹ for NO adsorbed on Pd ⁺ and Pd ²⁺ sites in Pd/H-CHA. NO stretching frequencies calculated by QMMM at the ωB97X-D/def2-sv(p) level of theory ($\nu_{\text{NO,DFT}}$) are shifted by adding the difference between the frequency for gas phase NO evaluated at the same level of theory (2097 cm ⁻¹) and the experimental value reported by NIST (1876 cm ⁻¹) to facilitate comparison with experimental IR spectra.	37
Table S2.5. Atoms included in the QM region for each of the attached XYZ files.	38
Table 3.1. Reaction free energies (ΔG_{rxn}) in kJ/mol under adsorption conditions (T = 348 K, $P_{\text{NO}} = 20$ Pa, $P_{\text{NO}_2} = 0.1$ Pa) for the reduction of Pd ²⁺ to Pd ⁺ at different Al pairs in the 6-rings and 8-rings in Pd/H-CHA before and after NO adsorption on the newly formed Pd ⁺ sites.	46
Table 3.2. Reaction free energies (ΔG_{rxn}) in kJ/mol under adsorption conditions (T = 348 K, $P_{\text{CO}} = 20$ Pa, $P_{\text{CO}_2} = 0.1$ Pa) for the reduction of Pd ²⁺ to Pd ⁺ at different Al pairs in the 6-rings and 8-rings in Pd/H-CHA before and after CO adsorption on the newly formed Pd ⁺ sites.	50
Table 3.3. Reaction free energies (ΔG_{rxn}) in kJ/mol for the reoxidation of Pd ⁺ to Pd ²⁺ at NNN Al pairs in the 6-rings and 8-rings in Pd/H-CHA, evaluated for various trace amounts of H ₂ O and O ₂ ($P_{\text{H}_2\text{O}}$ and P_{O_2} in Pa) at 773 K.	55
Table S3.1. 6-ring – NNN Al pair.	57
Table S3.2. 6-ring – NNNN Al pair.	59
Table S3.3. 8-ring – NNN Al pair.	61
Table S3.4. 8-ring – NNNN Al pair.	62
Table S3.5. 8-ring – NNNNN Al pair.	63

Acknowledgements

First, I would like to thank my advisor, Prof. Alexis T. Bell. For the last 6 years, Professor Bell has taught me so much about conducting research, giving presentations, and advice for converting my research results into an interesting story. I'm so thankful for the patience and wisdom he's shared with me during my PhD.

Next, I would like to thank the members of the Bell research group. Jeroen Van der Mynsbrugge, Neelay Phadke, Chris Ho, Julie Rorrer, and Danna Nozik were very welcoming and taught me what I needed to know to begin my research project. I would also like to thank the current members of the Bell Lab in Tan Hall: Natalie Lefton, Branden Leonhardt, and Afnan Alghannam, for their help and company.

I'd also like to thank Prof. Alexander Katz and Dr. Gregory Schoofs, with whom I helped teach Chemical Kinetics and Reaction Engineering as a Graduate Student Instructor in 2019 and 2022, respectively. Their lectures were pivotal in reinforcing my understanding of kinetics and reactor engineering, and they were very accommodating towards my efforts of balancing my research and my teaching assistant work. I am also grateful to Carlet Altamirano and Jeff King, who have helped me navigate the journey through the PhD program and enabled me to focus on my research.

Lastly, I would also like to thank the mentors I've had throughout my various research efforts. The opportunities and guidance they provided me were essential to my development as a student and researcher, and resulted in my desire to pursue a PhD. I'd like to thank the following people: Dr. Deokyang Kim, my high school research advisor, Professor Gary Brudvig, my undergraduate research advisor, Dr. Lukas Schmidt-Mende, my researcher supervisor during my summer abroad at the University of Konstanz, and Dr. Karla Reyes, my research supervisor during my internship at Sandia National Laboratories.

1 Introduction

1.1 Pd-based catalysts for passive NO_x storage

Air pollution has detrimental effects on the environment, resulting in climate change and substantial changes to global weather and temperatures. Of the many air pollution contributors, transportation, and the high density of cars in urban areas in particular, has been one of the largest sources of air pollution. Researchers and automakers are seeking ways to reduce the harmful emissions from vehicles to protect the environment. A particularly effective strategy for dealing with vehicular exhaust has been the three-way catalytic converter. First installed in 1972, it has led to orders of magnitude reductions in tailpipe emissions of CO, hydrocarbons (HC), and nitrogen oxides NO_x ($x = 1,2$).^{2,3} However, a remaining challenge in emissions control using catalytic converters is the time required to reach efficient operating temperatures (>523 K).² During this period, called the cold-start, the catalyst is not operating at its peak efficiency, and pollutants escape unconverted into the air. Under Tier 3 regulations of the US Environmental Protection Agency, automobiles will need to take additional steps to minimize the amount of NO_x and HC emitted during cold-start.³

One way to reduce NO_x emissions during cold-start is to adsorb NO together with CO and unburned hydrocarbons, and then to desorb these gases so that NO can be reduced in the catalytic converter once it reaches a temperature of 523-573 K. This can be done using a PNA, a device placed upstream of the catalytic converter that adsorbs NO_x emissions while the converter is heating up.⁴ PNAs will capture NO at lower temperatures, in the temperature window of cold start, and then release NO at appropriately high temperatures. This results in the release of any unconverted NO, which can then be dealt with by the operating catalytic converter.

The PNA consists of a metal dispersed on a high surface area support, such as a zeolite or mixed oxide.⁵ Research has been done on a number of both precious and transition metals for use in PNAs.⁵⁻⁸ Pd has been identified as a particularly attractive adsorbent for PNAs because of its high capacity for NO_x storage as molecular NO or as intermediates such as nitrites.⁹⁻¹¹ Pd is also more tolerant to sulfur poisoning compared to other precious metal candidates like Pt: this metal has similar adsorption capacity and can be superior under the right conditions.¹¹ However, Pt has been reported to bind NO more strongly than Pd, resulting in higher desorption energies and thus higher temperature requirements to release stored NO.¹¹ The ideal adsorbent releases NO at around 473-573 K, corresponding with the peak efficiencies of catalytic converters.

The method by which Pd-based catalysts capture NO varies depending on a variety of properties and the metal-support combination utilized. Feasible PNA development will require an understanding of the NO adsorption reaction mechanism. Honda Motor Company has conducted tests on Pd/ZSM-5, and shown that NO can be adsorbed without being oxidized to NO₂.¹² Ji et al have demonstrated that NO needs to adsorb in the form of a nitrite on Pd-promoted CeO₂-ZrO₂, but is ultimately desorbed as NO at higher temperatures. Additionally, they have also reported the benefits of co-adsorbed hydrocarbons (HC) alongside NO to improve not only the total storage but also increase the desorption temperature. These results suggest that Pd-based PNA materials can take advantage of HCs naturally present in exhaust gases to improve their storage properties.¹¹

There have been a number of articles analyzing the capabilities for NO storage of Pd-based catalysts, but a fair amount of debate still exists about the state of Pd that enables adsorption and how it is achieved.^{2,10,11} Previous work in the Bell group has reported that the catalyst pretreatment and Pd-loading can change the state of Pd.¹³ This work and prior studies also suggests that a number of factors can impact the available Pd used for NO storage, and consequently, results differ

from one group to another depending on the method of catalyst preparation and pretreatment. Pd for the most part is found to be present as isolated Pd cations, neutral PdO_x species, and Pd nanoparticles.¹⁴ The issues are further complicated by the fact that multiple states of Pd can exist for a given Pd loading or pretreatment, and not all of the Pd may be able to adsorb NO at all. For instance, PdO and Pd nanoparticles have been shown to be unable to adsorb NO.^{15–18} This leaves Pd cations as the primary adsorption species of interest.

The two oxidation states of most interest are the Pd²⁺ and Pd⁺ cations. Density functional theory calculations have been conducted, and most of the literature has come to an agreement that generally the Pd⁺ cation will bind NO more strongly than Pd²⁺.^{19–21} Pd²⁺ is commonly observed in NO adsorption experiments.^{1,13,15} However, the Pd⁺ oxidation state has proven elusive. Though many studies report the observation of Pd⁺, there is little direct evidence for this oxidation state due to a lack of reference materials.^{19,22,23} The strongest cases for the formation of Pd⁺ come from the production of NO₂ during the introduction of NO and electron paramagnetic resonance experiments on Pd zeolites in conditions very different from cold start (e.g. pretreatment and measurements taken at <10⁻⁵ torr).^{23–25} Additionally, most recent publications point to the observation of an IR feature at around 1800 cm⁻¹ as evidence for NO bound to Pd⁺. This band has been corroborated by theoretical calculations.^{17,22,23} The assignment of these IR features, however, are heavily debated and have been assigned to other possible NO adsorbed species such as NO bound on Pd²⁺ solvated in water molecules or a co-adsorbed complex of NO and OH on Pd²⁺.^{2,20,26} Assigning the band near 1800 cm⁻¹ and finding additional methods to identify Pd⁺ have been the largest hurdles in developing an adsorption reaction mechanism for NO on Pd.

1.2 Zeolite supports for PNA

Zeolites have been a popular choice of support for Pd due to their durable framework composition structures. These supports are crystalline, microporous silicoaluminates, possessing various 3D pores, channels, and cages, and possess high surface area.²⁷ In addition to their use in PNAs, zeolites have also been utilized as supports for selective catalytic reduction (SCR) of NO, thanks to their stability and ability to limit the formation of side products like N₂O.²⁸ The zeolite chabazite (CHA) has been identified as the most suitable support for Pd based on a number of characteristics. Its hydrothermal stability (stable up to 1023 K for up to 16 h in air and water) makes it a durable support that will not be in danger of dealumination during high temperature aging treatments.^{27,29,30} Their small pore size (0.22–0.39 nm) also inhibits Pd from agglomerating into less active species. Larger pore sizes have also been reported to lower the desorption temperatures of NO from the Pd zeolite.^{10,21,31} CHA also possesses a single Al site symmetry, which facilitates conducting theoretical studies to support the hypotheses presented in this dissertation.³²

Optimization of the zeolite support material is essential in order to maximize the cationic Pd content without sacrificing the durability of the catalyst. While small pores can inhibit Pd agglomeration, they increased risk of water condensation within the pores.³³ Another characteristic of the zeolite is its Si/Al ratio. Lowering this ratio increases the amount of Al atoms in the zeolite, which provides additional exchange sites for Pd and reduces the size of agglomerated Pd clusters.^{1,34} The former is particularly important for promoting the abundance of Al pairs that are the most stable exchange sites for Pd.^{19,35} It also reduces the zeolite hydrophobicity, which makes it easier for Pd to migrate deeper into the zeolite.^{34,36} Supports without any Al atoms adsorb little to no NO.³⁷ On the other hand, replacing more Si atoms with Al atoms in the zeolite reduces its stability, and can result in a more fragile support that cannot withstand high temperature aging treatments.³⁸ Another factor to consider is the Pd weight loading. Too high of a concentration of

Pd can be detrimental to the distribution of Pd species, since high weight loadings can result in Pd agglomeration and, hence, less stabilization of extra-framework Pd cations.^{39,40} The ideal amount of Pd loading lies between 1 and 2% weight.³⁴ These factors will be considered when developing Pd/H-CHA samples that are both durable and maximize the cationic Pd content.

1.3 Influence of co-adsorbates on NO storage

An additional consideration for PNAs is the composition of the exhaust gas: in addition to NO, other gases such as HCs, CO, CO₂, O₂, H₂O flow through the adsorbent and can impact its NO storage capabilities. One of the biggest questions regarding PNAs is whether the catalyst can take advantage of these other gases to improve NO storage. For instance, some studies have suggested that co-adsorbing HCs and CO together with NO can result in increased NO storage capacity and also delay the desorption to higher temperatures.^{17,41,42} At the same time, others have reported detrimental effects of flowing co-adsorbates, such as water blocking adsorption sites on Pd-based zeolites.^{34,43} Understanding how each of these co-adsorbates can impact NO storage will aid in developing a mechanism for NO storage on Pd.

Various theories that have been proposed regarding the effect of CO on NO storage. Co-adsorbed of CO with NO has been suggested to improve NO storage, but the mechanism still debated. Theis and Ura have theorized that CO reacts with NO to produce isocyanate species that are stored on Pd and decompose at high temperatures.⁴⁴ Other studies have suggested that CO and NO form a co-adsorbed complex on Pd²⁺ that will then lead to NO desorption at higher temperatures.^{26,45} CO has also been theorized to partially reduce Pd²⁺ to Pd⁺, and thus increase high temperature NO desorption by increasing the adsorption sites that bind NO more strongly.^{23,46} This last theory is of particular interest due to its close ties to the hypothesis that Pd⁺ is the high-temperature desorption site. The observation of CO₂ while adsorbing NO on Pd/H-CHA has been used as evidence that Pd⁺ is formed from Pd²⁺.^{46,47} In view of the various experimental studies of CO and NO co-adsorption and the divergence in their interpretation, there is still motivation to determine which of the proposed interpretations is right.

HCs such as ethene and propylene have been predicted to work similarly to CO in their ability to improve NO adsorption.^{47,48} Ethene has been reported to aid in delaying NO desorption by partially reducing Pd²⁺ to Pd⁺.^{9,47,49} Compared to CO however, ethene can compete with NO for Pd adsorption sites and impact the durability of the catalyst over repeated adsorption cycles.^{50,51} Propylene co-fed with NO on Pd/BEA had detrimental effects on the total NO_x storage but shifts more of the NO desorption to higher temperatures. The shift in desorption temperature is attributed to a mix of propylene blocking BAS, which typically desorb NO at lower temperatures, and the formation of propylene and NO complexes.^{48,52,53} The role of HCs in NO storage has similar questions as that of CO: though the effects are clearly observed during TPD, there are differences in how to interpret the influence of these reductants on the Pd adsorption site. While there is some evidence of the partial reduction of Pd due to the observation of acetaldehyde, most studies limit their conclusions to the possible formation of HC-NO complexes.^{23,48,54} Therefore, uncovering evidence for formation Pd⁺ in the presence of HCs or identifying the co-adsorbed complex remains a challenge in this field.

The influence of water has also been heavily studied as a part of the NO storage literature. PNAs needs to be stable at high temperatures in wet feeds to be of practical use in vehicles. Not only does water impact the availability of storage sites, but water can also adsorb on the Pd sites. The importance of water in the pretreatment step prior to NO exposure in order to maximize the total amount of available Pd cations has been noted.^{2,9} Others studies suggest that water poisons

active Pd sites, resulting in further agglomeration and formation of inactive PdO_x.⁵⁵ Water can outcompete NO for Brønsted acid sites and Pd²⁺ cations, inhibiting NO adsorption at these sites.^{43,47} At the same time, water has also been reported to react or co-adsorb with NO on Pd cations, resulting in one of the IR features reported.^{20,56} The dual effects of water are emblematic of the difficulties in studying NO adsorption: the particular conditions used in each study lead to different results. The aim of the present study was to develop a clearer understanding of the role of water on the and the identify of Pd cations in Pd/H-CHA and the adsorption of NO on both CHA and Pd cations exchanged into the zeolite.

2 Investigation of the Modes of NO Adsorption in Pd/H-CHAⁱ

2.1 Abstract

This study investigates NO adsorption on Pd-exchanged chabazite (Pd/H-CHA), a promising PNA for capturing cold-start NO_x emissions of gasoline- and diesel-powered vehicles. TPD and IR spectroscopy are combined with theoretical calculations to elucidate how and where NO is stored, and how water and O₂ affect this process. NO adsorption on Pd/H-CHA produces two TPD features, around 423 and 753 K, and IR bands centered at 1860 and 1810 cm⁻¹. Calculated NO stretching frequencies and maximum-desorption temperatures reveal that Pd²⁺ and Pd⁺ sites are responsible for these low- and high-temperature features, respectively, and that while the IR feature at 1810 cm⁻¹ is due to NO adsorption on Pd⁺, the 1860 cm⁻¹ feature contains contributions from both weakly-bound NO on Pd²⁺ and more strongly-bound NO on Pd⁺, consistent with experimentally observed effects of water and O₂.

2.2 Introduction

Several investigators have reported that the manner of Pd introduction onto a zeolite support and the subsequent pretreatment and usage conditions affect the NO storage capacity and release temperature of the PNA material.^{13,15,18} These studies and others have also shown that Pd can be present in multiple forms: isolated Pd cations (Pd²⁺, Pd(OH)⁺, Pd⁺), PdO_x (x = 1,2) nanoparticles, and metallic Pd nanoparticles.^{26,36,46,57-59} IR studies indicate that NO does not adsorb on PdO_x nanoparticles and adsorbs only weakly on metallic Pd nanoparticles.^{16,58,60} Therefore, isolated Pd cations are desired for PNAs, and the loss of such centers leads to a loss in the low-temperature NO adsorption capacity of the PNA.¹⁸

The critical role that isolated Pd cations have on NO adsorption is supported by recent work on Pd/H-CHA samples prepared so as to have Pd present predominantly as isolated Pd cations.²⁶ IR spectra of adsorbed NO showed bands at 2170 cm⁻¹, 1865 cm⁻¹, and 1805 cm⁻¹, which were assigned to NO⁺Z⁻, (NO) Pd²⁺(Z⁻)₂, and (NO) Pd⁺Z⁻, respectively, with the aid of DFT calculations^{26,34,61} (Z⁻ denotes a cation-exchange site in the zeolite framework created by the isomorphous substitution of tetravalent Si with trivalent Al). The presence of Pd²⁺ in as-prepared Pd/H-CHA samples has been supported by X-ray photoelectron spectroscopy, X-ray absorption spectroscopy, and diffuse reflectance UV-vis spectroscopy.¹⁷ Pd⁺ cations have been suggested to be produced upon NO adsorption via the reaction of Pd²⁺(Z⁻)₂ + 2 NO → (NO) Pd⁺Z⁻ + NO⁺Z⁻, based on the appearance of IR bands at 1805 cm⁻¹ and 2160 cm⁻¹,²⁶ and as discussed below, recent density functional theory (DFT) calculations that indicate that Pd/H-CHA treated in water vapor at high temperatures should thermodynamically favor the presence of Pd⁺ cations. DFT calculations using the GGA functional PW91-D2 by Khivantsev et al. have reported the electronic energies for binding NO to Pd²⁺ and Pd⁺ cations as -226 kJ/mol and -192 kJ/mol, respectively.¹⁷ However, Paolucci et al. have found that NO binding energies are highly sensitive to the choice of density functional and that using GGA functionals can overestimate the NO binding strength by up to 99 kJ/mol; hence, these authors report calculated NO binding energies of -175 kJ/mol for Pd⁺ and -70 kJ/mol for Pd²⁺ using the hybrid HSE06 functional.²⁰

ⁱ This chapter was originally published in Applied Catalysis B: Environmental and had been adapted for inclusion in this dissertation with permission from the coauthors J. Van der Mynsbrugge, H. Aljama, T. M. Lardinois, R. Gounder, M. Head-Gordon, and A. T. Bell. Dr. Van der Mynsbrugge contributed the theoretical calculations and Dr. Lardinois contributed the characterization of Pd/H-CHA.

Adsorption of NO on $[\text{Pd}(\text{OH})]^+$ sites in Pd-exchanged zeolites has also been proposed.^{2,23,47} It has been hypothesized that $[\text{Pd}(\text{OH})]^+$ is involved in the adsorption of NO, either as an adsorption site or as a precursor to the formation of Pd^+ according to the reaction: $\text{NO} + 2\text{Z}^- [\text{Pd}(\text{OH})]^+ \leftrightarrow 2\text{Z}^- \text{Pd}^+ + \text{NO}_2 + \text{H}_2\text{O}$.^{22,23} On the other hand, Mandal et al. have concluded that $[\text{Pd}(\text{OH})]^+$ does not form on samples with Pd content lower than the number of paired Al sites, as supported by DFT calculations and the absence of $[\text{Pd}(\text{OH})]^+$ bands in IR spectra of Pd/H-CHA acquired before and after NO.²⁰ We also note that Khivantsev et al. have suggested that $[\text{Pd}(\text{OH})]^+$ adsorbs NO to form $[\text{Pd}(\text{OH})(\text{NO})]^+$.²⁶ However, DFT studies reported by Van der Mynsbrugge et al. suggest that in the presence of air and water, Pd^+/H^+ and Pd^{2+} associated with pairs of Al atoms in the 6-rings and 8-rings of CHA are the thermodynamically favored species.¹⁹ These calculations also show that the stability of $[\text{Pd}(\text{OH})]^+$ is lower than that of Pd^{2+} and Pd^+/H^+ at Al pair sites, and under the conditions used in experimental studies $[\text{Pd}(\text{OH})]^+$ would readily react with the adjacent H^+ to form a Pd^{2+} and water.

The influence of other gas phase species on the adsorption of NO has also been studied. Water vapor present during NO adsorption has been reported to facilitate the mobility of PdO particles, leading to redispersion of Pd as cations,¹⁵ and water vapor has also been found to displace adsorbed NO from both the zeolite and Pd cations.⁴³ Oxygen, another component present in automotive exhaust, can also impact NO adsorption by forming NO_2 , which has been reported as a product upon NO desorption as well as an increase in the IR band associated with NO^+ on Pd/H-ZSM-5.¹³ Oxygen also prevents the reduction of Pd cations to small Pd particles, which do not adsorb NO.^{13,26} Additionally, heating Pd-exchanged zeolites in O_2 has been shown to convert metallic Pd nanoparticles to isolated Pd cations, thereby restoring the NO adsorption capacity of a PNA following use.⁶²

Another factor influencing the adsorption of NO is the location where Pd cations are exchanged into CHA. A recent theoretical study has shown that the relative stability Pd^{2+} and Pd^+ in cation-exchange sites in CHA strongly depends on the location of the Al atoms in the framework, as well as the operating conditions (e.g., exposure to water).¹⁹ Next-next-nearest neighbor (NNNN) Al pairs (separated by two Si atoms) in the 6-membered ring provide four zeolite oxygen atoms to coordinate Pd^{2+} cations in an ideal square planar configuration. As a result, Pd^{2+} is significantly more stable than Pd^+ at these Al pairs, over a wide range of conditions. By contrast, next-nearest neighbor (NNN) Al pairs (separated by a single Si atom) cannot provide the ideal square planar coordination to stabilize Pd^{2+} , such that the relative stability of Pd^+ and Pd^{2+} cations at these Al pairs depends on the temperature and partial pressure of water. The relative amounts of Pd^+ and Pd^{2+} cations exchanged at NNN Al pairs can therefore be altered by varying the temperature and partial pressure of water. The question of whether or not Pd^+ is present in as-prepared and pretreated Pd/CHA remains open, as several authors have suggested based on evidence inferred from IR spectroscopy that Pd^+ only forms upon NO adsorption via the process $\text{Pd}^{2+}(\text{Z}^-)_2 + 2 \text{NO} \rightarrow (\text{NO}) \text{Pd}^+ \text{Z}^- + \text{NO}^+ \text{Z}^-$; however, direct evidence of Pd^+ in zeolites in the absence of adsorbates has been reported by electron paramagnetic resonance spectroscopy (EPR).^{22,26,63}

The zeolite support onto which Pd cations are exchanged can also adsorb NO; hence, it is important to understand what fraction of the NO adsorbed in a PNA material is associated with the zeolite. IR spectroscopy has been used to identify the NO adsorption site in zeolites.⁶⁴ The principal feature observed in H-SSZ-13 (H-CHA) is a band at 2160 cm^{-1} ascribed to $\text{NO}^+ \text{Z}^-$. It has been suggested that this species forms via the reaction of two NO molecules (or NO and NO_2) with two Brønsted acid sites via $2 \text{NO} + 2 \text{H}^+ \text{Z}^- \rightarrow 2 \text{NO}^+ \text{Z}^- + \text{H}_2$ or via $\text{NO} + \text{NO}_2 + 2 \text{H}^+ \text{Z}^- \rightarrow 2 \text{NO}^+ \text{Z}^- +$

H₂O. The importance of proximate pairs of anion exchange sites to adsorb NO on acid sites in the zeolite has also been reported.⁵³

The present study was undertaken with the aim of identifying NO adsorption sites on Pd/H-CHA and the effect of water vapor and oxygen on the sites to which NO adsorbs. This effort has combined experimental studies and theoretical analysis based on DFT calculations. The questions addressed are the effects of adsorbent pretreatment on the formation of NO adsorption sites on both H-CHA and Pd/H-CHA, the relation between the oxidation state of Pd cations and the strength of NO adsorption, the vibrational frequencies for adsorbed NO on various binding sites, and the influence of H₂O and O₂ on NO adsorption on both H-CHA and Pd/H-CHA.

2.3 Experimental Methods

2.3.1 Adsorbent synthesis and characterization

The CHA zeolite (Si/Al = 12) was provided by BASF. This zeolite was the support utilized for the experiments described below. Additional CHA zeolite (Si/Al = 14) was prepared and used in experiments presented in the supplemental material. Palladium-exchanged zeolites were prepared by incipient wetness impregnation.³⁴ De-ionized water (18.2 MΩ) was added drop-wise to the NH₄-form zeolite while stirring until the total pore volume reached saturation, evidenced by a transformation from a powder-like substance to a liquid-like slurry. Assuming the same mass uptake as water, a Pd(NH₃)₄(NO₃)₂ solution (10 wt%, Sigma-Aldrich) was appropriately diluted with de-ionized water (18.2 MΩ) to achieve a desired Pd loading, using the same deposition procedure for the water-only trial. The Pd-form zeolite was dried in an oven at 393 K before treating in flowing air (Air Zero, Indiana Oxygen, 6000 cm³ h⁻¹ g⁻¹) to 823 K (120 K h⁻¹) for 5 h.

The framework topology was characterized with *ex situ* powder XRD, using a Rigaku Smartlab X-ray Diffractometer. Samples (0.01 g) were pressed onto low-dead volume holder (Rigaku), and patterns were collected from 4-40° 2θ with a scan rate of 60° h⁻¹ and a resolution of 0.01°.

Atomic absorption spectroscopy (AAS) was used to quantify the elemental contents using a Perkin Elmer model Analyst 300. Samples (0.02-0.05 g) were digested with 2.5 g of hydrofluoric acid (48 wt%, Alfa Aesar) for 3 days before diluting with 50 g of de-ionized water (18.2 MΩ). The Pd and Al contents in solution were determined by comparing to known elemental analysis standards. The Si/Al ratio was estimated by subtracting the contribution of extraframework cations and assuming a perfectly crystalline adsorbent with molar composition of [NH₄⁺]_x[Si_(1-x)O₂Al_x]^{x-}.

The amounts of cationic Pd and agglomerated PdO domains were quantified using H₂ temperature programmed reduction (TPR), using protocols we have reported previously.¹ H₂ TPR characterizations were performed with a Micromeritics Autochem II 2920 Chemisorption Analyzer, and H₂ consumption was quantified with a thermal conductivity detector (TCD). A TCD response factor determined by flowing different partial pressures (0.1-5 kPa) of H₂ in balance Ar, of which quantified a Micromeritics Ag₂O standard within 10%. Zeolites (0.05-0.10 g) were pretreated in flowing air (Air Zero, Indiana Oxygen, 1800 cm³ h⁻¹) to 473 K, 823 K, or 1023 K (600 K h⁻¹) for 1 h, cooled to 373 K before replacing the Air stream with Ar (UHP, Indiana Oxygen), then cooled to 203 K using a Micromeritics Cyrocooler II accessory. The Ar stream was replaced with 5 kPa H₂ in balance Ar (600 cm³ h⁻¹), then after achieving a stable TCD signal, the sample was treated to 573 K (600 K h⁻¹). H₂ TPR profiles, quantifications, and discussion can be found in the Supplemental Material (Section 2.8).

2.3.2 Temperature-programmed desorption (TPD) studies

All TPD studies were conducted in a quartz reactor. Typically, 100 mg of adsorbent were loaded into the reactor. A quartz wool plug was placed below the bed to prevent the adsorbent from entering the effluent gas line. Before NO adsorption measurements, the adsorbent underwent hydrothermal aging (HTA) in a stream of air containing 5% water from 348 K to 773 K at 2 K/min. The temperature was held at 773 K for 5 h, and then cooled back to 348 K in the absence of water vapor.

For adsorption, a feed stream containing the adsorbate was flowed over the adsorbent at 348 K until adsorbent was saturated. The composition of the feed stream varies between a number of experiments, and will be expanded upon in each section. The feed typically consisted of about 200 ppm of NO in a He flowing at 250 mL/min. 1000 ppm CH₄ was added to the NO/He stream as an inert tracer. He (purity of 99.999% from Praxair) was dried by passage through moisture trap (Restek Moisture Trap, <10 ppb water) and NO (1.03% NO in He balance from Praxair) was purified by passage through traps to remove moisture and NO₂ (Alltech Gas Drier, <1 ppm NO₂ and H₂O). The air carrier gas provided by Praxair is rated as extra dry (<10 ppm H₂O). The adsorption of NO was monitored using an MKS 2030 Multigas analyzer, a non-dispersive infrared (NDIR) spectroscopy instrument. The concentration of NO in the effluent was measured, and the NO and CH₄ were shut off once the effluent concentration of NO had reached the inlet value. The adsorbent was then purged with He until the concentration of NO had returned to the level observed before the start of the adsorption step. A purge stream of He (250 mL/min) was fed to the reactor immediately after adsorption to remove any weakly-bound adsorbates. The adsorbed NO was desorbed while the adsorbent was heated from 348 K to 773 K at 10 K/min, and then held at 773 K for 20 min. Throughout this period the concentration of NO and NO₂ in the effluent was monitored by the Multigas analyzer. Following a TPD experiment, the adsorbent was treated in one of several ways in order to prepare it for the next adsorption cycle. This typically involved cooling the adsorbent from 773 K back to 348 K in a defined gas mixture (e.g., He, air, air plus water vapor). This last step is referred to as a pretreatment, and for future discussion, the pretreatment refers to the step performed before an adsorption measurement when the adsorbent undergoes several adsorption/desorption cycles. Other pretreatment schemes involved the addition of either air, or O₂, in He, and are detailed as they are discussed subsequently. In this study, cycles typically refer to repeated experiments on the same adsorbent loading.

2.3.3 IR spectroscopy

The procedure for the initial treatment of Pd/H-CHA and pretreatment between NO adsorption experiments is similar to that used for the TPD experiments. About 30 mg of adsorbent was compressed into a pellet that was placed into a Harrick High Temperature cell with CaF₂ windows. The cell was heated resistively and the temperature was monitored with a K-type thermocouple. The adsorbent was exposed to NO for 15 min, after which the NO flow was stopped and the TPD ramp was started. *In situ* transmission IR experiments were conducted using a Nicolet 6700 spectrometer operated at 4 cm⁻¹ resolution. Each spectrum was obtained by averaging 256 scans. Background spectra of Pd/H-CHA, taken at the same temperatures as those at which spectra

were recorded during a TPD IR experiment, were subtracted from the spectra of NO adsorbed on Pd-CHA. Additional baseline subtraction was conducted using Origin.

2.3.4 Theoretical calculations

The crystallographic structure of CHA was obtained from the database maintained by the International Zeolite Association (IZA).⁶⁵ A large cluster model containing 696 tetrahedral atoms (T696) was constructed by selecting the framework atoms within a 25 Å radius of a central *cha* cage, and trimming the edges of the resulting fragment such that the cluster is terminated by double six-ring units. This large model avoids any boundary effects and prevents the introduction of unintended anisotropy in the description of long-range interactions.⁶⁶

Al pairs were placed in various next-nearest neighbor (NNN), next-next-nearest neighbor (NNNN) or next-next-next-nearest neighbor (NNNNN) configurations in the CHA framework. The resulting double charge defects were compensated by either Pd⁺/H⁺ or Pd²⁺. A total of 16 structures in which the Pd cations are accessible from the *cha* cage were selected to model potential NO adsorption sites. A hybrid quantum mechanics/molecular mechanics (QM/MM) approach was applied to limit the computational expense. A smaller fragment of the zeolite cluster and the adsorbates are treated quantum mechanically (QM), using the range-separated hybrid functional ω B97X-D^{67,68}, combined with def2 basis sets, which include an effective core potential for Pd. The QM region includes all neighboring T-atoms of each Al, as well as all Si and O atoms that are part of the 4-, 6- or 8-ring(s) connecting the pair of Al atoms. Where necessary, the QM region was extended further to fully account for the interactions of adsorbed NO with the zeolite framework. The remainder of the large cluster model is treated using molecular mechanics (MM).^{69,70} Fig. 2.1 shows the T696 cluster model and highlights the 4-, 6- and 8-rings facing the *cha* cages. Geometry optimizations and frequency calculations are performed at the ω B97X-D/def2-SV(P) level of theory, followed by single-point energy refinements at the ω B97M-V/def2-TZVPD level of theory. Paolucci et al. have pointed out that binding energies of NO to Pd are particularly sensitive to the choice of density functional.²⁰ In this study, we have selected the range-separated hybrid meta GGA functional ω B97M-V⁷¹ to evaluate the energetics, because it has emerged as the overall best performer out of the 200 density functionals evaluated by Mardirossian and Head-Gordon.⁷² The MM region is described with a CHARMM-type force field using the P2 parameter set.⁷⁰ Initial geometries were constructed with ZEOBUILDER.⁷¹ All QM/MM calculations were performed with a developmental version of Q-Chem.⁷³ Thermochemical quantities are calculated from a normal mode analysis using the quasi-rigid rotor/harmonic oscillator approximation (RRHO)^{70,74} on the optimized structures.

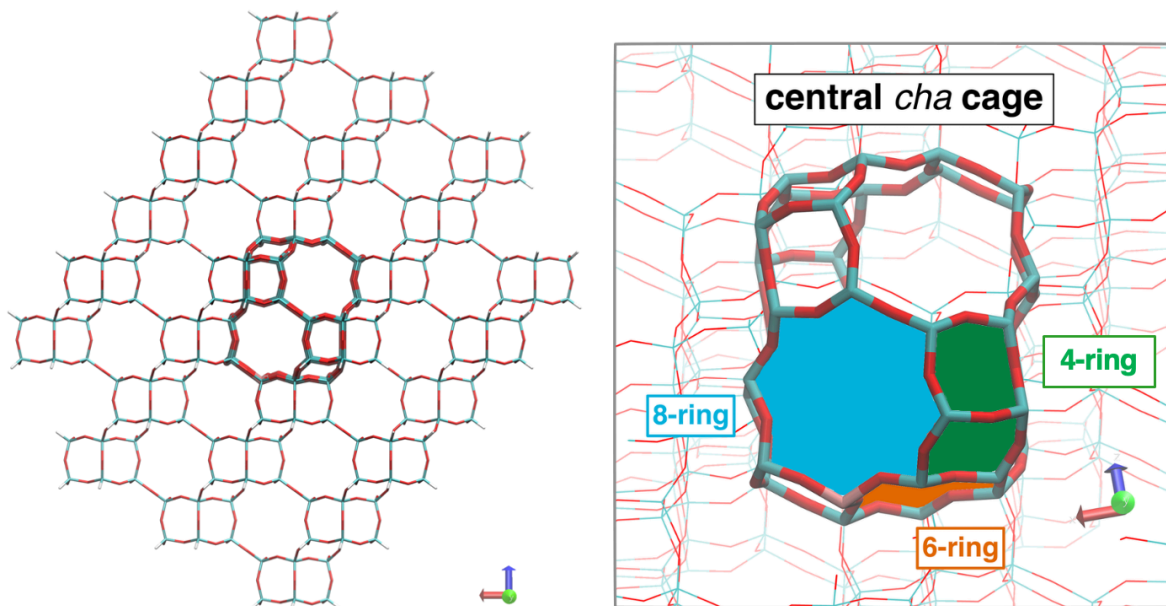
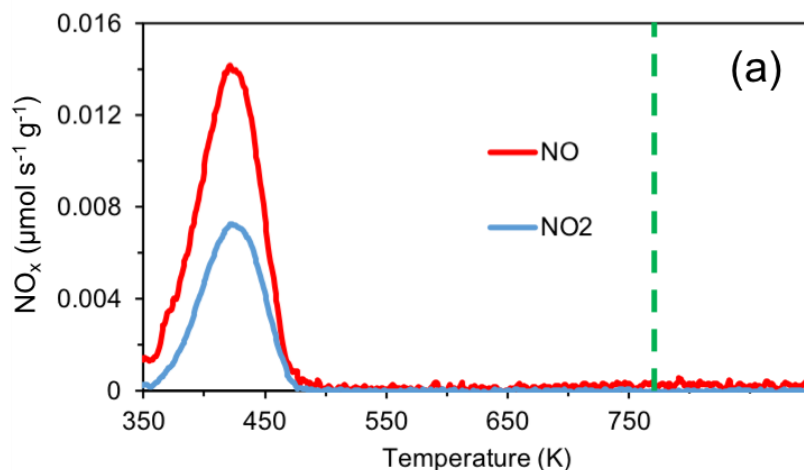


Figure 2.1: Left: T696 cluster model for CHA used in QM/MM calculations. Si atoms are represented in cyan, Al in pink, O in red, H in white. The central CHA cage containing the adsorption sites is shown in bold lines. Right: 6-, 8- and 4-rings in *cha* cage.

2.4 Results and Discussion

2.4.1 NO adsorption on H-CHA

NO adsorption on H-CHA (Si/Al = 12) was examined in order to characterize its interaction with the zeolite support. Fig. 2.2 shows the TPD profile after NO adsorption on H-CHA. Both NO and NO₂ were observed in the effluent in the ratio of 2/1, and the total amount of NO adsorbed is 5.4 μmol NO per gram of adsorbent. This amount of adsorbed NO corresponds to about 7.3×10^{-3} mol NO_x per mole of protons, indicating that only a small fraction of the zeolitic protons are involved in NO adsorption.



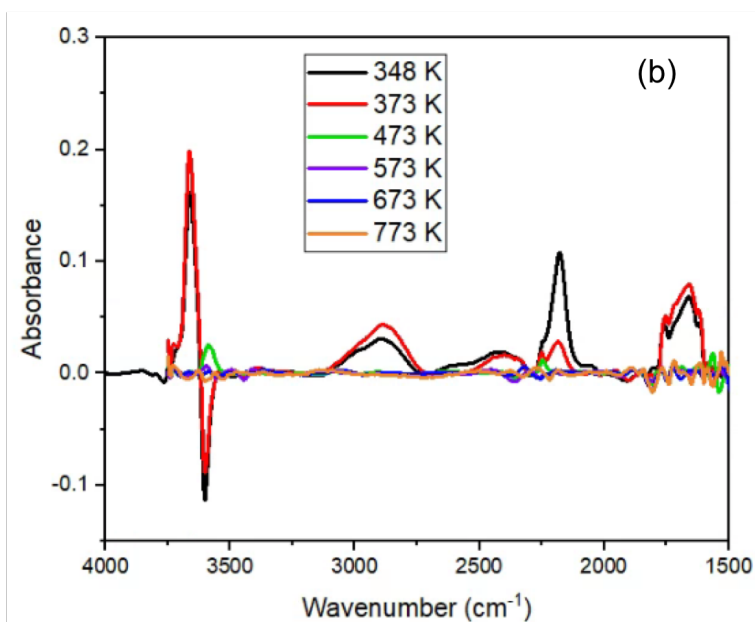


Figure 2.2: NO/NO₂ TPD profiles (a) and TPD IR spectra (b) for NO adsorbed on H-CHA. H-CHA was heated in air from 348 K to 773 K at 2 K/min and held at 773 K for 1 h. The sample was then cooled in air from 773 K to 348 K. Adsorption was from a flow of He (250 mL/min) containing 200 ppm of NO at 348 K. During TPD, the temperature was ramped from 348 K to 773 K at 10 K/min and then held at 773 K for 20 min in He. The dashed line corresponds to the maximum temperature of 773 K; the TPD profile beyond this line represents the continued temporal evolution of the system at constant temperature. Nearly identical results were obtained over four adsorption-desorption cycles. For the IR spectra, a reference spectrum was taken of H-CHA before NO adsorption, and then subtracted from the spectrum taken after NO adsorption. Scans were taken every 100 K during which the temperature was ramped at 2.5 K/min in He.

Fig. 2.2 also shows the IR spectra taken during TPD. At 348 K, the bands observed are the result of NO adsorption on H-CHA. The band at 2160 cm⁻¹, due to NO⁺Z⁻, appears to be comprised of two components, reflecting somewhat different environments.^{53,75} The appearance of this band is accompanied by a decrease in the band intensity at 3590 cm⁻¹ band due to Brønsted acidic O-H stretches.⁵³ There is also an increase in a band 3670 cm⁻¹, which is assigned to water adsorbed on the zeolite.⁷⁶ Additional evidence for the formation of water upon NO adsorption is the appearance of broad bands located 2830 cm⁻¹, 2390 cm⁻¹, and 1630 cm⁻¹, all of which have been reported for water strongly hydrogen-bonded to Brønsted acid sites in H-CHA.⁷⁶⁻⁷⁸ We note that the shape of the broad centered at 1630 cm⁻¹ does not match that expected for water vapor adsorbed on H-CHA, suggesting the presence of other species such as nitrates. The broad feature between 1500 and 1700 cm⁻¹ may also contain contributions from nitroso (NO₂⁻) and nitrates (NO₃⁻).^{23,76,79,80} These latter species very likely form during adsorption via the reaction of NO with small amounts of O₂ retained on the sample from the pretreatment in air. During TPD, the features associated with adsorbed NO and H₂O are retained when the temperature rises to 373 K, but by 473 K, all of the peaks have disappeared. This pattern is consistent with the TPD profile presented in Fig. 2.2a, which shows that all NO and NO₂ desorbs by 473 K. It is also notable that the band at 3590 cm⁻¹ for Brønsted acidic OH groups is restored during desorption of NO, suggesting that these species are associated with the adsorption of NO. This conclusion is confirmed by the observation that the TPD profile in the TPD IR spectra in Fig. 2.2b is reproducible after multiple adsorption and desorption cycles. Hadjiivanov et al. has proposed that NO and NO₂ react with two nearby

Brønsted acid sites to form two NO^+ bound to the zeolite, as well as a water molecule that is H-bonded to another Brønsted acid site.⁵³

The effect of water on NO adsorption on H-CHA was also investigated. To explore these effects, NO was first adsorbed on H-CHA by exposure to 200 ppm of NO in He, and then to a He stream containing 1% water for 10-20 min. After that, the sweep gas was switched to He and the temperature was ramped from 348 K to 773 K. Exposure of the pre-adsorbed NO to water resulted in the disappearance of the peaks for NO and NO_2 in the TPD profile. This figure is reported in the SI (Fig. S2.2). These results are similar to those reported for zeolite BEA, which have shown that water displaces NO adsorbed on the zeolite.⁴³ In addition, the inclusion of water in the pretreatment also prevented any NO adsorption on H-CHA.

The effect of air on the adsorption of NO on H-CHA was also examined. As seen in Fig. 2.3a, the adsorption of NO from air resulted in the desorption of nearly equivalent amounts of NO and NO_2 during TPD. The total amount of NO_x adsorbed (as either NO or NO_2) in this case is 63 μmol of NO_x per gram of adsorbent (5.7×10^{-2} mol NO /mol protons), which is considerably higher than the amount for NO adsorbed from He, 5.4 μmol NO_x /g of adsorbent (7.3×10^{-3} mol NO_x /mol protons).⁵³ The appearance of equivalent amounts of NO and NO_2 during TPD suggests that a fraction of the desorbing NO undergoes oxidation to NO_2 .

The TPD IR spectra for NO adsorbed from air onto H-CHA are shown in Figure 2.3b. Similar to the TPD IR results for the case of NO adsorbed from He (Fig. 2.2b), all of the bands disappear by 473 K. There is a sharp band at 2160 cm^{-1} due to NO^+ adsorbed on the zeolite, and a corresponding negative band at 3590 cm^{-1} indicating the loss of Brønsted acid sites. The band at 2160 cm^{-1} is also more intense when NO is adsorbed from air, supporting the mechanism proposed by Hadjiivanov et al.⁵³ When NO is adsorbed from air, the integrated area of the band for NO^+ is 4.8 times higher than that for NO adsorption from He, while the integrated area of the band for water around 2890 cm^{-1} is about 3.0 times higher, which agrees semi-quantitatively with what would be expected.⁵³

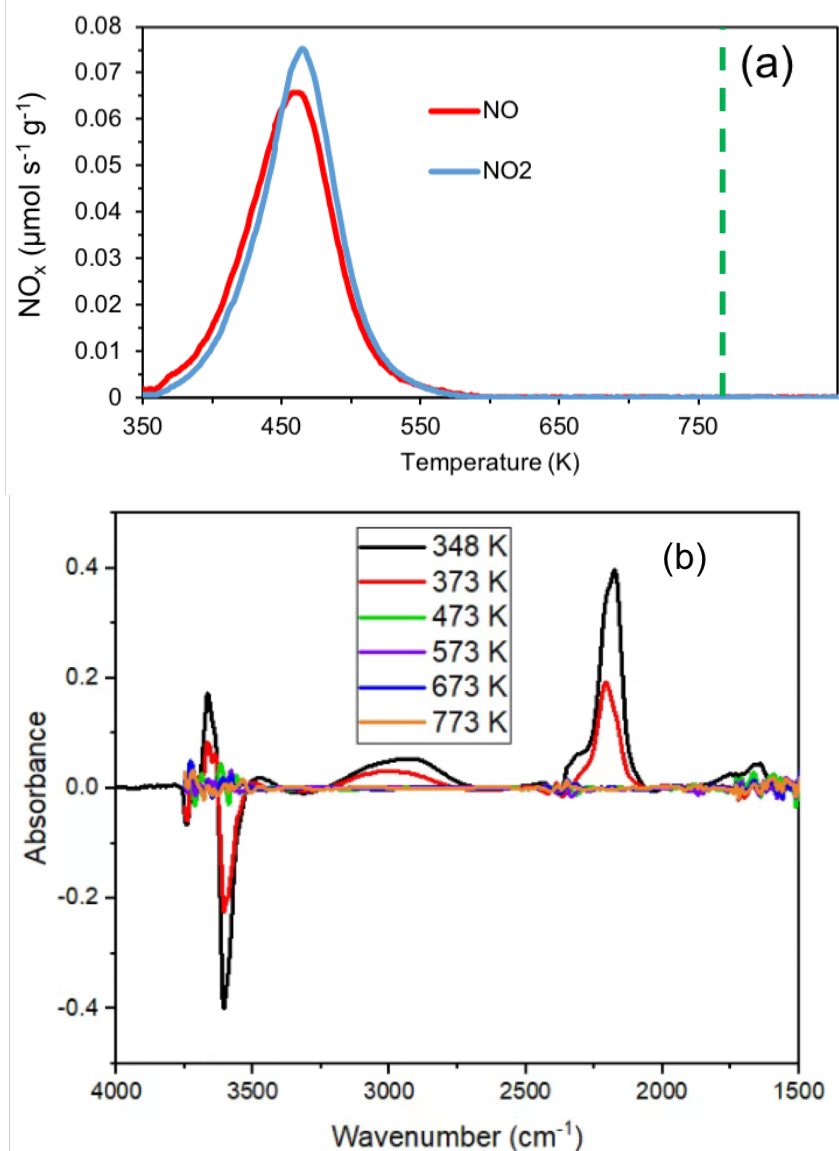


Figure 2.3: NO/NO₂ TPD profiles (a) and TPD IR spectra (b) for NO adsorbed on H-CHA. H-CHA was heated in air 348 K to 773 K at 2 K/min and held at 773 K for 1 h. The sample was then cooled in air from 773 K to 348 K. Adsorption was from a flow of air (250 mL/min) containing 200 ppm of NO at 348 K. During TPD, the temperature was ramped from 348 K to 773 K at 10 K/min and then held at 773 K for 20 min in air. The dashed line corresponds to the maximum temperature of 773 K; the TPD profile beyond this line represents the continued temporal evolution of the system at constant temperature. Nearly identical results were obtained over four adsorption-desorption cycles. For the IR spectra, a reference spectrum was taken of H-CHA before NO adsorption, and then subtracted from the spectrum taken after NO adsorption. Scans were taken every 100 K during which the temperature was ramped at 2.5 K/min.

2.4.2 NO adsorption on Pd/H-CHA

The adsorption of NO on Pd/H-CHA (Si/Al = 12, Pd/Al = 0.24) was investigated in order to identify the different states of NO adsorbed on Pd cations and the influence of adsorbent pretreatment on the distribution of these states of adsorbed NO. For these experiments, the adsorbent was first heated to 773 K at 2 K/min in air containing 5% H₂O, held at this temperature

for 5 h, and then cooled to 348 K in dry air (anhydrous). This pretreatment was chosen to attempt to maximize the amount of isolated Pd.¹ As seen in Fig. 2.4a, the TPD profile for NO adsorbed on Pd/H-CHA exhibits two prominent NO desorption peaks: a low-temperature peak around 423 to 473 K and a broad high-temperature peak ranging from 550 to 900 K with a maximum at about 753 K. The low-temperature peak comprises 29% of the desorbed NO and the high-temperature peak comprises 71%. No NO₂ was observed in the effluent during TPD. The total amount of NO adsorbed on Pd/H-CHA is about 57 μmol of NO per gram of adsorbent, which corresponds to a NO/Pd ratio of 0.73. This ratio agrees well with the fraction of isolated cations present in Pd/H-CHA measured by H₂ temperature programmed reduction (0.79), suggesting that each Pd cation adsorbs one NO molecule.

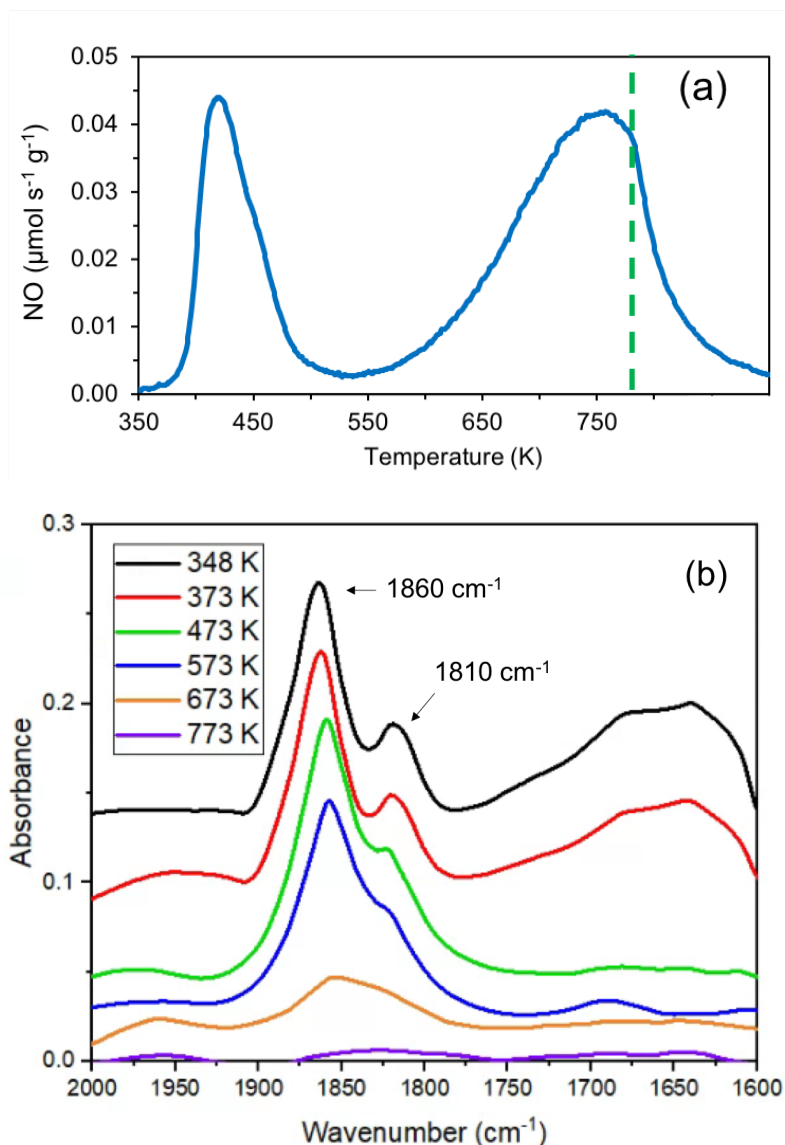


Figure 2.4: The NO TPD profile (a) and the TPD IR spectra (b) for NO adsorbed on Pd/H-CHA. Pd/H-CHA was heated in air and 5% H₂O from 348 K to 773 K at 2 K/min and held at 773 K for 5 h. The sample was cooled in He and 5% H₂O from 773 K to 348 K. NO adsorption was from a flow of He (250 mL/min) containing 200 ppm of

NO at 348 K. During TPD, the temperature was ramped from 348 K to 773 K at 10 K/min and then held at 773 K for 20 min in He. The dashed line corresponds to the maximum temperature of 773 K; the TPD profile beyond this line represents the continued temporal evolution of the system at constant temperature. Nearly identical results were obtained over four adsorption-desorption cycles. For the IR spectra, a reference spectrum was taken of Pd/H-CHA before NO adsorption, and then subtracted from the spectrum taken after NO adsorption. Scans were taken every 100 K during which the temperature was ramped at 2.5 K/min.

Fig. 2.4b shows the IR TPD spectra for NO adsorbed on Pd/H-CHA. For this experiment, the adsorbent was heated to 773 K at 2 K/min in a flow of air containing 5% H₂O and then held at this temperature for 5 h, and then cooled to 348 K in air (not containing water vapor) and held at this temperature for 5 h. After pretreatment, the sample was exposed to about 200 ppm NO in He for about 15 min. The principal bands associated with adsorbed NO occur at 1860 cm⁻¹ and 1810 cm⁻¹. Notably, the band at 2160 cm⁻¹ for NO⁺Z⁻ is absent. We attribute this to the retention of water vapor from the pretreatment step, which inhibits NO adsorption on the zeolite.⁴³ The bands at 1860 cm⁻¹ and 1810 cm⁻¹ have been observed previously in the IR spectrum of NO adsorbed on Pd-SSZ-13 and have been assigned to NO adsorbed on Pd²⁺ and Pd⁺ cations, respectively, on the basis of DFT calculations.²² The absence of a band at 2160 cm⁻¹ for zeolite-bound NO⁺, a consequence of the pretreatment of Pd/H-CHA in a He/H₂O mixture, indicates that all of the NO_x that desorbs during the TPD of Pd/H-CHA comes from NO adsorbed on Pd cations. As seen in Fig. S2.2, H-CHA cannot adsorb NO when pretreated in He and H₂O, due to water blocking BAS. Fig. 2.4b also shows a broad band around 1600-1775 cm⁻¹ attributable to water adsorbed on the zeolite during the pretreatment step. This band is also observed prior to NO adsorption, and very little NO₂ is observed during TPD. It's likely that most of this band is adsorbed water and adsorbed nitrates do not contribute significantly.²³

IR TPD experiments were performed to observe how the band intensities change as a function of temperature. Fig. 2.4b shows that the broad band at 1650 cm⁻¹, due to water adsorbed on the zeolite disappears between 358 K and 473 K, in agreement with previous observations.^{53,76} More notably, the band at 1810 cm⁻¹ significantly weakens above 373 K and loses most of its intensity by about 573 K. By contrast, the band at 1860 cm⁻¹ band only begins to lose intensity above 573 K and is no longer visible by 773 K. The relationship between band assignment and TPD behavior will be discussed in Section 2.5.

2.4.3 Effect of water on NO adsorption

Water vapor has been reported to affect the TPD profile of NO adsorbed on Pd-BEA. Khivantsev et al. have shown that when NO is co-adsorbed with O₂ and H₂O, only a high-temperature NO TPD feature is observed above 473 K, and Chen et al. have shown that water displaces the NO species responsible for the IR band at 1860 cm⁻¹.^{26,43} Consequently, we undertook experiments to assess whether water displaces either of the two forms of adsorbed NO observed during TPD and IR spectroscopy. The results of these experiments combined with theoretical analysis, enabled identification of the Pd species on which NO is adsorbed and the effects of water on the stability of adsorbed NO. Pd/H-CHA was pretreated by feeding a stream of air containing 5% water from 348 K to 773 K at 2 K/min. The temperature was held at 773 K for 5 h, and then cooled back to 348 K in the absence of water vapor. After pretreatment, Pd/H-CHA was exposed to 200 ppm of NO in He, and then to a He stream containing 1% water for 20 min. After that, the sweep gas was switched to He and the temperature was ramped from 348 K to 773 K. Fig. 2.5a shows that exposure of the sample containing adsorbed NO to water vapor caused a complete disappearance of the low-temperature NO desorption peak, but had no effect on the desorption of

NO at higher temperatures. Fig. 2.5b also shows that pre-adsorbed NO desorbed from the sample almost immediately after it was exposed to the He stream containing water vapor. In fact, the amount of NO displaced by water vapor ($12 \mu\text{mol NO per g of adsorbent}$ and 0.15 NO/Pd) corresponds closely to the amount of NO that would have desorbed in the low temperature NO desorption peak in the absence of water exposure ($16 \mu\text{mol NO per g of adsorbent}$ and 0.21 NO/Pd).

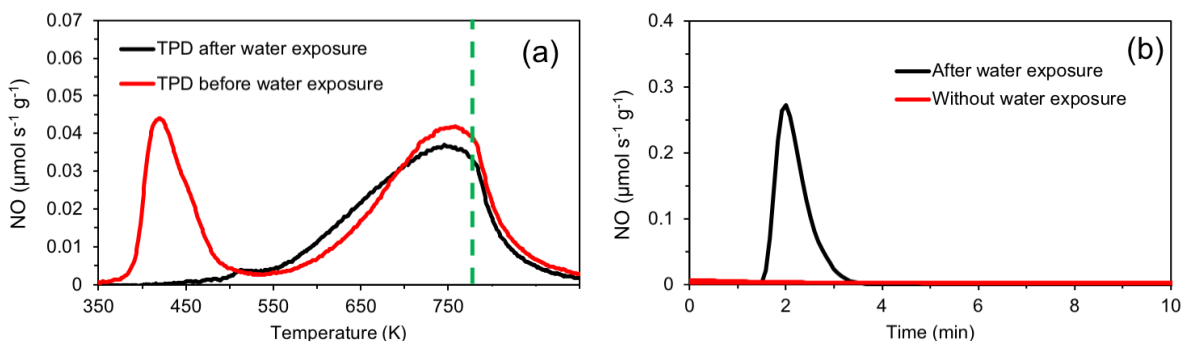


Figure 2.5: (a) NO TPD profile for Pd/H-CHA without and with exposure of adsorbed NO to water vapor prior to the onset of TPD. (b) The desorption of NO caused by exposure of NO adsorbed on Pd/H-CHA prior to the onset of TPD. Pd/H-CHA was heated in air and 5% H_2O from 348 K to 773 K at 2 K/min and held at 773 K for 5 h. After heating, the sample was cooled in He and 5% H_2O from 773 K to 348 K. NO adsorption was from a flow of He (250 mL/min) containing 200 ppm of NO at 348 K. To observe the effects of water vapor on adsorbed NO on Pd/H-CHA, the flow of NO in He was stopped and replaced by a He flow constraining 5% H_2O at 348 K. The water exposure was held for 20 min, after which the water flow was stopped and TPD started. During TPD, the temperature was ramped from 348 K to 773 K at 10 K/min and then held at 773 K for 20 min in He. The dashed line corresponds to the maximum temperature of 773 K; the TPD profile beyond this line represents the continued temporal evolution of the system at constant temperature.

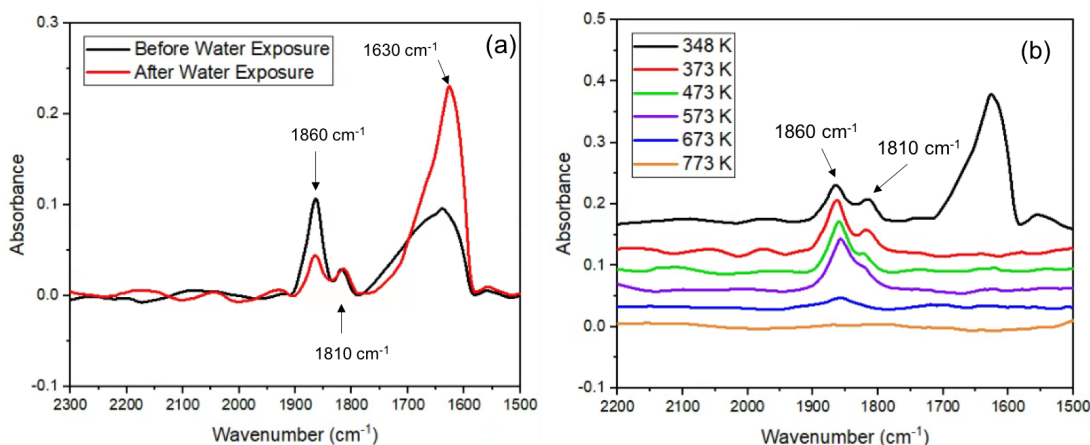


Figure 2.6: IR spectra (a) and TPD IR profiles (b) for NO adsorbed on Pd/H-CHA. Pd/H-CHA was heated in air and 5% H_2O 348 K to 773 K at 2 K/min and then held at 773 K for 5 h. After heating, the sample was cooled in He and 5% H_2O from 773 K to 348 K. NO adsorption was from a flow of He (250 mL/min) containing 200 ppm of NO at 348 K. To observe the effects of water vapor on adsorbed NO on Pd/H-CHA, the flow of NO in He was stopped and replaced by a He flow constraining 5% H_2O at 348 K. The water exposure was held for 20 min, after which the water flow was stopped and the acquisition of TPD IR spectra was initiated. During TPD IR, the temperature was ramped from 348 K to 773 K at 10 K/min and then held at 773 K for 20 min in He.

Fig. 2.6a shows IR spectra of NO adsorbed on Pd/H-CHA taken before and after exposure of the sample to water vapor. The spectrum recorded prior to water vapor exposure is identical to that shown in Fig. 2.4b. After exposure to water vapor, the band at 1630 cm^{-1} sharpens due to water adsorption onto the Brønsted acid sites.⁵³ The band centered at 1860 cm^{-1} loses intensity; however, the band at 1810 cm^{-1} is unaffected. Similar results have been reported by Mandal et al., who found that increasing the concentration of water in the feed preferentially reduces the intensity of the 1860 cm^{-1} band compared to the 1810 cm^{-1} band.²⁰ The loss in intensity of the band at 1860 cm^{-1} during water adsorption and the lack of NO desorption at low temperatures suggests that a portion of the adsorbed NO contributing to the band at 1860 cm^{-1} also contributes to low-temperature NO desorption. The band at 1860 cm^{-1} does not disappear completely, suggesting that it may comprise multiples forms of adsorbed NO associated with Pd cations, as will be discussed below. The absence of an effect of water exposure on the band at 1810 cm^{-1} suggests that the NO-Pd species contributing to this band and the part of the 1860 cm^{-1} band unaffected by water vapor account for the NO desorption observed above 500 K.

Fig. 2.6b also shows the IR spectra of adsorbed NO taken during TPD following the exposure of adsorbed NO to water vapor. The band for water adsorbed on the zeolite disappears completely, as soon as the temperature increases above 373 K. The bands remaining at 1860 cm^{-1} and 1810 cm^{-1} follow a pattern very similar to that shown in Fig. 2.4b. With increasing temperature, the band at 1810 cm^{-1} decreases first and loses intensity before the band at 1860 cm^{-1} loses intensity. All IR bands disappear by 773 K.

2.4.4 Effect of O_2 on the adsorption of NO on Pd/H-CHA

Since air is present in automobile exhaust gas, it is important to determine how air affects the adsorption of NO on Pd/H-CHA. For these experiments, NO was adsorbed on Pd/H-CHA from flowing air stream using the same protocol described above for the adsorption of NO on H-CHA. The results of these experiments are shown in Fig. 2.7.

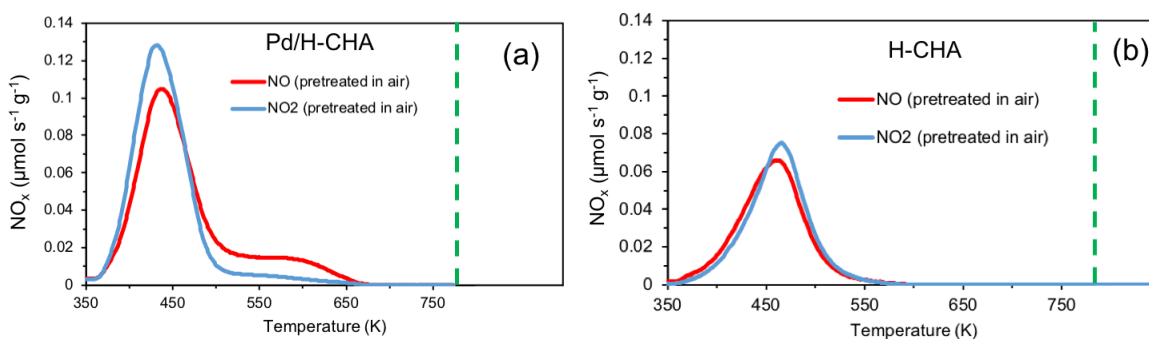


Figure 2.7: Comparison of NO and NO₂ TPD profiles for NO adsorbed from air on Pd/H-CHA (a) and for NO adsorbed from air on H-CHA (b) Pd/H-CHA was heated in air and 5% H₂O from 348 K to 773 K at 2 K/min and then held at 773 K for 5 h. H-CHA was heated in air from 348 K to 773 K at 2 K/min and then held at 773 K for 1 h. Following initial heating, both samples were cooled in air from 773 K to 348 K. Adsorption was from a flow of air (250 mL/min) containing 200 ppm of NO at 348 K. During TPD, the temperature was ramped from 348 K to 773 K at 10 K/min and then held at 773 K for 20 min in air. The dashed line corresponds to the maximum temperature of 773 K; the TPD profile beyond this line represents the continued temporal evolution of the system at constant temperature.

When NO is adsorbed from air, the TPD profile shows prominent peaks for NO and NO₂ centered at about 450 K. A smaller, broad feature is also observed for both species centered at

about 575 K, but a large peak centered at 750 K is not observed, as otherwise appears in the TPD profile of NO adsorbed from He (Fig. 2.4b). The total amount of NO desorbing as either NO or NO₂ is 99 μmol/g of adsorbent, which is 1.7 times larger than that for NO adsorbed on Pd/H-CHA from He. Also plotted for comparison is the TPD profile for NO adsorbed from air taken for H-CHA (see Fig. 2.3). While the shape and position of the low-temperature features for NO and NO₂ are similar for Pd/H-CHA and H-CHA, the amounts desorbed at low temperatures for Pd/H-CHA are smaller. As noted earlier, the amounts of NO and NO₂ desorbed from H-CHA are 31 μmol per gram of adsorbent and 32 μmol per gram of adsorbent, respectively. This comparison suggests that roughly one third of the NO/NO₂ desorbing from Pd/H-CHA may be due to NO/NO₂ adsorption on the zeolite.

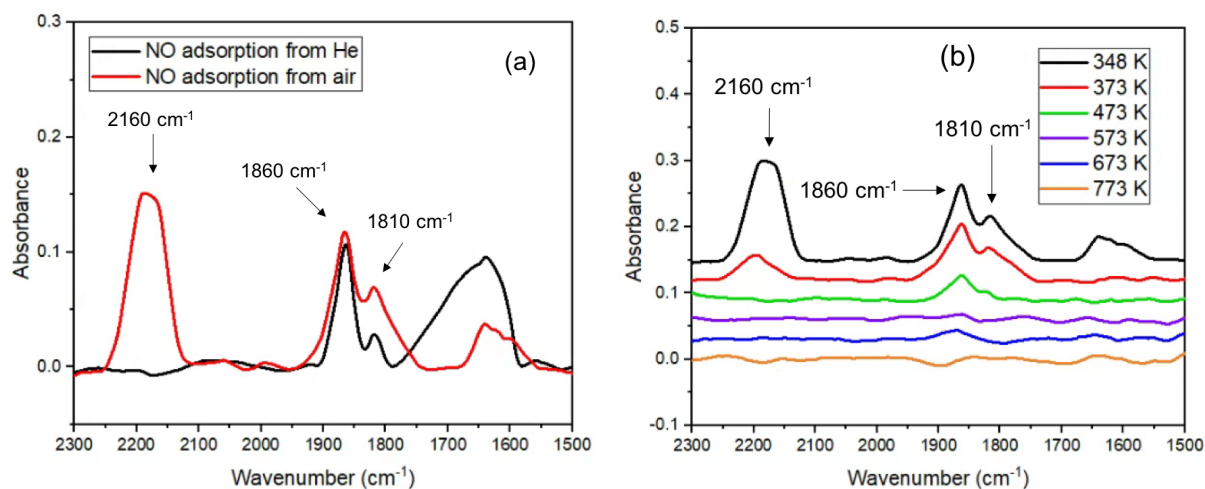


Figure 2.8: (a) IR spectra of NO adsorbed from He or air on Pd/H-CHA. For the case of NO adsorption from He, Pd/H-CHA was heated in air and 5% H₂O from 348 K to 773 K at 2 K/min and held at 773 K for 5 h. In 8a, for the NO adsorption from He, the sample was cooled in He and 5% H₂O from 773 K to 348 K. For the NO adsorption from air, the sample was cooled in air from 773 K to 348 K. Adsorption occurred at 348 K from a flow (250 mL/min) containing 200 ppm NO in He or air. A reference spectrum was taken of Pd/H-CHA before NO adsorption and then subtracted from the spectrum taken after NO adsorption. (b) TPD IR spectra taken during heating at a rate of 2.5 K/min in flowing air (250 mL/min).

An IR spectrum of NO adsorbed on Pd/H-CHA from air is shown in Fig. 2.8a and the same IR bands are present as were observed in the spectrum for NO adsorbed from He (Fig. 2.4b), except that the band at 2160 cm⁻¹ is now significantly more intense. There is a small broad band around 1630 cm⁻¹, attributable to water produced during the formation of NO⁺Z⁻ and to nitrates formed via the reaction of NO with O₂ during NO adsorption.^{23,53,79,80} We also note that the appearance of this band is accompanied by a loss in Brønsted acidic O-H intensity upon NO adsorption. These features are similar to those seen in Fig. 2.3 for the adsorption of NO from air on H-CHA. Fig. 2.8a also shows an apparent increase in the intensity of band at 1810 cm⁻¹ relative to that observed for the case of NO adsorption from He. The increase is designated as apparent because a new, broad band appears beneath the feature at 1810 cm⁻¹, which on the low-wavenumber side extends to 1750 cm⁻¹. The identity of this band is not known. Fig. 2.8b shows the TPD IR spectra taken during NO desorption from Pd/H-CHA in flowing air. As seen in the TPD IR spectrum for H-CHA (Fig. 2.2), the 2160 cm⁻¹ band disappears by about 473 K, as does the broad feature at 1650 cm⁻¹ attributed to adsorbed water (which is likely associated with NO⁺ formation).⁵³ The two bands at 1860 cm⁻¹ and 1810 cm⁻¹ attenuate in a different manner compared to that seen in the IR TPD spectra shown in Fig. 2.4b for NO adsorbed onto Pd/H-CHA from He. Both the band centered at

1810 cm^{-1} and the one centered at 1860 cm^{-1} band disappear by around 573 K. This is consistent with the TPD results but differs from the experiment in which NO is adsorbed from He; there, the band at 1860 cm^{-1} does not disappear until higher temperatures. The observed effect of O_2 on the adsorption of NO on the zeolite as NO^+ cations is very similar to that reported by Hadjiivanov et al. for ZSM-5.⁵³ The authors of this study propose that O_2 enhances the formation of NO^+ via the reaction $2 \text{H}^+\text{Z}^- + 2 \text{NO} + 0.5 \text{O}_2 \rightarrow 2 \text{NO}^+ \text{Z}^- + \text{H}_2\text{O}$. An assessment of this possibility and alternatives are discussed below.

2.5 Theoretical Interpretation

2.5.1 NO adsorption in Pd/H-CHA

To elucidate which forms of adsorbed NO contribute to the low-temperature and high-temperature features observed in the TPD experiments (see Fig. 2.4b), as well as the different bands observed in the transmission IR experiments, theoretical calculations of NO adsorption on a variety of Pd^+ and Pd^{2+} sites, that can be expected to be present in Pd/H-CHA after the pretreatment in wet air ($T = 773 \text{ K}$ and $P_{\text{H}_2\text{O}} = 5 \text{ kPa}$), were conducted. In a recent theoretical study, it was shown that in the presence of air and water, Pd dispersed as Pd^+ and Pd^{2+} cations is thermodynamically most favorable at Al pairs in the 6-rings and 8-rings in CHA.¹⁹ The speciation of Pd was found to be more sensitive to the partial pressure of water than that of oxygen. Additionally, the preference for Pd^+ or Pd^{2+} was found to depend strongly on the precise configuration of the Al pair. These findings are illustrated in the phase diagrams shown in Fig. 2.9. Because the NNNN Al pairs in the 6-ring allow for a near-perfect square planar coordination of the Pd^{2+} cation with four framework oxygen atoms, Pd^{2+} is lower in free energy than the next most favorable species at the NNNN Al pair by $>30 \text{ kJ/mol}$ over a wide range of conditions. Consequently, it can be considered unchangeable throughout repeated adsorption-desorption-regeneration cycles on the Pd/H-CHA samples. By contrast, at NNN Al pairs in the 6-ring or 8-ring, Pd^{2+} and Pd^+/H^+ might be interconverted depending on the temperature and the water partial pressure. Finally, at NNNN and NNNNN Al pairs in the 8-ring, Pd^+/H^+ is more favorable than Pd^{2+} , as the Al atoms in these configurations are too far apart to efficiently stabilize a single divalent cation.

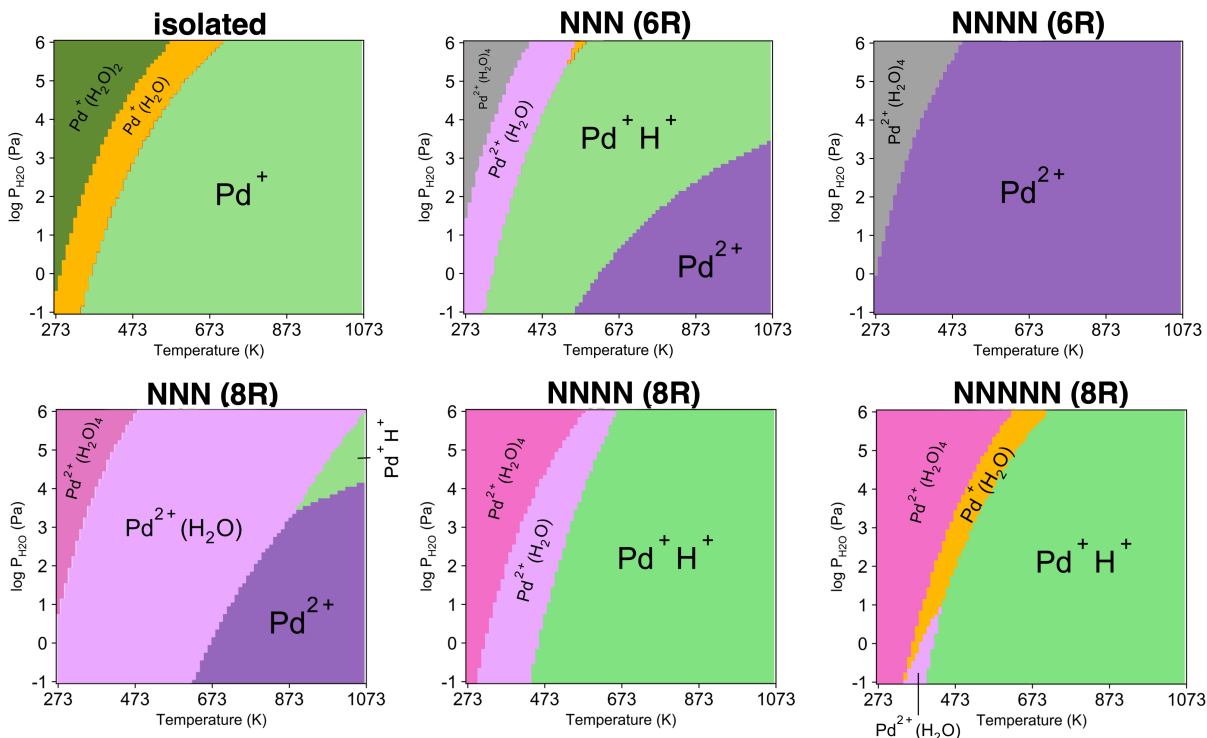
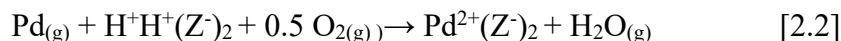
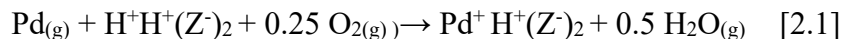


Figure 2.9: $[P_{\text{H}_2\text{O}}, T]$ phase diagrams showing the thermodynamically preferred Pd species at isolated Al and next-nearest neighbor (NNN), next-next-nearest (NNNN) neighbor and next-next-next-nearest neighbor NNNNN) Al pair in the 6- and 8-rings of CHA under flowing air ($P_{\text{O}_2} = 20$ kPa). Reprinted with permission from ref.¹⁹

In this study, we have examined NO adsorption and desorption from the Pd^+ and Pd^{2+} sites predicted by the phase diagrams in Fig. 2.9 to be present at Al pairs in the 6-rings and 8-rings. Additionally, we have considered Pd^+ and Pd^{2+} sites that may be present due to NNN Al pairs in the 4-rings and NNNN Al pairs spanning two or more adjacent rings, identified in a high-throughput study on the stability of Pd cation sites in zeolites by Aljama et al.⁸¹ In these structures, the charge-compensating Pd cations are also located in a nearby 6- or 8-ring, such that they are accessible to adsorbates in the *cha* cage. Table 1 shows for each of the Pd sites considered in this study the formation energy (ΔE_{form}) relative to the Brønsted acid protons at the same Al pair:



For all Al pairs except NNNN Al pairs in the 6-ring, the formation energy of $\text{Pd}^+\text{H}^+(\text{Z}^-)_2$ is more negative than that of $\text{Pd}^{2+}(\text{Z}^-)_2$. For the NNN Al pairs in the 6-ring and the 8-ring, the formation energy of $\text{Pd}^+\text{H}^+(\text{Z}^-)_2$ is lower than that of $\text{Pd}^{2+}\text{Z}^-\text{Z}^-$ by 50 kJ/mol and 30 kJ/mol, respectively. As shown by the phase diagrams in Fig. 2.9, both Pd^+ and Pd^{2+} sites may be present at these Al pairs, depending on the temperature and the partial pressure of water. By contrast, for the NNNN and NNNNN Al pairs in the 8-ring, for which the phase diagrams predict the presence of only Pd^+ sites, the formation energy of $\text{Pd}^+\text{H}^+(\text{Z}^-)_2$ is 165-199 kJ/mol lower than that of $\text{Pd}^{2+}(\text{Z}^-)_2$. Consequently, we can reasonably expect that both Pd^+ and Pd^{2+} sites may occur at the NNN Al pairs in the 4-ring and the NNNN Al pairs in adjacent rings for which the formation energy of

$\text{Pd}^{2+}(\text{Z}^-)_2$ is at most 50 kJ/mol higher than that of $\text{Pd}^+\text{H}^+(\text{Z}^-)_2$. A schematic representation of the various Al pairs is included in the Supplemental Material (Fig. S2.5).

Table 2.1: Formation energies (ΔE_{form}) in kJ/mol for Pd^+ and Pd^{2+} sites relative to the Brønsted acid protons at the same Al pair reported in ref. [19] (†) and ref. [81] (‡).

	$\text{Pd}^+ \text{H}^+(\text{Z}^-)_2$	$\text{Pd}^{2+}(\text{Z}^-)_2$
6-ring [†]		
NNN	-266	-215
NNNN	-245	-303
8-ring [†]		
NNN	-220	-181
NNNN	-238	-74
NNNNN	-237	-38
4-ring [‡]		
NNN-1	-250	-154
NNN-2	-256	-233
other [‡]		
NNNN-1	-280	-270
NNNN-2	-284	-243
NNNN-3	-286	-263
NNNN-4	-271	-130
NNNN-5	-284	-143

To elucidate which NO adsorption modes contribute to the low-temperature and high-temperature features observed in the TPD experiments (see above, Fig. 2.4b), we have combined NO adsorption free energies ($\Delta G_{\text{ads,NO}}$) predicted by QM/MM for each of the potential sites with an equilibrium desorption model to estimate the temperature at which the desorption of NO reaches a maximum (T_{max}). Details on the calculation of the maximum desorption temperatures as well as XYZ coordinates of the optimized geometries of all NO adsorption complexes are included in the Supplemental Material (Section 2.8.7 and 2.8.10). To aid in the assignment of the bands observed in the transmission IR experiments, we also examined the NO stretching frequency in each of the

model complexes. To mitigate systematic errors in DFT-predicted stretching frequencies caused by both the harmonic approximation as well as the specific functional employed for the electronic structure calculations, we have shifted the calculated NO stretching frequencies ($\nu_{\text{NO,DFT}}$) by adding the difference between the frequency for gas phase NO evaluated at the same level of theory (2097 cm^{-1}) and the experimental value reported by NIST (1876 cm^{-1}).⁵³ The resulting values ($\nu_{\text{NO,est}}$) are then directly comparable with the spectra obtained in the transmission IR experiments. This comparison is shown in Fig. 2.10, which juxtaposes our theoretical estimates for the maximum desorption temperatures (T_{max}) and NO stretching frequencies ($\nu_{\text{NO,est}}$) with the results of the IR-TPD experiments discussed in Section 2.4.2. Numerical values of the maximum desorption temperatures and calculated stretching frequencies are listed in Table S2.4 in the Supplemental Material. The results presented in Fig. 2.10 show that the TPD desorption feature centered at 430 K is due exclusively to NO adsorbed on Pd^{2+} cations at NNN Al pairs in the 6-rings. The vibrational frequency associated with this form of NO is predicted to be in the region of 1860 cm^{-1} . By contrast, the high-temperature NO desorption feature is due to NO adsorbed on Pd^+ cations in a variety of environments. Between 550 and 750 K, NO will desorb from Pd^+ cations at the NNN Al pairs in the 6-rings and the NNNNN Al pairs in the 8-rings. As a result, a decrease in IR intensity is expected in the range of the lower-frequency band (i.e., 1810 cm^{-1}). Finally, above 750 K, NO will desorb from Pd^+ cations at NNN Al pairs in the 8-rings, resulting in the disappearance of the IR feature around 1860 cm^{-1} . Pd^{2+} cations at NNN Al pairs in the 8-rings might also provide very strong NO binding sites that contribute to both the high-temperature TPD feature and the 1860 cm^{-1} IR band.

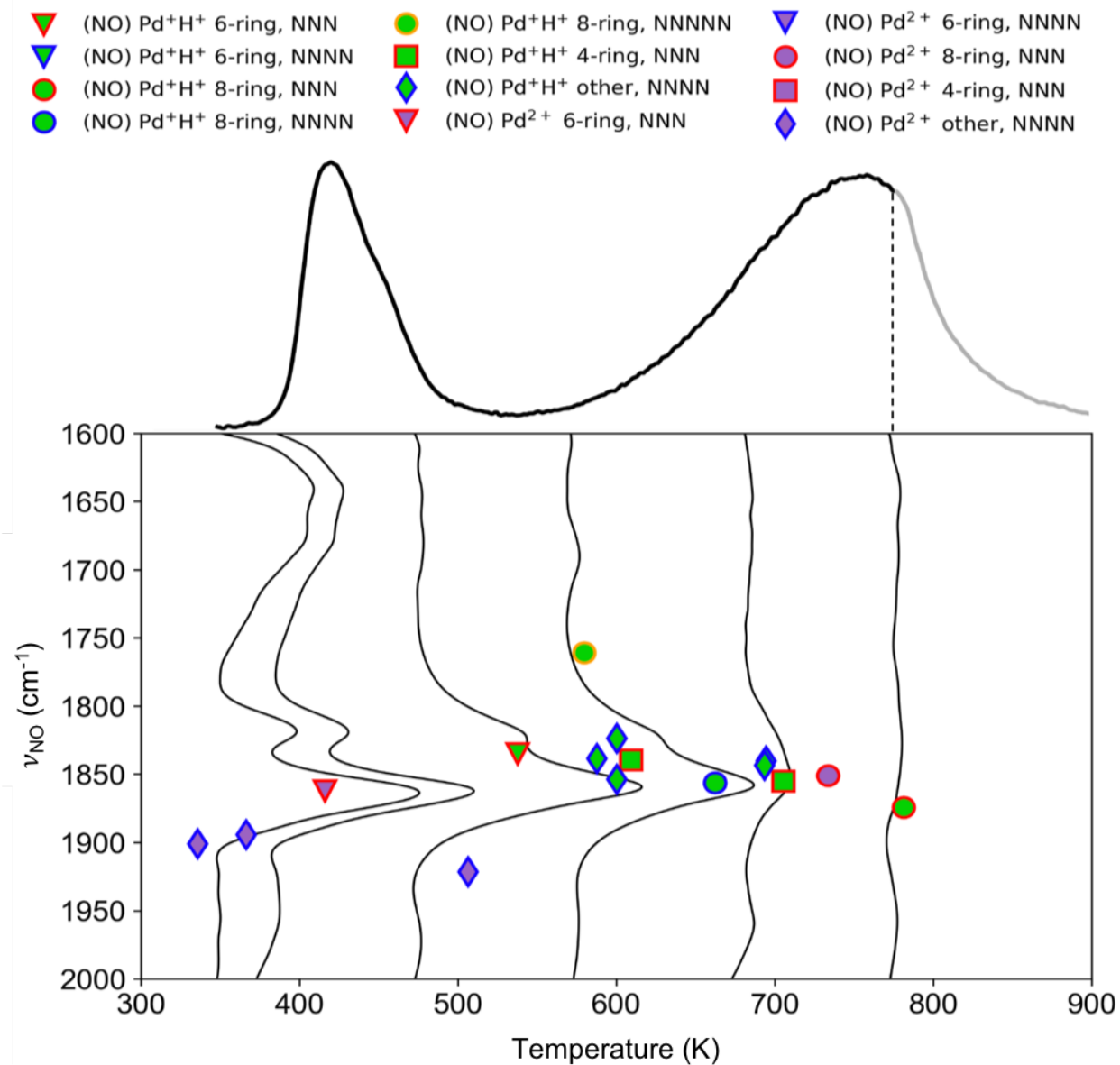


Figure 2.10: Theoretical estimates of IR stretching frequencies for NO ($\Delta_{\text{NO, est}}$) adsorbed on Pd⁺ and Pd²⁺ sites in Pd/H-CHA vs. calculated temperatures of maximum desorption (T_{max}) from the respective sites. Experimental IR spectra collected at 348K, 373K, 473K, 573K, 673K and 773K are shown as solid black lines. The corresponding TPD profile is shown above the graph. During TPD, the temperature was ramped from 348 K to 773 K at 10 K/min and then held at 773 K for 20 min in He. The dashed line corresponds to the maximum temperature of 773 K; the TPD profile beyond this line represents the continued temporal evolution of the system at constant temperature.

Combined, our calculated desorption temperatures and IR stretching frequencies provide an interpretation that is consistent with the experimental observations from both TPD and IR TPD spectra. The main conclusion from this analysis is that the IR stretching frequencies for NO adsorbed on different Pd sites cover a broad frequency range and that NO adsorbed on Pd⁺ and Pd²⁺ contribute to the broad band observed in the region of 1860 cm⁻¹. This finding is consistent with that of Mandal et al.²⁰ who calculated frequencies of 1866 cm⁻¹ and 1853 cm⁻¹ for NO adsorbed on Pd²⁺ and Pd⁺ cations, respectively. They proposed that the band at 1810 cm⁻¹ is likely

due to the presence of NO adsorbed on partially hydrated Pd²⁺ cations.²⁰ However, our experimental conditions are different from those used by Mandal et al. who included both water and oxygen in the NO feed,²⁰ and therefore their interpretation cannot explain our observations. Fig. 2.7 demonstrates that the band at 1810 cm⁻¹ also appears in the IR spectrum when NO is adsorbed in the absence of water, on a Pd/H-CHA sample that was pretreated in dry air. Furthermore, Fig. 2.5 shows that exposure of adsorbed NO to water vapor has no effect on the band at 1810 cm⁻¹, but instead decreases the intensity of the band at 1860 cm⁻¹. We suggest that this lower frequency band is best attributed to NO adsorbed on Pd⁺H⁺ species at NNNN Al pairs in a 6-ring or at NNNNN Al pairs in an 8-ring, which have calculated frequencies of 1800 cm⁻¹ and 1760 cm⁻¹, respectively.

It is also noteworthy that NO adsorption on the thermodynamically most favorable Pd²⁺ species at NNNN Al pairs in the 6-ring appears to be too weak to be relevant. The predicted maximum desorption temperature for these sites (270 K) is well below the temperature of the initial adsorption step (348 K). Nevertheless, it has been suggested that these sites might undergo partial reduction upon NO adsorption via the following reaction²⁶:



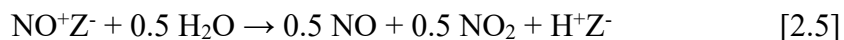
Our calculations show that Reaction 2.3 is strongly exergonic, except for the highly stable Pd²⁺ sites at the NNNN pair in the 6-ring (for T = 348 K, P_{NO} = 20 Pa, ΔG_{rxn} = +26 kJ/mol). However, the experimental results presented here (see Fig. 2.6) show no evidence for the concurrent formation of NO⁺Z⁻ species when NO is adsorbed from He on Pd/H-CHA. Therefore, we conclude that Reaction 2.3 is unlikely to occur. Furthermore, the experimentally observed NO storage capacity of Pd/H-CHA typically approaches a 1:1 ratio, 1 mol NO per mol of atomically dispersed Pd in the sample, indicating a low abundance of the thermodynamically most favorable Pd²⁺ sites at NNNN Al pairs in the 6-ring.

We have also calculated the thermodynamics for forming NO⁺Z⁻ on H-CHA via the reaction



The formation of NO⁺Z⁻ is observed to occur on H-CHA (see Fig. 2.2), as evidenced by the appearance of the IR band at 2160 cm⁻¹ at 348 K and the concurrent consumption of zeolite protons and formation of adsorbed H₂O. Reaction 2.4 is predicted to have a free energy of reaction (ΔG⁰_{rxn}) of -12 kJ/mol for 200 ppm of NO (p_{NO} = 20 Pa) at 348 K, assuming only trace amounts of O₂ and H₂O (p_{O2} = p_{H2O} = 0.1 Pa) are present in the zeolite after the pretreatment. Our calculations predict an NO stretching frequency (ν_{NO,est}) for NO⁺Z⁻ of 2073 cm⁻¹, consistent with the frequency range in which the IR band is observed in the experiments.

We have also considered the possibility that desorption occurs via the reaction



Reaction 2.5 would explain how NO and NO₂ are formed in equivalent quantities, as can be seen in Fig. 2.3. Assuming only trace amounts of NO and NO₂ are present in the gas phase (p_{NO} = p_{NO2} = 0.1 Pa) at 348 K, ΔG⁰_{rxn} = -28 kJ/mol if the water consumed in the desorption of NO⁺Z⁻

was retained on a Brønsted site, and $\Delta G_{\text{rxn}}^0 = -18$ kJ/mol if trace amounts of gas phase water ($p_{\text{H}_2\text{O}} = 0.1$ Pa) are consumed instead. The results of our thermodynamic calculations for reactions 4 and 5 suggest that during the TPD, NO^+Z^- is much more likely to desorb via reaction 5 than the reverse of reaction 4, consistent with the observation of significant amounts of NO_2 desorbing concurrently with NO .

2.5.2 Effect of water on NO adsorption on Pd^+ and Pd^{2+} sites

To rationalize the effect of water vapor on NO adsorbed on $\text{Pd}/\text{H-CHA}$, we compare adsorption free energies for NO and water under typical conditions (200 ppm NO , 5% water, 348 K). These values are listed in Table 2.2 for a selection of Pd^+ and Pd^{2+} sites. We find that water adsorbs more than NO on Pd^{2+} sites, but weakly on Pd^+ sites. Therefore, a purge with He-containing water vapor after the NO adsorption step, as described in Section 2.4.3, is expected to displace NO from Pd^{2+} sites, but not from Pd^+ sites. Our previous assignment of Pd^{2+} and Pd^+ sites to the low-temperature and high-temperature TPD peaks, respectively, is therefore in agreement with the experimental observation that the low-temperature feature is missing in the TPD profile obtained after a wet purge. Similarly, the observation that the 1810 cm^{-1} feature in the IR spectrum is unaffected by the purge with He containing water vapor while the 1860 cm^{-1} feature is somewhat diminished in intensity agrees with our theoretical interpretation that the former is due to NO on Pd^+ sites while the latter is due to a combination of NO on weak-binding Pd^{2+} and strong-binding Pd^+ sites.

Table 2.2: Adsorption free energies (ΔG_{ads}) in kJ/mol for 200 ppm NO ($P_{\text{NO}} = 20$ Pa) and 5% water ($P_{\text{H}_2\text{O}} = 5$ kPa) at 348.15 K on Pd^{2+} sites at NNN Al pairs, Pd^+ and Pd^{2+} sites at NNN Al pairs in the 6-ring and 8-ring and Brønsted acid sites in CHA.

	$\Delta G_{\text{ads, NO}}$	$\Delta G_{\text{ads, H}_2\text{O}}$
$\text{Pd}^+ \text{H}^+(\text{Z}^-)_2$		
NNN (6R)	-31	-8
NNNN (6R)	-40	-4
NNN (8R)	-79	-55
NNNN (8R)	-59	-34
NNNNN (8R)	-41	-44
$\text{Pd}^{2+}(\text{Z}^-)_2$		
NNN (6R)	-9	-35
NNNN (6R)	+14	+33
NNN (8R)	-62	-113

2.5.3 Effects of O₂ on the adsorption of NO on Pd⁺ and Pd²⁺ sites

As discussed in Section 2.4.4, when NO is adsorbed from air, the TPD profile exhibits strong peaks for NO and NO₂ centered at about 450K and smaller, broader features around 575 K, but no high-temperature peak around 750 K. Using our theoretical analysis, in Section 2.5.1, we have attributed the low-temperature features to NO adsorbed on Pd²⁺ sites and the high-temperature features to NO adsorbed on Pd⁺ sites. Therefore, the experimental observations suggest that NO storage on Pd²⁺ sites increases, while NO storage on Pd⁺ sites decreases upon adsorption from air. This interpretation appears to be consistent with the phase diagrams shown in Fig. 2.9. These phase diagrams show that for NNN pairs in the 6-rings and 8-rings, Pd⁺ sites could be converted to Pd²⁺ sites under oxidizing conditions, with Pd²⁺ becoming more favorable relative to Pd⁺ at lower partial pressures of water. As argued above, the same is likely to be true for Al pairs in the 4-rings and those spanning adjacent rings for which the formation energy of Pd²⁺ is less than 50 kJ/mol higher than that of the corresponding Pd⁺ site at the same Al pair. Consequently, exposing Pd/H-CHA to air could result in an increased abundance of Pd²⁺ sites with maximum desorption temperatures below 500 K, formed by re-oxidation of Pd⁺ sites with maximum desorption temperatures between 500 and 750 K. As illustrated in Fig. 2.11, this change in the Pd speciation is consistent with the observed shift in the TPD profiles when NO is adsorbed from air instead of from He. Finally, Table S2.4 in the SI shows that the IR signatures of NO adsorbed on the Pd⁺ sites that are lost in the re-oxidation process and those of NO adsorbed on the corresponding Pd²⁺ sites fall within the range of the broad band at 1860 cm⁻¹, such that this interconversion of Pd sites may not be evident in the IR spectra.

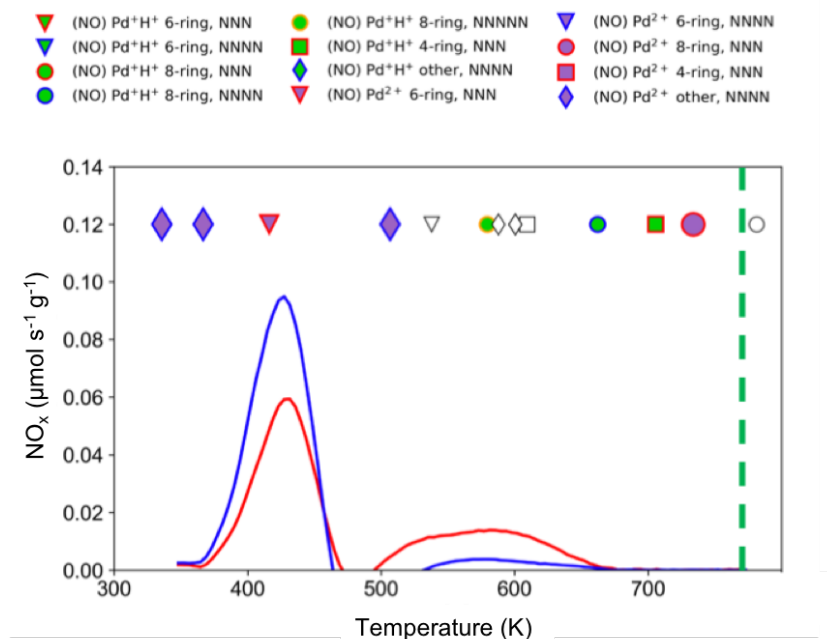


Figure 2.1: Calculated temperatures of maximum desorption (T_{\max}) from Pd^+ and Pd^{2+} sites in Pd/H-CHA vs. corresponding experimental desorption profiles for NO (blue) and NO_2 (red) after NO adsorption from air. The blue and red curves in this graph represent the difference between the TPD profiles on Pd/H-CHA and H-CHA (see Figures 7a and 7b) in order to isolate NO adsorption associated with the Pd sites. The dashed line corresponds to the maximum temperature of 773 K; the TPD profile beyond this line represents the continued temporal evolution of the system at constant temperature. The Pd^+ sites that may be re-oxidized to Pd^{2+} sites by air exposure are represented by open symbols with black outlines. The corresponding Pd^{2+} sites at the same Al pairs, which may become more abundant by the oxidation of these Pd^+ sites, are represented by enlarged symbols.

2.6 Conclusions

In this study, we have investigated the adsorption of NO on H-CHA and Pd/H-CHA, and the effects of H_2O and O_2 on this process. NO adsorption on H-CHA involves a small percentage ($\sim 7\%$) of the Brønsted sites on the zeolite support and is characterized by an IR feature around 2160 cm^{-1} , and NO storage on the zeolite support is enhanced by the presence of O_2 and inhibited by the presence of water. Theoretical calculations of free energies support the interpretation of this adsorbed species as NO^+Z^- and its formation being thermodynamically favorable. During TPD, this species can react with small amounts of adsorbed or free water to form NO and NO_2 in comparable amounts resulting in peaks centered at about 450 K. TPD profiles for NO adsorbed on Pd-CHA show two distinct desorption features, a low-temperature peak between 423 and 473 K and a broad high-temperature feature between 553 and 853 K which has a maximum at about 753 K. IR spectra of NO adsorbed on Pd/H-CHA exhibit two characteristic bands, around 1860 and 1810 cm^{-1} . The low-temperature desorption feature is eliminated in the presence of water, while the high-temperature feature is unaffected, while the opposite behavior is observed when NO is adsorbed in the presence of O_2 . DFT calculations were used to determine the Gibbs free energies for NO adsorption on Pd^+ and Pd^{2+} cations in different environments and the corresponding NO stretching frequencies. We find that NO generally binds more strongly on Pd^+ sites than on

Pd^{2+} sites, suggesting that the former are responsible for the high-temperature desorption peak observed in the TPD experiments, while the latter contribute to the low-temperature feature. Calculated NO stretching frequencies reveal that the IR feature at 1810 cm^{-1} is due to NO adsorption on Pd^+ sites with intermediate binding strength and a maximum-desorption temperature of about 550 K. The 1860 cm^{-1} feature contains contributions from both weakly-bound NO on Pd^{2+} sites desorbing below 500 K, and NO bound on Pd^+ sites in different environments with peak desorption temperatures between 550 and 800 K. These findings show that the experimentally observed TPD and IR features cannot be assigned unambiguously to specific NO-Pd adsorption complexes. Taken in combination, the calculated desorption temperatures and IR stretching frequencies for NO adsorbed on Pd cations in different environments provide an interpretation that is consistent with the experimental observations from both TPD and IR spectroscopy. Our calculations also show that water can displace NO from Pd^{2+} sites, but not from Pd^+ sites, corroborating the experimentally observed changes in the TPD and IR spectra upon exposure to water. These findings further support our interpretation of the underlying modes of NO adsorption.

2.7 Acknowledgements

This material is based upon work supported by the U.S. Department of Energy's Office of Energy Efficiency and Renewable Energy (EERE) under the Vehicle Technologies Program Award Number DE-EE0008213. The presented theoretical work was conducted by Dr. Jeroen Van der Mynsbrugge. Additional support for computational modeling for JvDM, MHG and ATB was provided through the the U.S. Department of Energy, Office of Science, Office of Advanced Scientific Computing Research and Office of Basic Energy Sciences, Scientific Discovery through Advanced Computing (SciDAC) program. Computational resources were provided by UC Berkeley's Molecular Graphics and Computation Facility (supported by NIH S10OD023532). We also acknowledge useful discussions with our collaborators on this project at the University of Kentucky, Oak Ridge National Laboratory, Ford Motor Co., and BASF Chemical Company.

2.8 Supporting Information

2.8.1 X-ray diffraction

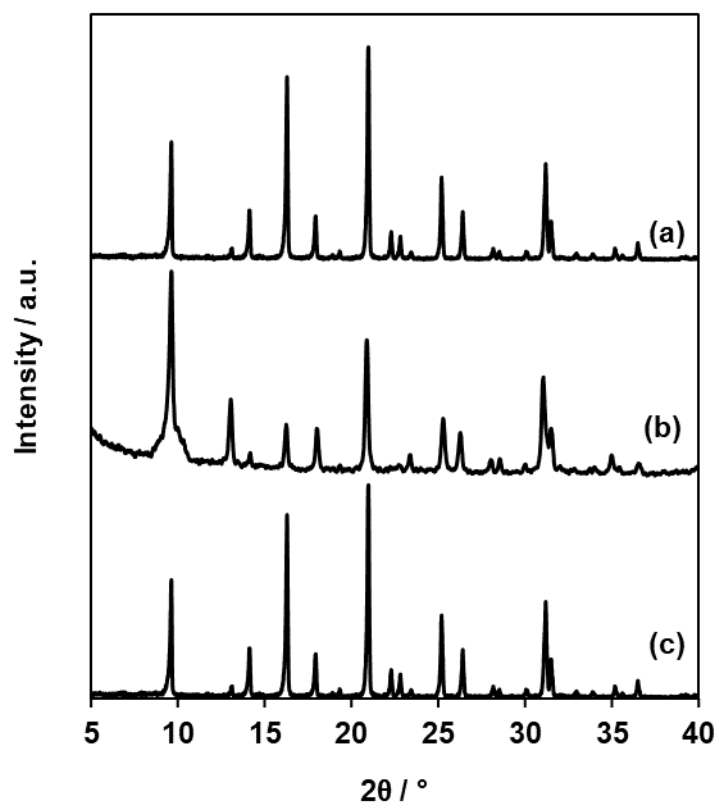


Figure S2.1: Ex-situ X-ray diffraction patterns of a (a) reference purely siliceous CHA, (b) H-CHA (Si/Al = 12), and (c) H-CHA (Si/Al = 14).

2.8.2 Synthesis of H-CHA and Pd/H-CHA

The CHA zeolite (Si/Al = 12) was provided by BASF. The CHA zeolite (Si/Al = 14) was synthesized hydrothermally using a molar synthesis ratio of 1 SiO₂/0.0667Al/0.25TMAOH/0.25Na/44H₂O.⁸² Trimethyladamantylammonium hydroxide (25 wt%, Sachem) and de-ionized water (18 MΩ) were mixed under ambient conditions in a perfluoroalkoxy alkane container (Saville Corporation) with a magnetic Teflon stir bar for 0.25 h. Next, aluminum hydroxide (98 wt%, SPI Pharma) and sodium hydroxide pellets (98 wt%, Alfa Aesar) were added to the mixture. Once homogenized, Ludox-HS-40 (40 wt%, Sigma Aldrich) was added, and the final synthesis solution was stirred for 2 h. The synthesis gel was transferred to Teflon-lined, stainless steel metal autoclaves (Parr Instruments), sealed under autogenous pressure, and placed in a convection oven at 433 K. The synthesis was quenched every other day, then vigorously stirred with a Teflon stir rod before re-sealing and returning to the oven. After 7 days, the solids were recovered with centrifugation and washed (30 mL per g-solid) a total of seven times, alternating between water (18.2 MΩ) and acetone (99.9 wt%, Sigma Aldrich) and ending with a water wash. The solid zeolites were dried in a static oven at 373 K before characterizing the topology with X-ray diffraction (SI Fig. S2.1). The CHA zeolites were treated in flowing air (Air Zero, Indiana Oxygen, 6,000 cm³ h⁻¹ g⁻¹) to 853 K (60 K h⁻¹, 10 h) to combust occluded organic compounds from synthesis, and XRD was performed again to ensure no crystalline degradation occurred (SI Fig. S2.1). The resultant Na-form CHA zeolite was contacted with 1 M NH₄NO₃ at a ratio of 150 g-solution per g-solid for 24 h under ambient conditions. The solids were recovered by centrifugation, washed four times (30 mL per g-solid) with de-ionized water (18.2 MΩ), and dried in a static oven at 373 K, resulting in the NH₄-form zeolite.

Table S2.1: Table comparing the characteristics of the Pd/H-CHA samples analyzed in this paper and supplemental material. Note that the main manuscript only examines Pd/H-CHA (Si/Al = 12). Percentage of isolated Pd was determined by temperature programmed reduction (TPR) in H₂: the Pd/H-CHA samples were pretreated in air to 773 K prior to TPR.¹

Sample Name	Si/Al	Pd weight %	Isolated Pd %
Pd/H-CHA (Si/Al = 14)	14	0.68	79
Pd/H-CHA (Si/Al = 12)	12	0.83	30

2.8.3 Effect of water on NO adsorption on H-CHA

The effect of water on the H-CHA (Si/Al = 12) sample was also investigated. Fig. S2.2 shows the TPD profile after exposing a H-CHA sample saturated with NO to 1% H₂O. All of the NO was displaced and only a small amount of NO₂ was observed. This matches previously reported results for adsorbed NO species being displaced by water.⁴³

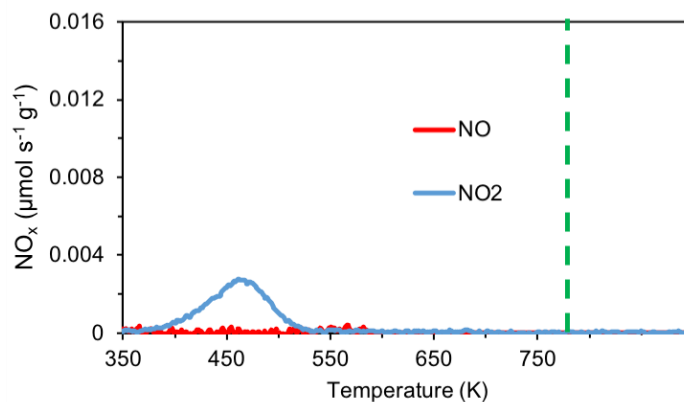


Figure S2.2: Effects of water vapor on the NO TPD. H-CHA (Si/Al = 12) was heated from in air 348 K to 773 K at 2 K/min and held at 773 K for 1 h. The sample was then cooled in air from 773 K to 348 K. H-CHA adsorption was from a flow of He (250 mL/min) containing 200 ppm of NO at 348 K. After saturating with NO, the flow of NO in He was stopped and replaced by He flow constraining 5% H₂O. During TPD, the temperature was ramped from 348 K to 773 K at 10 K/min. It was then held at 773 K for 20 min. The dashed line corresponds to 773 K; beyond this line, the temperature was held at 773 K for 20 min.

2.8.4 Effect of water in pretreatment on Pd/H-CHA

Previous studies have noted the importance of water vapor on the activation of Pd/H-CHA for NO adsorption.¹⁵ To develop a better understanding of the presence of water vapor during the pretreatment, the regenerative step between adsorption cycles, was investigated. After TPD, the sample sits at 773 K and needs to be cooled down to 348 K for the next cycle. The gas composition flowed during this cooling period was varied to see the effect on NO adsorption. The pretreatment was found to be important for regenerating the adsorption sites on the adsorbent. There were three different pretreatment feed gas compositions explored: (1) He and 5% H₂O, (2) He, and (3) air. These compositions were chosen to explore the importance of O₂ and H₂O in regenerating adsorption sites. Note that these experiments were conducted on a different sample of Pd/H-CHA: the one in the paper will be called Pd/H-CHA (Si/Al = 12, isolated Pd % = 79) and the sample for this pretreatment study will be called Pd/H-CHA (Si/Al = 14, isolated Pd % = 30).

Table S2.2: Table comparing the NO/Pd ratios resulting from applying different pretreatments (cooling from 773 K to 348 K) to Pd/H-CHA (Si/Al = 14) adsorbent before adsorption and TPD.

Pretreatment	NO/Pd Desorption	NO _x /Pd Desorption
He and H ₂ O	0.50	0.50
He	0.67	1.01
Air	0.56	0.77

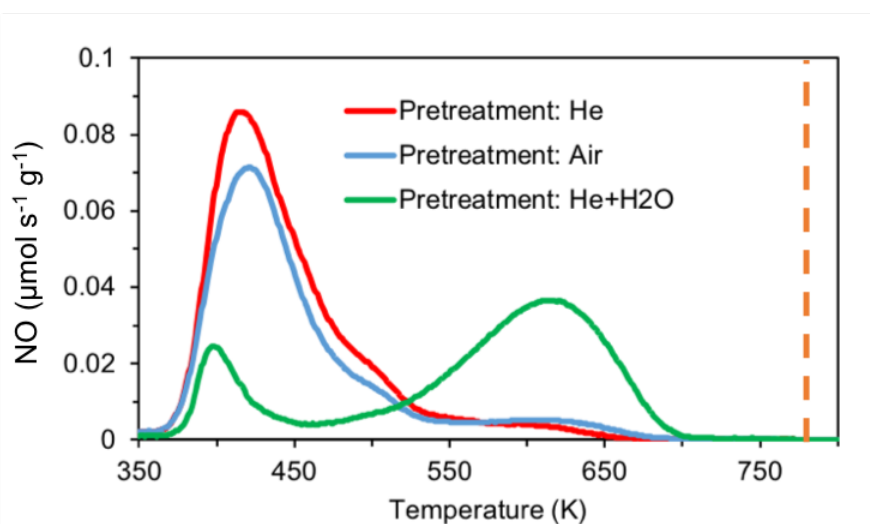


Figure S2.3: Desorption curves that result from the different pretreatment conditions on Pd/H-CHA (Si/Al = 14). Pd/H-CHA was heated in air and 5% H₂O from 348 K to 773 K at 2 K/min and held at 773 K for 5 h. The sample was cooled in He and 5% H₂O from 773 K to 348 K. These TPD profiles result from flowing about 200 ppm of NO with CH₄ tracer in He or air at a flow rate of about 250 mL/min. Adsorption occurred at 348 K. During TPD, the temperature is ramped from 348 K to 773 K at 10 K/min. It was then held at 773 K for 20 min. The dashed line corresponds to 773 K; beyond this line, the temperature was held at 773 K. Each pretreatment condition was performed on the same sample of Pd/H-CHA (Si/Al = 14).

Fig. S2.3 compares the results of the TPD of NO after various pretreatments. Notably, the presence of H₂O is the only reactant that will lead to NO desorption at high temperatures. When

the adsorbent is treated with H₂O in the pretreatment, it desorbs NO at two temperatures, around 400 K and 623 K. In the absence of water, there is significantly more NO desorbed at low temperatures: this matches previous evidence that water will block zeolite sites that will desorb NO at lower temperatures. In addition to more NO, the He and air pretreatments also result in significantly more NO₂ desorption that is not observed in the water pretreatment. It is likely that the NO₂ is produced as a result of forming N_xO_y adsorbed complexes.⁵³ However, without water, there are no NO species that desorb at higher temperatures, which is the goal of using Pd/H-CHA as a PNA material. Despite the lower NO/Pd, water was present in all pretreatments for the experiments conducted in this paper in order to ensure the stability of adsorbed NO species to higher temperatures.

2.8.5 Effect of increasing ion-exchanged Pd on NO adsorption

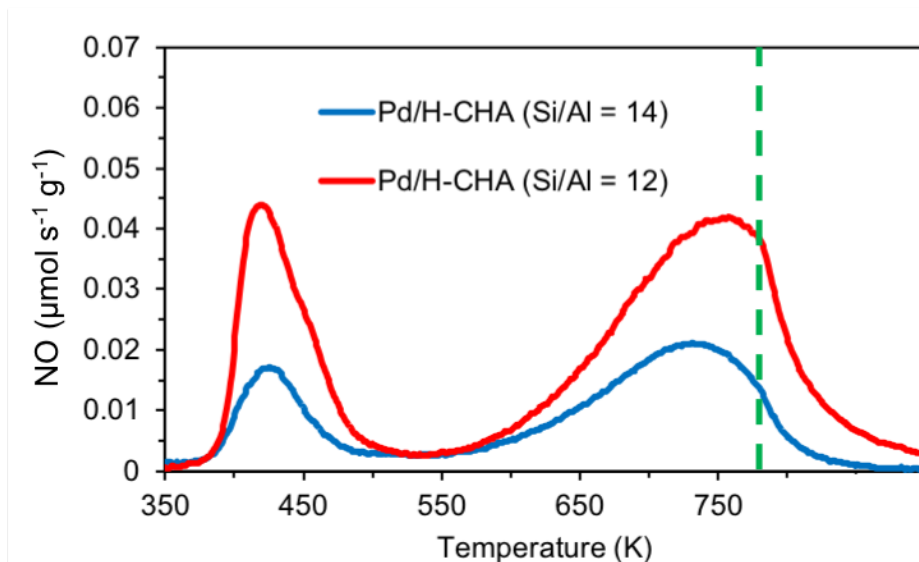


Figure S2.4: The TPD profiles for NO desorption from Pd/H-CHA (Si/Al = 12) and Pd/H-CHA (Si/Al = 14). The peak concentration values were adjusted for the weight of CHA zeolite. Both Pd/H-CHA samples were heated in air and 5% H₂O from 348 K to 773 K at 2 K/min and held at 773 K for 5 h. The samples were then cooled in He and 5% H₂O from 773 K to 348 K. About 200 ppm NO, 20% O₂, and CH₄ tracer were flowed in a He at a flow rate of about 250 mL/min. Adsorption occurred at 348 K. During TPD, the temperature was ramped from 348 K to 773 K at 10 K/min. It was then held at 773 K for 20 min. The dashed line corresponds to 773 K; beyond this line, the temperature was held at 773 K.

Fig. S2.4 compares the NO TPD profiles for Pd/H-CHA (Si/Al = 12) and Pd/H-CHA (Si/Al = 14). The shapes of the TPD profiles for both materials are roughly the same but the amount of NO desorbed is significantly higher for Pd/H-CHA (Si/Al = 12) than Pd/H-CHA (Si/Al = 14). The NO/Pd ratio for Pd/H-CHA (Si/Al = 14) is 0.44, whereas that for Pd/H-CHA (Si/Al = 12) is 0.81. The amount of NO adsorbed appears to be essentially one NO per Pd cation. The higher isolated Pd content of Pd/H-CHA (Si/Al = 12) results in a larger amount of NO adsorbed on Pd sites and consistently with more intense NO desorption features at both low and high temperatures.

2.8.6 Details of experiments reported in the manuscript

Table S2.3 summarizes the experimental findings from the manuscript and compares the amounts of NO_x adsorbed, both per Pd atom and per gram of adsorbent.

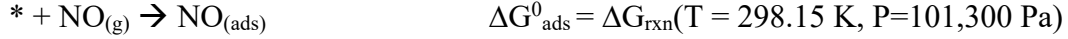
Table S2.3 List of pretreatment conditions, adsorption composition, carrier gas used for TPD, and the amounts of NO adsorbed for different experiments reported in the manuscript. The table is split into two for easier viewing.

Figure	Pretreatment	Adsorption Feed	Second Adsorption	TPD	Adsorbent	NO/Pd
2.2	air	NO in He	N/A	He	H-CHA	N/A
2.3	air	NO in air	N/A	Air	H-CHA	N/A
2.4	He+H ₂ O	NO in He	N/A	He	Pd/H-CHA	0.73
2.5	He+H ₂ O	NO in He	H ₂ O in He	He	Pd/H-CHA	0.67
2.7	Air	NO in air	N/A	Air	Pd/H-CHA	0.62

Figure	NO _x /Pd	NO $\mu\text{mol/g}$ adsorbent	NO _x $\mu\text{mol/g}$ adsorbent	Water present in IR spectrum (Source)	Water introduced?
2.2	N/A	5.4	8.1	Yes (formed by NO adsorption)	No
2.3	N/A	31	63	Yes (formed by NO adsorption)	No
2.4	0.73	57	57	Yes (retained from pretreatment)	Yes
2.5	0.67	52	52	Yes (retained from pretreatment and from exposure of adsorbed NO to water vapor)	Yes
2.7	1.22	52	99	Yes (formed by NO adsorption)	Yes

2.8.7 Calculated peak desorption temperatures

For each Pd⁺ and Pd²⁺ site, the temperature at which the desorption of NO reaches a maximum (T_{max}) was calculated from the adsorption enthalpy (ΔH_{ads}) and free energy (ΔG_{ads}) obtained from the QM/MM calculations:



The corresponding equilibrium coefficient K is given by:

$$K = K^0 \exp\left(-\frac{\Delta H_{ads}^0}{RT}\right)$$

We assume that the relation between NO coverage of a given site, θ, the partial pressure of NO_(g), p, and the equilibrium coefficient, K, can be described by a Langmuir isotherm:

$$\theta = \frac{Kp}{1+Kp} \quad (1)$$

Throughout the TPD experiment, the instantaneous temperature T is defined by the initial temperature T₀ and the heating rate β:

$$T = T_0 + \beta t$$

We can then write the following mass balance, which states that the amount of NO desorbing from the adsorption sites equals the amount of NO captured by the mass spectrometer:

$$-\frac{d\theta}{dt} = -\beta \frac{d\theta}{dT} = \frac{Qp}{RT_{MS}N_s} \quad (2)$$

In equation 2, Q is the flow rate of the sweep gas applied during TPD, p is the partial pressure of NO in the sweep gas, R is the universal gas constant, T_{MS} is the temperature in the mass spectrometer, N_s is the number of adsorption sites.

Combine equations 1 and 2:

$$\frac{Qp}{RT_{MS}N_s} = -\beta \left[\frac{K \frac{dp}{dT} + p \frac{dK}{dT}}{1+Kp} - Kp \frac{K \frac{dp}{dT} + p \frac{dK}{dT}}{(1+Kp)^2} \right] \quad (3)$$

To solve for the temperature, T_{max}, at which the partial pressure of NO, p, reaches its maximum, set $\frac{dp}{dT} = 0$. Because $Kp \ll 1$, equation 3 reduces to

$$\frac{Qp}{RT_{MS}N_s} = -\beta K^0 \exp\left(-\frac{\Delta H_{ads}^0}{RT}\right) \frac{\Delta H_{ads}^0}{RT^2}$$

Such that T_{max} is given by:

$$T_{max} = \frac{-\frac{\Delta H_{ads}^0}{R}}{2W\left(\frac{Qp}{\sqrt{-RT_{MS}N_s\beta K^0\frac{\Delta H_{ads}^0}{R}\left(-\frac{\Delta H_{ads}^0}{2R}\right)}}\right)} \quad (4)$$

T_{max} can be calculated for each of the Pd^+ and Pd^{2+} sites using equation 4: the NO adsorption enthalpy (ΔH_{ads}^0) is obtained from QM/MM. The temperature in the mass spectrometer is room temperature (T_{MS}) is 298.15K. The heating rate applied in the TPD experiments (β) is 10 K/min. The flow rate of the sweep gas (Q) is 250 ml/min. The typical sample size of Pd/H-CHA is 100 mg, containing 1 wt% of Pd. Assuming full atomic dispersion of the Pd, the number of adsorption sites (N_s) is approximated by the number of moles in 1 mg Pd, i.e., 9.3967×10^{-6} mol. The function $W(x)$ in the denominator of equation 4 is known as the Lambert W function.

2.8.8 Al pairs considered in QMMM study

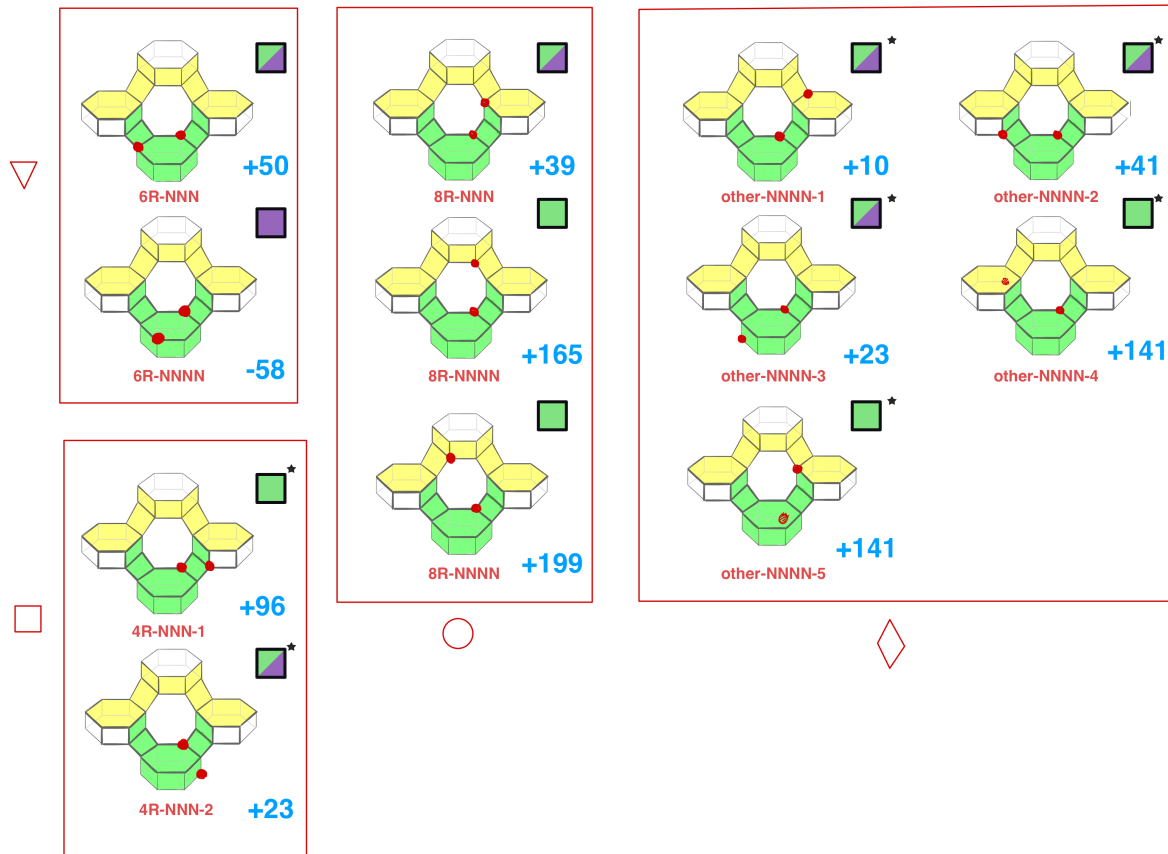


Figure S2.5: Schematic representation of the different NNN, NNNN and NNNNN Al pairs considered in the QMMM study. The difference in formation energy ($\Delta\Delta E_{form}$) in kJ/mol between Pd^{2+} and Pd^+H^+ at each Al pair is shown in blue. Schematic representations of the corresponding $P_{H_2O,T}$ phase diagrams are also

shown (purple square: Pd²⁺ most favorable over entire range of conditions; green square: Pd⁺H⁺ most favorable over entire range of conditions; split green and purple square: Pd²⁺ or Pd⁺H⁺ most favorable, depending on P_{H2O}, T). * = inferred on the basis of $\Delta\Delta E_{\text{form}}$.

2.8.9 Calculated vibrational frequencies for NO adsorbed on Pd⁺ and Pd²⁺ sites

Table S2.4: Calculated maximum desorption temperatures in K and vibrational frequencies in cm⁻¹ for NO adsorbed on Pd⁺ and Pd²⁺ sites in Pd/H-CHA. NO stretching frequencies calculated by QMMM at the $\omega\text{B97X-D/def2-sv(p)}$ level of theory ($\nu_{\text{NO,DFT}}$) are shifted by adding the difference between the frequency for gas phase NO evaluated at the same level of theory (2097 cm⁻¹) and the experimental value reported by NIST (1876 cm⁻¹) to facilitate comparison with experimental IR spectra.

	Pd⁺ H⁺(Z)₂		Pd²⁺(Z)₂	
	T _{max} (K)	$\nu_{\text{NO,est}}$ (cm ⁻¹)	T _{max} (K)	$\nu_{\text{NO,est}}$ (cm ⁻¹)
6-ring				
NNN	538	1835	416	1862
NNNN			270	1888
8-ring				
NNN	781	1874	734	1851
NNNN	662	1856		
NNNNN	580	1761		
4-ring				
NNN-1	705	1855		
NNN-2	609	1840	273	1889
other				
NNNN-1	600	1824	507	1921
NNNN-2	609	1839	336	1901
NNNN-3	600	1854	366	1894
NNNN-4	695	1840		
NNNN -5	694	1844		

2.8.10 XYZ coordinates of optimized structures

See attached ZIP archive. The atoms included in the QM region for each of the complexes are specified in Table S5.

Table S2.5: Atoms included in the QM region for each of the attached XYZ files

filename	QM atoms
6-ring	
pd1-no-6R-NNN.xyz	1-24
pd1-h2o-6R-NNN.xyz	1-25
pd2-no-6R-NNN.xyz	1-23
pd2-no-6R-NNNN.xyz	1-23
pd2-h2o-6R-NNN.xyz	1-24
pd2-h2o-6R-NNNN.xyz	1-24
8-ring	
pd1-no-8R-NNN.xyz	1-28
pd1-no-8R-NNNN.xyz	1-28
pd1-no-8R-NNNNN.xyz	1-28
pd1-h2o-8R-NNN.xyz	1-29
pd1-h2o-8R-NNNN.xyz	1-29
pd1-h2o-8R-NNNNN.xyz	1-29
pd2-no-8R-NNN.xyz	1-27
pd2-h2o-8R-NNN.xyz	1-28
4-ring	
pd1-no-4R-NNN-1.xyz	1, 2, 3, 4, 5, 13, 14, 15, 16, 23, 24, 26, 27, 28, 29, 30, 31, 43, 44, 46, 47, 48, 101, 102, 113, 168, 178, 192, 193, 219, 228, 229, 240, 241, 367, 368, 369, 2185, 2186, 2187, 2188
pd1-no-4R-NNN-2.xyz	1, 2, 3, 4, 5, 6, 7, 8, 10, 11, 12, 13, 14, 15, 16, 17, 18, 20, 22, 24, 26, 27, 28, 30, 31, 32, 33, 38, 39, 40, 42, 44, 46, 47, 49, 50, 54, 57, 58, 61, 154, 201, 202, 203, 206, 268, 269, 291, 292, 293, 2185, 2186, 2187, 2188

pd2-no-4R-NNN-2.xyz 1, 2, 3, 4, 5, 6, 7, 8, 10, 11, 12, 13, 14, 15, 16, 17, 18, 20, 22, 24, 26, 27, 28, 30, 31, 32, 33, 38, 39, 40, 42, 44, 46, 47, 49, 50, 54, 57, 58, 61, 154, 201, 202, 203, 206, 268, 269, 291, 292, 293, 2185, 2186, 2187

other

pd1-no-other-NNNN-1.xyz 1, 2, 3, 4, 5, 6, 7, 8, 10, 11, 12, 13, 14, 15, 16, 17, 18, 20, 22, 24, 26, 27, 28, 30, 31, 33, 38, 39, 42, 44, 46, 47, 50, 57, 58, 61, 152, 153, 154, 201, 268, 269, 270, 271, 444, 509, 525, 591, 609, 697, 735, 853, 912, 925, 967, 987, 1051, 1080, 1214, 1354, 1451, 1463, 1507, 1627, 1874, 1884, 1960, 2185, 2186, 2187, 2188

pd1-no-other-NNNN-2.xyz 1, 2, 3, 4, 5, 13, 14, 15, 16, 24, 25, 26, 27, 28, 30, 31, 44, 45, 46, 47, 228, 229, 230, 231, 234, 235, 236, 237, 238, 239, 240, 241, 367, 368, 369, 370, 371, 378, 379, 519, 2185, 2186, 2187, 2188

pd1-no-other-NNNN-3.xyz 1, 2, 3, 4, 5, 6, 7, 8, 9, 10, 11, 12, 13, 14, 15, 16, 17, 18, 19, 20, 21, 22, 24, 26, 27, 28, 29, 30, 31, 33, 34, 37, 38, 39, 40, 41, 42, 44, 46, 47, 48, 50, 51, 54, 57, 201, 202, 203, 206, 218, 2185, 2186, 2187, 2188

pd1-no-other-NNNN-4.xyz 1, 2, 3, 4, 5, 13, 14, 15, 16, 24, 26, 27, 28, 29, 30, 31, 44, 46, 47, 48, 192, 193, 194, 195, 196, 197, 198, 200, 291, 292, 294, 357, 358, 359, 360, 361, 362, 363, 364, 365, 366, 443, 531, 565, 587, 1590, 1639, 1798, 1962, 2185, 2186, 2187, 2188

pd1-no-other-NNNN-5.xyz 19, 35, 36, 52, 53, 62, 64, 65, 66, 67, 68, 70, 242, 243, 244, 245, 246, 247, 248, 251, 252, 254, 296, 297, 298, 299, 300, 301, 303, 304, 305, 306, 318, 319, 320, 321, 322, 325, 348, 349, 350, 353, 354, 355, 864, 930, 984, 1810, 1923, 2185, 2186, 2187, 2188

pd2-no-other-NNNN-1.xyz 1, 2, 3, 4, 5, 6, 7, 8, 10, 11, 12, 13, 14, 15, 16, 17, 18, 20, 22, 24, 26, 27, 28, 30, 31, 33, 38, 39, 42, 44, 46, 47, 50, 57, 58, 61, 152, 153, 154, 201, 268, 269, 270, 271, 444, 509, 525, 591, 609, 697, 735, 853, 912, 925, 967, 987, 1051, 1080, 1214, 1354, 1451, 1463, 1507, 1627, 1874, 1884, 1960, 2185, 2186, 2187

pd2-no-other-NNNN-2.xyz 1, 2, 3, 4, 5, 13, 14, 15, 16, 23, 24, 25, 26, 27, 28, 30, 31, 43, 44, 45, 46, 47, 219, 220, 221, 222, 223, 224, 225, 226, 228, 229, 230, 231, 234, 235, 236, 237, 238, 239, 240, 241, 367, 368, 369, 370, 371, 373, 374, 377, 378, 379, 380, 519, 952, 2185, 2186, 2187

3 Experimental and Theoretical Studies of Pd Cation Reduction and Oxidation During NO Adsorption on and Desorption from Pd/H-CHA^j

3.1 Abstract

PNAs have been proposed for trapping NO_x present in automotive exhaust during the period of cold start during which the three-way converter is not yet hot enough to be effective for NO_x reduction. Pd-exchanged chabazite (Pd/H-CHA) is a good candidate for passive NO_x adsorption due to its ability to store NO and retain it to high temperatures (>473 K). Previous research suggests that NO adsorbs on both Pd²⁺ and Pd⁺ cations, and that NO desorption from Pd²⁺ cations occurs at lower temperatures than from Pd⁺ cations. Since experimental evidence shows that Pd exchanges into CHA exclusively as Pd²⁺, it is not clear how these cations are reduced to Pd⁺. In this study we show through experiments and theoretical analysis that Pd⁺ cations can form via two processes, each of which involves water adsorbed on Brønsted-acid sites of the zeolite. The first of these processes is $1.5 \text{ NO} + \text{Pd}^{2+}\text{Z}^-\text{Z}^- + 0.5 (\text{H}_2\text{O})\text{H}^+\text{Z}^- \rightarrow (\text{NO})\text{Pd}^+\text{Z}^-\text{H}^+\text{Z}^- + 0.5 \text{ NO}_2 + 0.5 \text{ H}^+\text{Z}^-$. Experiments confirm that the ratio of NO₂ upon NO adsorption to the NO desorbing at elevated temperatures from Pd⁺ corresponds to 0.5. Pd²⁺ can also be reduced via the reaction $1.5 \text{ CO} + \text{Pd}^{2+}\text{Z}^-\text{Z}^- + 0.5 (\text{H}_2\text{O})\text{H}^+\text{Z}^- \rightarrow (\text{CO})\text{Pd}^+\text{Z}^-\text{H}^+\text{Z}^- + 0.5 \text{ CO}_2 + 0.5 \text{ H}^+\text{Z}^-$. Upon subsequent adsorption of NO, NO fully displaces CO from Pd⁺ to form (NO)Pd⁺Z⁻H⁺Z⁻. In this case the amount of CO₂ formed upon CO adsorption is 0.5 of the NO desorbing at elevated temperatures from Pd⁺. Gibbs free energy calculations for the above processes at various potential ion-exchange sites in the cha framework indicate that these reactions are thermodynamically feasible. We also find that Pd⁺ is not formed in the absence of adsorbed water and is readily reoxidized to Pd²⁺ by trace amounts of O₂.

3.2 Introduction

Automotive emissions of NO_x (x = 1, 2) can be controlled very effectively using a catalytic converter placed downstream of the engine.^{2,3} To attain high NO_x conversion, the converter must operate at temperatures above 473 K; however, over a period of several minutes following engine startup, a significant amount of NO_x is emitted at the automobile tailpipe because the converter has not yet reached its ideal operating temperature.⁸³ To address this issue, it has been proposed that a PNA be placed upstream of the catalytic converter to capture and store NO_x until the PNA and the converter reach the temperature (> 473 K) at which full NO_x reduction occurs.⁴

PNAs consist of a metal dispersed on a high surface area support.⁵ A promising choice for a PNA is Pd supported on chabazite zeolite (Pd/H-CHA) because CHA exhibits hydrothermal stability (up to 1023 K in air and water) and Pd is resistant to poisoning by other tailpipe emissions such as sulfur dioxide.^{11,16,18} A number of studies have investigated the adsorption capacity and desorption characteristics of Pd/H-CHA under both oxidizing and reducing conditions.^{2,23,42,59} These efforts have shown that Pd/H-CHA is capable of NO storage and release at temperatures suitable for PNA applications and have motivated follow-up research devoted to understanding the modes of NO adsorption on Pd/CHA.

^j This chapter was originally published in Journal of Physical Chemistry C and had been adapted for inclusion in this dissertation with permission from the coauthors J. Van der Mynsbrugge, M. Head-Gordon, and A. T. Bell. Dr. Van der Mynsbrugge contributed the theoretical calculations. Dr. Chatterjee contributed the EPR results.

TPD studies of NO adsorbed on Pd/H-CHA have shown that NO desorption can occur at both low (423-473 K) and/or high (550-900 K) temperatures depending on the method of adsorbent pretreatment and the conditions of NO adsorption, i.e., the presence of co-adsorbates such as O₂, CO, and H₂O, and the adsorption temperature.^{2,23,48,50} The low-temperature and high-temperature TPD features have been attributed to NO adsorbed on Pd²⁺ cations and Pd⁺ cations, respectively. IR spectra of NO adsorbed on Pd/H-CHA show bands at ~2170 cm⁻¹, ~1860 cm⁻¹, and ~1810 cm⁻¹. The first of these features has been assigned to NO⁺ bound directly to the ion-exchange site of the zeolite, whereas the latter two features have often been attributed to NO adsorbed on Pd²⁺ and Pd⁺ cations, respectively.^{26,61} Density functional theory (DFT) simulations of NO adsorption on Pd/H-CHA have been used to confirm the assignments of the features observed in both TPD and IR studies.^{20,37,84} DFT calculations support the assignment of the low-temperature and high-temperature TPD features to NO adsorbed on Pd²⁺ and Pd⁺ cations, respectively. However, while DFT calculations also support the assignment of the IR band observed at 1810 cm⁻¹ to NO adsorbed on Pd⁺ cations, we recently reported that the band at 1860 cm⁻¹ consists of contributions from NO adsorbed on both Pd²⁺ and Pd⁺ cations.⁸⁴

A question not fully addressed in previous studies is the process by which Pd⁺ cations are formed and the stability of Pd⁺ to oxidation back to Pd²⁺. Lardinois et al. have shown that Pd in as-prepared Pd/CHA is present as either PdO or Pd²⁺, and that the fraction of the Pd present as Pd²⁺ cations ion-exchanged into the zeolite depends on the Si/Al ratio and preparation method of the parent CHA. This work shows that the stabilization of Pd²⁺ cations requires pairs of framework Al atoms in next-nearest neighbor (NNN) and next-next-nearest neighbor (NNNN) configurations.¹ Therefore, the greater the fraction of proximate Al atoms in CHA, the greater the fraction of Pd present as Pd²⁺ cations. It has also been found the ratio of adsorbed NO to total Pd increases with the fraction of Pd cations exchanged into the zeolite, since PdO does not adsorb NO.^{16,58} It is still possible, though, that Pd²⁺ cations can be present as [Pd(OH)]⁺ cations associated with isolated Al cation-exchange sites.^{16,23,59}

Several proposals have been advanced to explain the reduction of Pd²⁺ cations to Pd⁺ cations. In these reactions, Z⁻ represents a charge-exchange site in the zeolite (CHA). The simplest is that Pd⁺ is produced upon NO adsorption via the reaction of Pd²⁺ Z⁻Z⁻ + 2 NO → (NO) Pd⁺ Z⁻ + NO⁺Z⁻ based on the simultaneous appearance of IR bands at 1805 cm⁻¹ and 2160 cm⁻¹, assigned to NO adsorbed on Pd⁺Z⁻ and NO⁺Z⁻ respectively.²⁶ However, Kim et al. have shown that pretreatment of Pd/H-CHA in a stream of air containing 5% water prior to adsorption of NO from He results in NO adsorption on both Pd²⁺ and Pd⁺ sites and the absence of an IR band for NO⁺Z⁻.⁸⁴ These authors have proposed Pd²⁺ is reduced by the reaction Pd²⁺Z⁻Z⁻ + 0.5 H₂O → Pd⁺Z⁻/H⁺Z⁻ + 0.25 O₂, and found that the reaction free energy for this process is negative for all Al pairs, except NNNN(6R) Al pairs under the pretreatment conditions used. We note, however, that neither the precise mechanism for the formation of Pd⁺ nor the possible role of NO in this process were considered. In this connection, Gupta et al. have suggested that the precursor to Pd⁺ is [Pd(OH)]⁺, and that Pd⁺ forms according to the reaction: 0.5 NO + [Pd(OH)]⁺ Z⁻ ↔ Pd⁺Z⁻ + 0.5 NO₂ + 0.5 H₂O.^{22,23} This idea is supported by the observation of water and NO₂ desorption in the low-temperature portion of NO TPD spectra.^{22,23} We note, however, that Mandal et al. have not observed an IR band for isolated [Pd(OH)]⁺ species and DFT calculations by Van der Mynsbrugge et al. show that [Pd(OH)]⁺ located near framework Al that is part of an NNN or NNNN Al pair (i.e., in close proximity to a Brønsted acid proton) is not stable relative to Pd²⁺Z⁻Z⁻.⁸⁴ In this situation, [Pd(OH)]⁺/H⁺Z⁻ readily dehydrates via the reaction: [Pd(OH)]⁺Z⁻H⁺Z⁻ → (H₂O)Pd²⁺Z⁻Z⁻. This, however, does not exclude the possibility that [Pd(OH)]⁺ cations associated with isolated Al

exchange sites might undergo reduction in the presence of NO via the proposed reaction. Thus, it remains unclear whether Pd⁺ sites are formed during the pretreatment in water vapor or upon NO adsorption on Pd/H-CHA.

It has also been reported that CO, another component of exhaust gas, is able to increase the uptake of NO on Pd zeolites. Two possibilities by which CO does this include the formation of a co-adsorbed CO/NO complex on Pd or an isocyanate intermediate.^{42,47,85} Another hypothesis, proposed by Ambast et al., is that the strength of NO adsorption is enhanced by the reduction of Pd²⁺ to Pd⁺ via the reaction $\text{CO} + [\text{Pd}(\text{OH})]^+ \text{Z}^- \rightarrow 0.5 \text{Pd}^+ \text{Z}^- + 0.5 (\text{CO})\text{Pd}^+ \text{Z}^- + 0.5 \text{CO}_2 + 0.5 \text{H}_2\text{O}$.⁴⁷ For the reasons discussed above, this process should only be plausible for [Pd(OH)]⁺ cations associated with isolated Al cation-exchange sites. Finally, it is important to note that none of the previous studies have examined the stability of Pd⁺ to reoxidation to Pd²⁺ and the processes by which this might occur.

The present study was undertaken to elucidate the pathways by which Pd²⁺ cations in Pd/H-CHA are reduced to Pd⁺ cations, and to identify the roles that adsorbed H₂O, NO and CO play in this process. The resistance of Pd⁺ cations to reoxidation to Pd²⁺ cations during the desorption of NO was also examined. To these ends, we have used a combination of TPD experiments, IR spectroscopy, and DFT calculations.

3.3 Experimental Methods

3.3.1 Adsorbent synthesis and characterization

The NH₄-CHA zeolite was provided by BASF. Palladium-exchanged CHA was prepared by incipient wetness impregnation. De-ionized water (18.2 MΩ) was added drop-wise to the NH₄-form zeolite while stirring until the total pore volume reached saturation, evidenced by a transformation of the mixture from a powder-like substance to a slurry. Assuming the same mass uptake as water, a Pd(NH₃)₄(NO₃)₂ solution (10 wt%, Sigma-Aldrich) was dissolved in de-ionized water (18.2 MΩ) to achieve a desired Pd loading. The Pd-exchanged CHA form was then dried overnight at room temperature (~298 K). The weight loading of Pd was determined by atomic absorption spectroscopy to be 1.2 wt%, which corresponds to a Pd/Al ratio of ~ 0.1.

The distribution of Pd present on the CHA support was determined by H₂ temperature-programmed reduction (TPR). Previous studies have shown that Pd in Pd/H-CHA can be present as Pd cations and PdO.^{36,46,58,59} H₂ TPR was carried out to determine the fractions of Pd present in each of the two forms by analyzing the effluent gas during H₂ TPR using a MKS Cirrus 3 mass spectrometer.¹ For these experiments, the adsorbent (0.05-0.10 g) was first pretreated in flowing air (Air Zero, Indiana Oxygen, 1800 cm³ h⁻¹) to 773 K (10 K/min) for 5 h, then cooled to 303 K. The air stream was replaced with 15 mL/min of 1000-50000 ppm of H₂ in He. After achieving a stable signal for m/e = 2, the sample was heated to 773 K at 10 K/min. Based on these experiments, the ionic Pd content was estimated to be 100% of the Pd in the sample, meaning that there was no PdO present. To determine the content of paired Al sites in Pd/H-CHA, Co²⁺ titration was conducted. The zeolite was mixed with CoCl₂ solutions, and the amount of exchanged Co was determined by recovering the solids with centrifugation, washing samples with deionized water, and drying in stagnant air. The Co exchanged sample was then treated in flow dry air at 773 K for 4 h, and then the sample was digested for elemental analysis.¹ For the Pd/H-CHA used in this study, the Co²⁺/Al ratio was estimated to be 0.16, corresponding to about 32% of Al in pairs.¹ Taking these figures and the measured weight loading of Pd into account, suggests that most of the Pd²⁺ cations are exchanged into NNN or NNNN pairs of Al charge-exchange sites as Pd²⁺(Z⁻

)2. This interpretation is supported by our theoretical calculations showing that proximate pairs of Al charge-exchange sites are the preferred locations for accommodation of Pd²⁺ cations.^{19,81}

3.3.2 Temperature-programmed desorption studies

All TPD studies were conducted in a quartz reactor. Typically, 100 mg of adsorbent was loaded into the reactor. A quartz wool plug placed below the bed prevented the adsorbent from entering the effluent gas line. Before NO adsorption, the adsorbent underwent hydrothermal aging (HTA) in a stream of air containing 5% water heated from 348 K to 773 K at 2 K/min. The temperature was held at 773 K for 5 h in air and water vapor, and then cooled to 348 K in the absence of water vapor.

For adsorption, a feed stream containing the adsorbate was flowed over the adsorbent at 348 K until the adsorbent was saturated. The feed typically consisted of about 200 ppm of NO in a He balance flowing at 250 mL/min. 1000 ppm CH₄ was added to the NO/He stream as an inert tracer. For experiments using CO, about 100 ppm of CO was added to the He stream. He (purity of 99.999% from Praxair) was dried by passage through moisture trap (Restek Moisture Trap, <10 ppb water) and NO (1.03% NO in He balance from Praxair) was purified by passage through traps to remove moisture and NO₂ (Alltech Gas Drier, <1 ppm NO₂ and H₂O). The air carrier gas was provided by Praxair and was rated as extra dry (<10 ppm H₂O). The adsorption of NO was monitored using an MKS 2030 Multigas analyzer, a non-dispersive infrared (NDIR) instrument. The concentration of NO in the effluent was measured, and the NO and CH₄ were shut off once the effluent concentration of NO had reached the inlet value. The adsorbent was then purged with He until the concentration of NO had returned to the level observed before the start of the adsorption step. A purge stream of He (250 mL/min) was fed to the reactor immediately after adsorption to remove any weakly bound adsorbates. The adsorbed NO was then desorbed as the adsorbent was heated from 348 K to 773 K at 10 K/min, and subsequently held at 773 K for 20 min. Throughout this period the concentrations of NO and NO₂ in the effluent were monitored by non-dispersive IR spectroscopy. Following a TPD experiment, the adsorbent was treated in one of several ways in order to prepare it for the next adsorption cycle. This typically involved cooling the adsorbent from 773 K back to 348 K in a defined gas mixture (e.g., He, air, air plus water vapor). This last step is referred to as a pretreatment, and for future discussion, pretreatment refers to the steps performed before an adsorption measurement when the adsorbent undergoes several adsorption/desorption cycles.

3.3.3 IR spectroscopy

The procedure for the initial treatment of Pd/H-CHA and pretreatment between NO adsorption experiments is similar to that used for the TPD experiments. About 30 mg of adsorbent was compressed into a pellet that was placed into a Harrick High Temperature cell with CaF₂ windows. The cell was heated resistively and the temperature was monitored with a thermocouple. The adsorbent was exposed to NO for 15 min, after which the NO flow was stopped and the TPD ramp was started. In-situ transmission IR experiments were conducted using a Nicolet 6700 spectrometer operated at 4 cm⁻¹ resolution. Each spectrum was obtained by averaging 256 scans. Background spectra of Pd/H-CHA, taken at the same temperatures as spectra recorded during a TPD IR experiment, were subtracted from the spectra of NO adsorbed on Pd-CHA.

3.3.4 Theoretical calculations

The crystallographic structure of CHA was obtained from the database maintained by the International Zeolite Association (IZA).⁶⁵ A large cluster model containing 696 tetrahedral atoms (T696) was constructed by selecting the framework atoms within a 25 Å radius of a central *cha* cage and trimming the resulting fragment to be terminated at double six-ring units. This large model allows representing the periodic crystal structure of the zeolite lattice by a finite cluster without introducing boundary effects or spurious anisotropy in the description of long-range interactions.⁶⁶

Al pairs were placed in various next-nearest neighbor (NNN), next-next-nearest neighbor (NNNN) and next-next-next-nearest neighbor (NNNNN) configurations in 6-rings and 8-rings within the CHA framework. Charge-compensating cations (either Pd⁺/H⁺ or Pd²⁺) that are accessible from the *cha* cage represent potential NO adsorption sites within Pd/H-CHA. A hybrid quantum mechanics/molecular mechanics (QM/MM) approach was used to reduce the computational cost. A smaller fragment of the zeolite cluster and the adsorbates are treated quantum mechanically (QM), using the range-separated hybrid functional ω B97X-D^{67,68}, combined with def2 basis sets (detailed below), which include an Ar+3d effective core potential for Pd. The QM region includes all neighboring T-atoms of each Al, as well as all Si and O atoms that are part of the 6- or 8-ring(s) connecting the pair of Al atoms. The remainder of the large cluster model is treated using molecular mechanics (MM).^{69,70} Fig. 1 shows the T696 cluster model and highlights the 6- and 8-rings facing the *cha* cages. Geometry optimizations and frequency calculations are performed at the ω B97X-D/def2-SV(P) level of theory, followed by single-point energy refinements at the ω B97M-V/def2-TZVPD level of theory. Paolucci et al. have pointed out that binding energies of NO to Pd are particularly sensitive to the choice of density functional.²⁰ In this study, we have selected the range-separated hybrid meta GGA functional ω B97M-V⁷¹ to evaluate the energetics, because it has emerged as the overall best performer out of the 200 density functionals evaluated by Mardirossian and Head-Gordon.⁷² The MM region is described with a CHARMM-type force field using the P2 parameter set.⁷⁰ Initial geometries were constructed with ZEOBUILDER.⁷¹ All QM/MM calculations were performed with a developmental version of Q-Chem.⁷³ Thermochemical quantities are calculated from a normal mode analysis using the quasi-rigid rotor/harmonic oscillator approximation (RRHO)^{70,74} on the optimized structures.

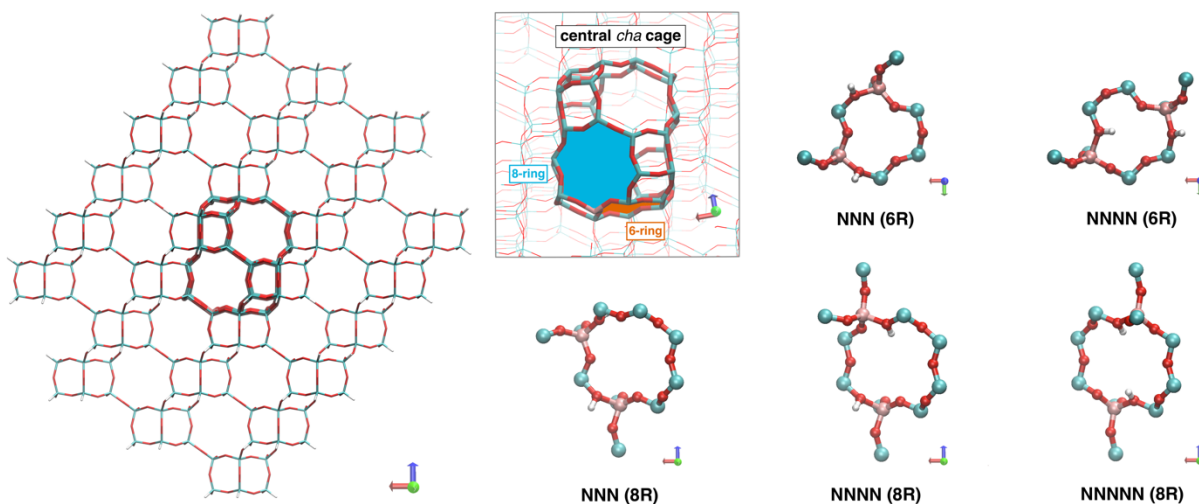


Figure 3.1: Left: T696 cluster model for CHA used in QM/MM calculations. Si atoms are represented in cyan, Al in pink, O in red, H in white. The central CHA cage containing the adsorption sites is shown in bold lines. Center: 6-ring

and 8-ring in the *cha* cage. Right: Al pairs in next-nearest neighbor (NNN), next-next-nearest neighbor (NNNN) and next-next-next-nearest neighbor (NNNNN) configurations in the 6-ring (6R) and 8-ring (8R). Adapted with permission from [19].

3.3.5 EPR spectroscopy

Electron paramagnetic resonance spectroscopy experiments were carried out using a Bruker EMX plus EPR spectrometer. Samples were first treated in a quartz reactor in a similar manner to the TPD experiments. Depending on the condition being tested, samples were taken from different parts of the TPD methodology, such as before and after saturation with NO: they were cooled to room temperature and then removed from the quartz reactors. 25-50 mg samples were loaded into 4 mm OD Clear Fused-Quartz tubes. They were attached to a Schlenk line through a Teflon stopcock. The Schlenk line was utilized to put each sample under vacuum. Once connected, three cycles of flushing with high purity N₂ gas and then evacuation were conducted. After the third cycle, the stopcock was closed to keep the reactor under vacuum and separate it from the Schlenk line. This line was then flame sealed using a gas-oxygen torch.

Following flame seal, EPR experiments were performed by Dr. Ruchira Chatterjee and Kaitlyn Engler. EPR spectra were acquired at X-Band at 20 K in a Bruker EN 4118X-MD4 resonator on a E580 Eleksys spectrometer equipped with an Oxford Instruments CF935 helium cryostat. Three gauss modulation was applied during acquisition. Power and modulation levels were varied to ensure the spectra were not saturated or broadened due to overmodulation.

3.4 Results and Discussion

3.4.1 NO adsorption on Pd/H-CHA

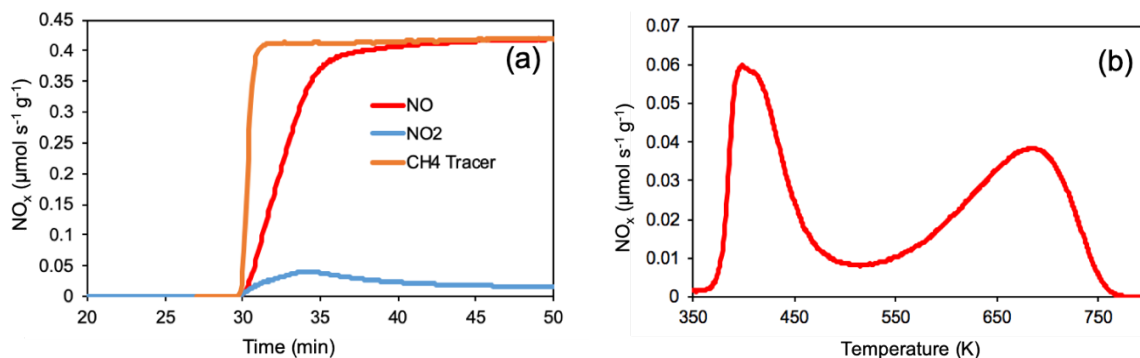
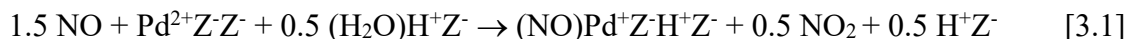


Figure 3.2: a) NO/NO₂ profile for NO adsorbed on Pd/H-CHA during the adsorption step. NO adsorption was from a flow of He (250 mL/min). (b) NO TPD profile for NO adsorbed on Pd/H-CHA. Nearly identical results were obtained over four adsorption-desorption cycles.

A set of experiments was performed to assess whether NO is involved in the reduction of Pd²⁺ to Pd⁺. The Pd/H-CHA catalyst used in the present study has a Si/Al ratio of 13 and a Pd weight loading of 0.64%. This catalyst in particular has been extensively studied thanks to its tunability as a zeolite and great hydrothermal stability, making it ideal for usage in the hot and wet conditions of exhaust gas.¹¹ The Pd/H-CHA was first heated in air containing 5% H₂O to 773 K at 2 K/min, held at this temperature for 5 h, and then cooled to 348 K in 5% H₂O in He. NO adsorption was from a flow of He (250 mL/min) containing 200 ppm of NO at 348 K. During TPD, the temperature was ramped from 348 K to 773 K at 10 K/min and then held at 773 K for 20 min in

He. This protocol is identical to that used in our earlier work and was found to result in the appearance at high-temperature NO desorption peak during TPD, attributable to NO desorption from Pd⁺ cations. Fig. 3.2a shows the composition of the effluent from the reactor upon exposure of pretreated Pd/CHA to NO. Traces are seen for both NO and NO₂. Since the NO fed to reactor is free of NO₂, the NO₂ observed is formed during the adsorption process by reacting with the Pd or the zeolite support.⁸⁴ The integral of the trace of NO₂ corresponds to approximately 15 μmol of NO₂ per gram of adsorbent. Fig. 3.2b shows the TPD spectrum for NO. Two NO desorption peaks are observed: one at low-temperatures (423-473 K) and one at high temperatures (550-773 K) that can be attributed to NO desorption from Pd²⁺ and Pd⁺, respectively. The total amount of NO desorbed is 57 μmol of NO per gram of adsorbent, which corresponds to a NO/Pd ratio of 0.51. The fractions of NO desorbing from Pd²⁺ and Pd⁺ are 0.43 and 0.57, respectively. The ratio of NO desorbing from Pd⁺ to NO₂ formed during NO adsorption is 2.1, consistent with what would be expected for the following process.



The ratio of NO desorbing from the high-temperature desorption peak, attributed to Pd⁺, to NO₂ formed upon adsorption may vary due to the conversion of NO to NO₂ catalyzed by the zeolite.⁸⁴ The water involved in this reaction is assumed to be H₂O retained on unexchanged Brønsted acid sites during the cool-down phase of the adsorbent pretreatment.

To determine whether Reaction 3.1 is thermodynamically feasible, we calculated the reaction free energy for this process. The calculated reaction free energies for Reaction 3.1 under NO adsorption conditions (T = 348 K, P_{NO} = 20 Pa, P_{NO₂} = 0.1 Pa) are listed in Table 3.1 for Pd cations at the various Al pairs in the 6- and 8-rings. This reaction is thermodynamically favorable for all Al pairs, except for next-next-nearest neighbor Al pairs in 6-rings (NNNN(6R)).

Table 3.1: Reaction free energies (ΔG_{rxn}) in kJ/mol under adsorption conditions (T = 348 K, P_{NO} = 20 Pa, P_{NO₂} = 0.1 Pa) for the reduction of Pd²⁺ to Pd⁺ at different Al pairs in the 6-rings and 8-rings in Pd/H-CHA before and after NO adsorption on the newly formed Pd⁺ sites.

Charge-Exchange Site	Reaction 3.1
	ΔG_{rxn} [kJ/mol]
NNN(6R)	-87
NNNN(6R)	+9
NNN(8R)	-123
NNNN(8R)	-224
NNNNN(8R)	-241

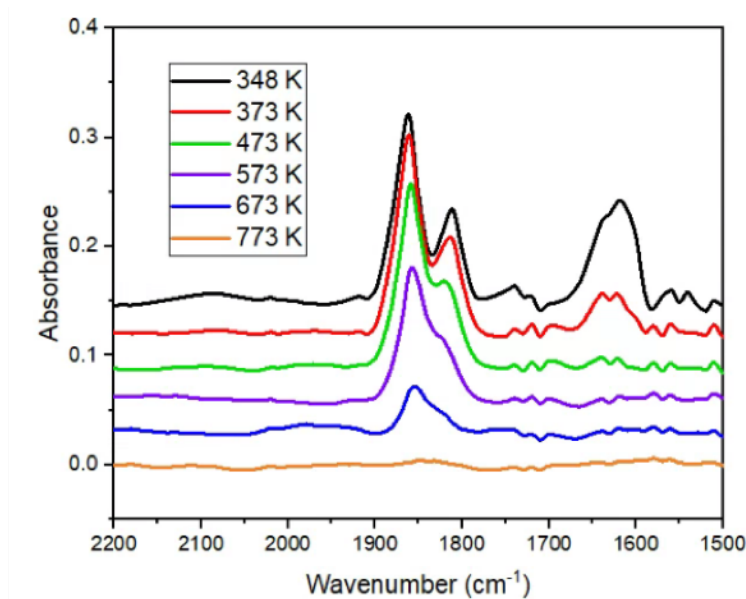


Figure 3.3: TPD IR spectra for NO adsorbed on Pd/H-CHA. A reference spectrum was taken of Pd/H-CHA before NO adsorption, and then subtracted from the spectrum taken after NO adsorption. Scans were taken every 100 K during which the temperature was ramped at 2.5 K/min.

IR experiments were also carried out in order to identify adsorbed NO species. Fig. 3.3 shows IR TPD spectra for NO adsorbed on the Pd/H-CHA. Pd/H-CHA was de-greened by heating in air and 5% H₂O from 348 K to 773 K at 2 K/min and holding at 773 K for 5 h. The sample was then cooled to 75°C in air. NO adsorption was from a flow of He (250 mL/min) containing 200 ppm of NO at 348 K. During TPD, the temperature was ramped from 348 K to 773 K at 10 K/min and then held at 773 K for 20 min in He. As previously reported, the main features associated with NO adsorbed on Pd occur at 1860 cm⁻¹ and 1810 cm⁻¹.^{2,17,43} While these bands have been attributed to NO bound to Pd²⁺ and Pd⁺, respectively, recent work by Kim et al. indicates that the band at 1860 cm⁻¹ has contributions from NO adsorbed on Pd⁺ as well as Pd²⁺.⁸⁴ DFT calculations reveal that the frequency of the band for NO adsorbed on Pd⁺ is quite sensitive to the location of the charge exchange site at which the Pd⁺ cation is located within the unit cell of CHA. These findings demonstrate that IR spectroscopy cannot be used unambiguously to identify NO adsorbed on Pd⁺.

3.4.2 Effect of CO on NO adsorption on Pd/H-CHA

Prior studies have suggested that CO can improve NO adsorption by either the reduction of Pd²⁺ to Pd⁺ or via formation of an NO-Co complex.^{10,17,23} To test these alternatives, we carried out experiments using CO. Pd/H-CHA was de-greened by heating in air and 5% H₂O from 348 K to 773 K at 2 K/min and holding at 773 K for 5 h. The sample was then cooled to 75°C in air. A few different adsorption experiments were conducted, in which 100 ppm of CO was either co-adsorbed with NO, or CO was adsorbed prior to NO adsorption. In both experiments, adsorption was from a flow of He at 348 K. During TPD, the temperature was ramped from 348 K to 773 K at 10 K/min and then held at 773 K for 20 min in He.

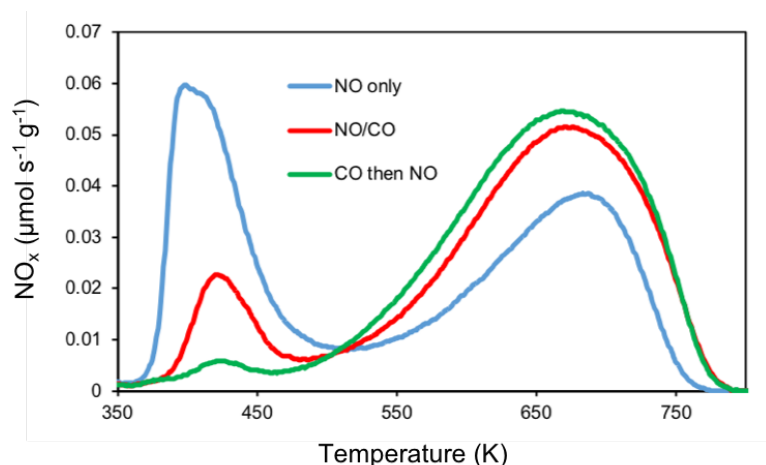


Figure 3.4: NO TPD profiles for NO adsorbed on Pd/H-CHA. Additional gas feeds were tested: NO and CO were co-adsorbed in one case, and the Pd/H-CHA was pre-saturated with CO prior to NO adsorption in the other.

As seen in Fig. 3.4, the co-adsorption of CO and NO significantly reduces the area of the low-temperature TPD peak and increases the area of the high-temperature peak relative to what is observed when NO is adsorbed alone. Adsorption of CO prior to the adsorption of NO has a similar effect. In this case, though, the low-temperature NO desorption feature is almost completely suppressed and the high-temperature feature increases further relative to what is seen for the co-adsorption of CO and NO. Notably, in all these experiments, the total amount of NO adsorbed remains the same at 0.51 NO/Pd. Additionally, neither of these experiments shows any evidence for CO desorption coincident with the desorption of NO in the high-temperature peak. Therefore, we conclude that NO and CO does not form a co-adsorbed NO/CO complex and that it is more likely that CO reduces Pd^{2+} to Pd^+ (as suggested by Ambast et al.⁴⁷), which binds NO more strongly than Pd^{2+} .

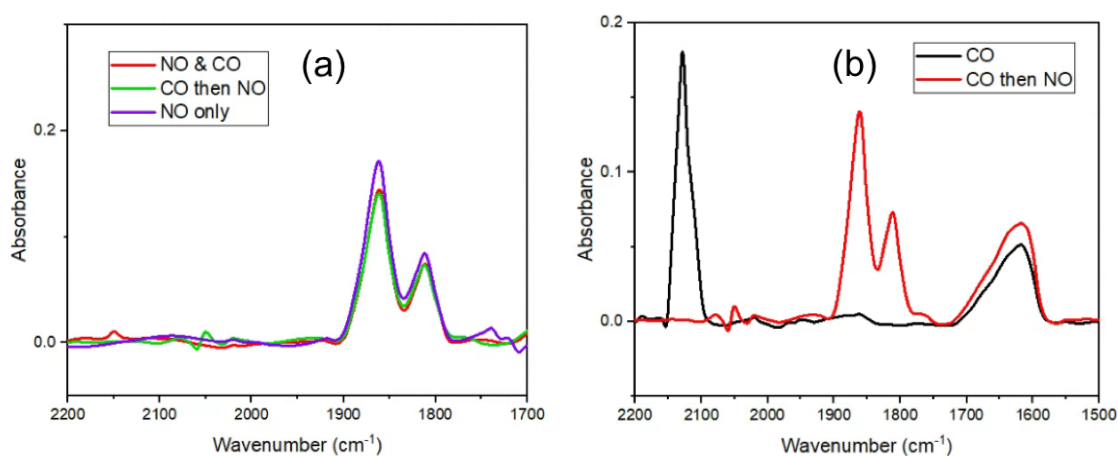


Figure 3.5: TPD IR spectra for NO adsorbed on Pd/H-CHA. In (a), additional gas feeds were tested: NO and CO were co-adsorbed in one case, and the Pd/H-CHA was pre-saturated with CO prior to NO adsorption in the other. In (b) the sample was first pre-saturated with CO from a flow of He (250 mL/min) at 348 K. A scan was taken after CO adsorption and prior to NO adsorption. This scan is then compared to a scan taken after NO adsorption.

To help relate the change in TPD behavior to a change in NO-Pd speciation, IR spectra were collected. Pd/H-CHA was de-greened by heating in air and 5% H₂O from 348 K to 773 K at 2 K/min and holding at 773 K for 5 h. The sample was then cooled to 75°C in air. NO adsorption was from a flow of He (250 mL/min) containing 200 ppm of NO at 348 K. In Fig. 3.5a, additional gas feeds were tested: NO and 100 ppm of CO were co-adsorbed in one case, and the Pd/H-CHA was pre-saturated with 100 ppm of CO prior to NO adsorption in the other. A reference spectrum was taken of Pd/H-CHA before NO and CO, and then subtracted from the spectrum taken after NO and CO adsorption. Spectra in Fig. 3.5a were taken just prior to TPD. In Fig. 3.5b the sample was first pre-saturated with 100 ppm of CO from a flow of He (250 mL/min) at 348 K. A scan was taken prior to NO adsorption, revealing the IR features associated with CO adsorption on Pd/H-CHA. Then NO adsorption was from a flow of He (250 mL/min) containing 200 ppm of NO at 348 K. A reference spectrum was taken of Pd/H-CHA before NO and CO adsorption, and then subtracted from the spectrum taken after NO and CO adsorption.

IR spectra taken after the adsorption of NO for each of the three experiments reported in Fig. 3.4 are presented in Fig. 3.5a. Surprisingly, for all three scenarios – NO adsorption alone, CO and NO co-adsorption, and CO adsorption followed by NO adsorption – the spectra are virtually the same, exhibiting bands at 1810 cm⁻¹ and 1860 cm⁻¹. Therefore, despite the distinct differences in the TPD spectra for these scenarios, IR spectroscopy provides little insight into the changes in Pd adsorption sites produced by exposure of the adsorbent to CO either prior to or together with NO adsorption. As described previously, the IR band at 1860 cm⁻¹ contains contributions from NO adsorbed on Pd⁺ and Pd²⁺ located in NNN and NNNN sites. If CO only redistributes the adsorbed sites without creating additional ones (as indicated by the similar amounts of NO adsorbed with and without CO), then those changes may not be reflected in the IR spectra. Fig. 3.5b shows a spectrum of CO adsorbed on Pd/H-CHA. The band at 2130 cm⁻¹ is attributable to CO adsorbed on either Pd⁺ or Pd²⁺.^{18,26,40} The absence of this band after NO adsorption or after co-adsorption of CO and NO is consistent with the stronger adsorption of NO than CO (see more on this topic below) and the displacement of adsorbed CO by NO illustrated in Fig. 3.5b. This result matches the aforementioned TPD experiments which demonstrate that there is no formation of a NO/CO co-adsorbed complex.

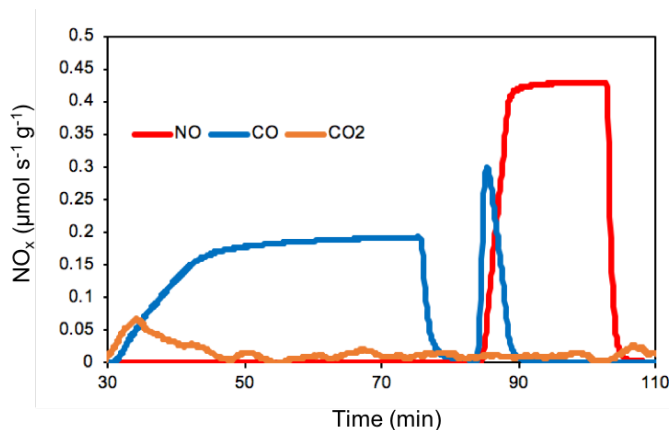
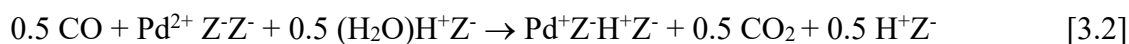


Figure 3.6: NO/CO/CO₂ profiles during adsorption for CO and NO adsorbed on Pd/H-CHA. The profiles for NO, CO, and CO₂ were recorded during the adsorption step for Pd/H-CHA that was pre-saturated with CO prior to NO adsorption.

Further insights into the role of CO were obtained from monitoring the composition of the gas leaving the reactor for the experiment in which CO is pre-adsorbed prior to the adsorption of NO. Pd/H-CHA was de-greened by heating in air and 5% H₂O from 348 K to 773 K at 2 K/min and holding at 773 K for 5 h. The sample was then cooled to 75°C in air. The profiles for NO, CO, and CO₂ were recorded during the adsorption step for Pd/H-CHA that was pre-saturated with CO prior to NO adsorption. Fig. 3.6 shows that upon adsorption of CO a small amount of CO₂ is formed during a period of about 15 min, corresponding to ~ 0.24 mol CO₂/mol Pd. The partial pressure of CO reaches a plateau about 40 min after its introduction but then is completely removed during by the He flush.

It is notable that upon CO adsorption, a small amount of CO₂ is formed. We suggest that reduction might occur via Reaction 3.2 or 3.3.



As discussed for the case of NO adsorption in Section 3.4.1, the water required to perform the chemistry is assumed to have been retained on the zeolite during its pretreatment.

The reaction free energies under adsorption conditions (T = 348 K, P_{CO} = 20 Pa, P_{CO₂} = 0.1 Pa) were calculated for Reaction 3.2 and 3.3, and the results are listed in Table 3.2 for Pd cations associated with various Al pairs in the 6- and 8-rings. This table shows that Reaction 3.2 and 3.3 are both thermodynamically favorable for all Al pairs, including the next-next-nearest neighbor Al pair in the 6-ring (NNNN(6R)), and that the reaction free energy is more favorable for Reaction 3.3.

Table 3.2: Reaction free energies (ΔG_{rxn}) in kJ/mol under adsorption conditions (T = 348 K, P_{CO} = 20 Pa, P_{CO₂} = 0.1 Pa) for the reduction of Pd²⁺ to Pd⁺ at different Al pairs in the 6-rings and 8-rings in Pd/H-CHA before and after CO adsorption on the newly formed Pd⁺ sites.

	Reaction 3.2	Reaction 3.3
	ΔG_{rxn} [kJ/mol]	ΔG_{rxn} [kJ/mol]
NNN(6R)	-157	-180
NNNN(6R)	-53	-100
NNN(8R)	-145	-226
NNNN(8R)	-266	-320
NNNNN(8R)	-301	-360

Fig. 3.6 also shows that upon initial exposure to NO, a sharp burst of CO is recorded, indicating that all of the CO that was previously adsorbed on the Pd/H-CHA is displaced by NO. The absence of CO during TPD also indicates that NO and CO do not form a co-adsorbed complex for the conditions investigated in this study. In addition, we note that the amount of CO₂ (0.24 CO₂/Pd) formed is approximately equal to half the amount of NO desorbing from Pd⁺ at high 0.51 NO/Pd⁺, consistent with Reaction 3.2 or 3.3. These results show that CO can reduce Pd²⁺ completely to Pd⁺, resulting in the exclusive desorption of NO at higher temperatures (>500 K).

3.4.3 Electron paramagnetic resonance experiments on NO adsorbed Pd/H-CHA

Co-adsorbate studies have shown evidence for the formation of Pd⁺. However, direct observation of this oxidation state has remained a challenge in this field.¹⁹ EPR spectroscopy is a technique that can detect radical electrons, making it one of the last bastions of experimental techniques remaining that can be used to detect the formation of Pd⁺. These experiments were conducted with the assistance of the Dr. Junko Yano from the Molecular Biophysics and Integrated Bioimaging Division at Lawrence Berkeley National Lab.

Prior to EPR experiments, samples were first pretreated and saturated with NO. In Fig. 3.7, three samples were compared. The first sample was H-CHA (Si/Al = 12) that was de-greened by heating in air from 348 K to 773 K at 2 K/min, and held at 773 K for 1 h. The sample was then cooled to 348 K in air. NO adsorption was carried out from a flow of He (250 mL/min) containing 200 ppm of NO at 348 K. The second sample was Pd/H-CHA (Si/Al = 12, Pd/Al = 0.24) that was de-greened by heating in air and 5% H₂O from 348 K to 773 K at 2 K/min and held at 773 K for 5 h. The sample was then cooled to 348 K in air. This sample was not saturated with NO. The third sample was a Pd-CHA-10 that was de-greened by heating in air and 5% H₂O from 348 K to 773 K at 2 K/min and held at 773 K for 5 h. The sample was then cooled to 348 K in air. NO adsorption was from a flow of He (250 mL/min) containing 200 ppm of NO at 348 K.

Following each adsorption step (for Pd_zeolite, following the end of the de-greening step), the samples were removed from their quartz reactors and transferred to EPR tubes inside a fume hood. They were connected to a Schlenk line, where the samples were put under vacuum. Using a valve, the EPR tube was separated from the Schlenk line and then flame sealed.

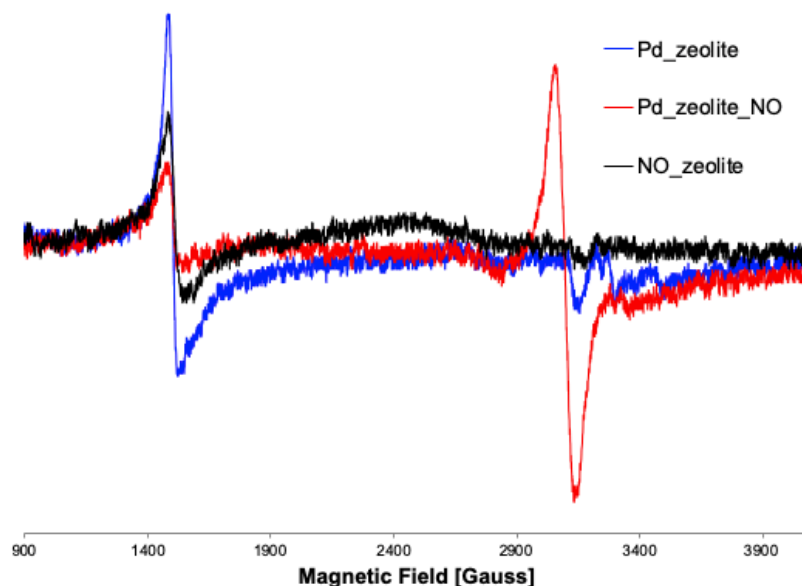


Figure 3.7: EPR spectra of Pd/H-CHA and H-CHA samples. Samples were pretreated in He and 5% H₂O. Samples were removed from the quartz reactor and transferred to quartz EPR tubes. They were then moved to a Schlenk line to put under vacuum. A stopcock was used to separate the vacuum sealed EPR tube from the Schlenk line. Samples were then flame sealed. The Pd_zeolite sample was removed immediately after pretreatment. The NO_zeolite sample was the H-CHA sample that was saturated with NO after pretreatment. The Pd_zeolite_NO sample was the Pd/H-CHA sample that was saturated with NO after pretreatment.

There are two notable features observed in these EPR spectra: the peak around 1400 Gauss is typical of iron impurities that is found in zeolites. The feature of interest is the one located at around 3000-3300 Gauss or a g-value of about 2.1. This feature has been assigned to Pd⁺.^{24,25} Fig. 3.7 shows that following the de-greening step, there is no Pd⁺ present prior to the introduction of NO. Lardinois et al. have used H₂ temperature programmed reduction experiments to determine that, using a similar pretreatment, Pd should be predominantly in the form of Pd²⁺ or PdO.¹ But upon adsorbing NO, the EPR spectrum exhibits a peak, matching the hypothesis proposed in Chapter 2 where it was suggested that NO is required to produce Pd⁺.

However, subsequent experiments have failed to reproduce this feature at g~2.1. Fig. 3.8 showcases several additional EPR experiments conducted under similar conditions to those reported in Fig. 3.7. In part a, the samples were first saturated with NO before sealing off the reactor and transferring it to a glove box. The catalyst was then transferred to the EPR tube under inert conditions. In part b, the sample was de-greened, and then transferred to the Schlenk line. In the Schlenk line, the catalyst was exposed to NO and then put under vacuum for flame sealing. However, neither of these methods resulted in the observation of the peak at a g-value of 2.1.

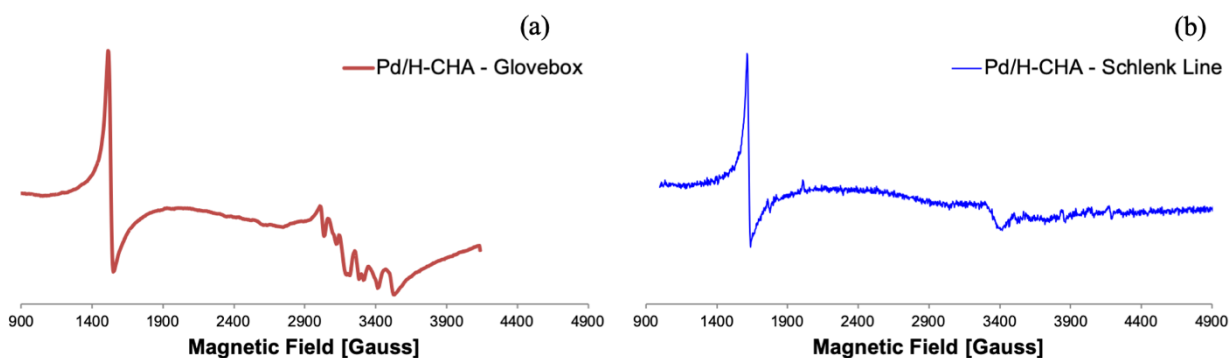


Figure 3.8: EPR spectra of Pd/H-CHA samples taken using two different methodologies. In Fig. 3.8a, a Pd/H-CHA sample was saturated with NO. Afterwards, two valves installed around the reactor were closed to seal the sample from the air, and then the reactor was transferred to a glove box. In the glove box, the sample was transferred to an EPR quartz tube before being sealed with a stopcock and connected to a Schlenk line to be put under vacuum. In Fig. 3.8b, a Pd/H-CHA sample was pretreated in a quartz reactor, and then transferred to an EPR quartz tube. Once connected to a Schlenk line, the sample was exposed to NO before being put under vacuum for flame sealing.

Both experiments sought to create environments free of air and H₂O to maintain the stability of the Pd⁺ cation when moving from the quartz reactor to the EPR spectrometer. Given the lack of consistency in EPR results, direct observation of Pd⁺ proved difficult to confirm. One potential issue is that even at very low temperatures (20-100 K), the Pd⁺ signal in EPR possesses a very short relaxation time which makes it difficult to detect.⁸⁶ Theoretical calculations also demonstrate the sensitivity of the Pd oxidation state to temperature, so the necessary low temperatures (10-20 K) possibly convert Pd⁺ to an EPR-silent species instead.^{19,25,40} High Si/Al can also make EPR experiments difficult due to the very low population of exchanged Pd in the catalyst.^{10,40} Successful studies have observed Pd⁺ in more extreme conditions such as high vacuums and thermal reduction by H₂, which were not employed in the above experiments.^{20,24,25,87} Potential fixes could include increasing the Pd weight loading, which has been reported to monotonically increase along with the EPR signal up to about 3% weight loading, or approaching even lower temperatures (<10 K).⁸⁸ However, it is possible that using an *in situ* EPR spectrometer and adsorbing NO without the need to transfer the sample between instruments can overcome the stability concerns of Pd⁺.

3.4.4 Retention of Pd⁺ sites following NO TPD

A significant question is whether the Pd⁺ sites responsible for the desorption of NO at high temperature are retained after NO desorption. To address this issue the following experiment was carried out. Pd/H-CHA (Si/Al = 14, Pd wt% = 0.68) was de-greened by heating in air and 5% H₂O from 348 K to 773 K at 2 K/min and holding at 773 K for 5 h. The sample was then cooled to 348 K in air. NO adsorption was from a flow of He (250 mL/min) containing 200 ppm of NO at 348 K. During TPD, the temperature was ramped from 348 K to 773 K at 10 K/min and then held at 773 K for 20 min in He. Immediately after the desorption of NO from Pd/H-CHA pretreated in He and 5% H₂O prior to NO adsorption, the sample was cooled in pure He and then exposed to NO. Under these conditions, 39 μmol NO_x/g of adsorbent was stored. A second experiment was carried out in which, following cooling in pure He, the catalyst was exposed to CO and then to NO. Under these conditions, a similar amount, 44 NO_x/g of adsorbent, was stored as in the first experiment.

After the first TPD experiment (with a pretreatment of He and H₂O), the TPD spectrum exhibits the high-temperature NO desorption feature. Fig. 3.9 shows that if the pretreatment in H₂O is not repeated prior to the second adsorption of NO, the TPD spectrum of adsorbed NO exhibits primarily the low temperature NO desorption peak and very little of the high-temperature feature. The results suggest that any Pd⁺ sites that had formed during the adsorption of NO following pretreatment in He containing 5% H₂O were not retained after NO TPD. This observation suggests that all Pd⁺ sites were oxidized to Pd²⁺ sites during the first NO TPD process. There is also a noticeable peak due to NO₂ desorbing: NO₂ is typically not observed in the TPD when using pretreatments involving water. Prior work has shown that NO₂ is formed by the reactions of NO with trace amounts of O₂ retained on the Brønsted acid sites of the zeolite.^{53,84}

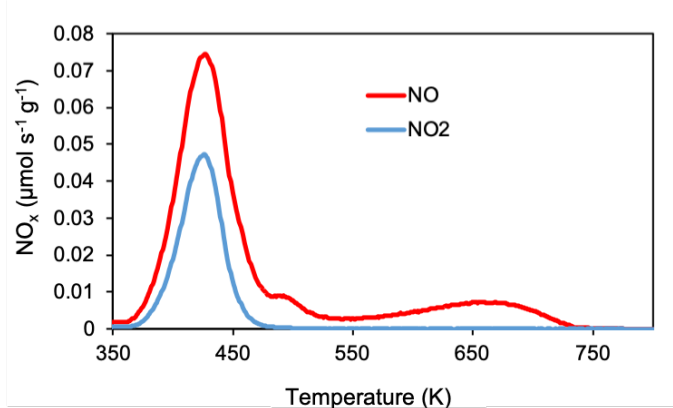


Figure 3.9: NO/NO₂ TPD profile for NO adsorbed on Pd/H-CHA. The spectra above were collected after de-greening the Pd/H-CHA in air and H₂O, adsorbing NO, and then doing TPD. Afterwards, the sample was cooled in He from 773 K to 348 K, NO was adsorbed again at 348 K, and then the TPD was done again, resulting in the spectrum presented above.

Further support for the conclusion that all Pd⁺ sites are oxidized to Pd²⁺ during NO TPD from Pd/H-CHA pretreated in 5% H₂O and He is provided by inspection of the reactor effluent during NO adsorption. Fig. 3.10a indicates that after Pd/H-CHA pretreatment in He, no NO₂ is observed during the adsorption of NO in contrast to what was observed in Fig. 3.2a. Fig. 3.10b examines the adsorption step of CO on Pd/H-CHA after a pretreatment in He (and no H₂O). In this case, there is no notable CO₂ formed in contrast to what was observed in Fig. 5b. The resulting

TPD curve for this case (Fig. 3.10b) is similar to that shown in Fig. 3.10a, exhibiting little high-temperature NO desorption. This is particularly notable for the CO experiment, because as depicted in Fig. 3.5, the addition of CO in the adsorption protocol should have significantly increased the amount of NO desorbing at higher temperature.

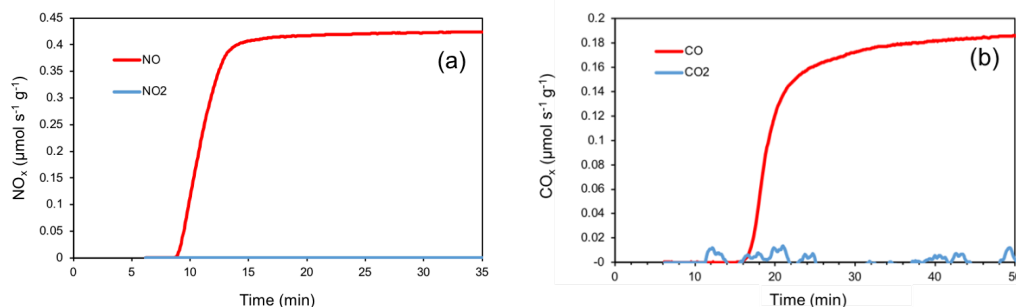
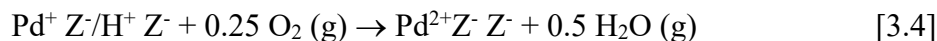


Figure 3.10: a) The NO/NO₂ profile for NO adsorbed on Pd/H-CHA during the adsorption step. NO adsorption was from a flow of He (250 mL/min) containing 200 ppm of NO at 348 K. b) The CO/CO₂ profile for CO adsorbed on Pd/H-CHA during the adsorption step. CO adsorption was from a flow of He (250 mL/min) containing 100 ppm of CO at 348 K.

The absence of a high-temperature NO peak from Pd/H-CHA that had not undergone pretreatment in the presence of H₂O prior to the adsorption of NO (or adsorption of CO and then NO) suggests that Pd⁺ is only formed through the interactions of adsorbed H₂O with either NO or CO (Reactions 3.1 and 3.3) and that upon NO desorption, Pd⁺ is re-oxidized to Pd²⁺. We hypothesize that this process involves trace amounts (~1 ppm) of O₂ present in the feed (either during pretreatment in He/air and 5% H₂O or the adsorption in He and 200 ppm NO) and occurs via the reaction:



Trace amounts are suggested because moisture and NO₂ (Alltech/Restek) traps were used to assure the purity of the He and NO feed during the pretreatment and adsorption steps (as described in the Methods Section).

To examine the possibility of reoxidation of Pd⁺ sites due to trace amounts of oxygen via Reaction 3.4, we calculated the reaction free energy at 773 K (the temperature at the end of TPD/pretreatment in He). The tables below list the reaction free energies (in kJ/mol) for a range of O₂ and H₂O partial pressures (in Pa) for the NNN Al pairs in the 6-ring and 8-ring. It is important to note that the oxidation to Pd⁺ to Pd²⁺ in the presence of only O₂ and H₂O is only possible at the listed pairs of framework Al sites. For the NNNN(6R) pair of Al sites, Pd²⁺ prevails regardless of P_{O2} and P_{H2O}. By contrast, at the NNNN(8R) and NNNN(8R) pairs of Al sites, Pd⁺ prevails regardless of P_{O2} and P_{H2O}. In light of all the experimental observations, the latter finding strongly suggests that Pd⁺ cations are not formed at these Al pairs, since they would always be strong-binding Pd⁺ sites that would be impossible to reoxidize. The results show that reoxidation of Pd⁺ due to trace amounts of O₂ is possible for Pd⁺ associated with NNN(6R) and NNN(8R) Al pairs, provided the amount of H₂O is sufficiently low. This conclusion agrees with the earlier finding that H₂O in the pretreatment is crucial for generation of high-T NO desorption sites.

Table 3.3: Reaction free energies (ΔG_{rxn}) in kJ/mol for the reoxidation of Pd^+ to Pd^{2+} at NNN Al pairs in the 6-rings and 8-rings in Pd/H-CHA, evaluated for various trace amounts of H_2O and O_2 ($P_{\text{H}_2\text{O}}$ and P_{O_2} in Pa) at 773 K.

NNN(6R)

$P_{\text{O}_2} / P_{\text{H}_2\text{O}} \rightarrow$	0.1	1	10
0.1	-4.3	3.1	10.5
1	-8.0	-0.6	6.8
10	-11.7	-4.3	3.1

NNN(8R)

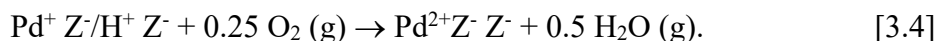
$P_{\text{O}_2} / P_{\text{H}_2\text{O}} \rightarrow$	0.1	1	10
0.1	-14.8	-7.4	-0.0
1	-18.5	-11.1	-3.7
10	-22.2	-14.8	-7.4

3.5 Conclusions

This study has examined the chemistry by which Pd^{2+} cations present in Pd-exchanged H-CHA (Pd/H-CHA) are reduced to Pd^+ cations and the stability of the latter cations to reoxidation. The results show that the reduction of Pd^{2+} to Pd^+ involves the reaction of small amounts of water, retained on the zeolite following pretreatment in water vapor, with either NO or CO via the Reactions 3.1 or 3.3:



The free energy of reaction for both processes is negative but much more strongly so for Reaction 3.3, consistent with the observation that saturating the Pd/H-CHA with CO beforehand will shift the distribution of NO desorption such that all of the NO desorbs at high temperatures. This result demonstrates that nearly all Pd^{2+} cations are reduced to Pd^+ cations via this reaction but only a subset of the Pd^{2+} cations are reduced via Reaction 3.1. Additionally, CO adsorbed on Pd^+ cations formed in Reaction 3.3 appears to be readily displaced by NO at 333 K. Finally, Pd^+ cations are found to be reoxidized to Pd^{2+} cations following TPD in He. It is suggested that this could occur via Reaction 3.4:



In summary, this work provides new insights into the redox chemistry of Pd cations present in Pd/H-CHA and the role of this chemistry in adsorption and desorption of NO.

3.6 Acknowledgements

This material is based upon work supported by the U.S. Department of Energy's Office of Energy Efficiency and Renewable Energy (EERE) under the Vehicle Technologies Program Award Number DE-EE0008213. The presented theoretical work was conducted by Dr. Jeroen Van der Mynsbrugge. Additional support for computational modeling for JVdM, MHG and ATB was provided through the U.S. Department of Energy, Office of Science, Office of Advanced Scientific Computing Research and Office of Basic Energy Sciences, Scientific Discovery through Advanced Computing (SciDAC) program. Computational resources were provided by UC Berkeley's Molecular Graphics and Computation Facility (supported by NIH S10OD023532).

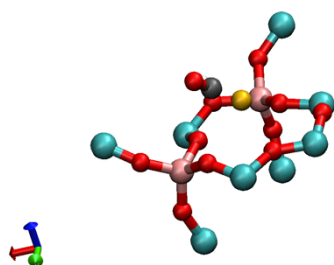
3.7 Supporting Information

XYZ coordinates of all QM/MM optimized structures used in the thermodynamics calculations are provided in the attached ZIP archive. The tables below show thumbnail images of the QM region in each structure, and specify which atoms in the corresponding XYZ file are included in the QM region.

Table S3.1: 6-ring – NNN Al pair

structure	filename	QM atoms
Pd ²⁺ Z ⁻ Z ⁻	pd2-6R-NNN.xyz	1-21
Pd ⁺ Z ⁺ H ⁺ Z ⁻	pd1-6R-NNN.xyz	1-22
(NO)Pd ⁺ Z ⁺ H ⁺ Z ⁻	pd1-no-6R-NNN.xyz	1-24

(CO)Pd⁺Z⁻H⁺Z⁻



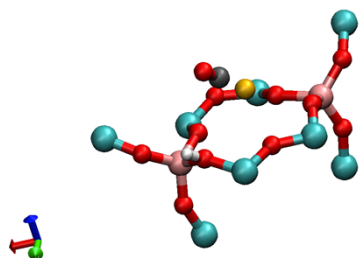
pd1-co-6R-NNN.xyz

1-24

Table S3.2: 6-ring – NNNN Al pair

structure		filename	QM atoms
$\text{Pd}^{2+}\text{Z}^-\text{Z}^-$		pd2-6R-NNNN.xyz	1-21
$\text{Pd}^+\text{Z}^-\text{H}^+\text{Z}^-$		pd1-6R-NNNN.xyz	1-22
$(\text{NO})\text{Pd}^+\text{Z}^-\text{H}^+\text{Z}^-$		pd1-no-6R-NNNN.xyz	1-24

(CO)Pd⁺Z⁻H⁺Z⁻



pd1-co-6R-NNNN.xyz

1-24

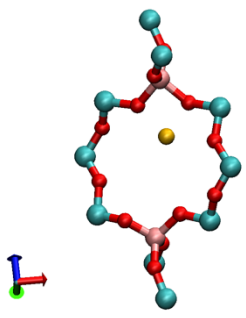
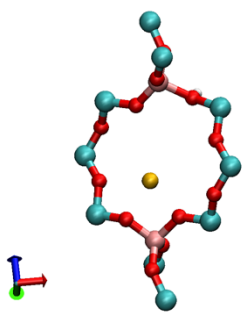
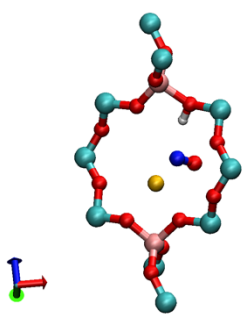
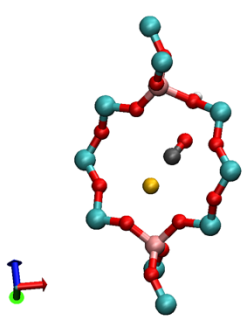
Table S3.3: 8-ring – NNN Al pair

structure	filename	QM atoms
Pd ²⁺ Z ⁻ Z ⁻	pd2-8R-NNN.xyz	1-25
Pd ⁺ Z ⁺ H ⁺ Z ⁻	pd1-8R-NNN.xyz	1-26
(NO)Pd ⁺ Z ⁺ H ⁺ Z ⁻	pd1-no-8R-NNN.xyz	1-28
(CO)Pd ⁺ Z ⁺ H ⁺ Z ⁻	pd1-co-8R-NNN.xyz	1-28

Table S3.4: 8-ring – NNNN Al pair

structure	filename	QM atoms
Pd ²⁺ Z ⁻ Z ⁻	pd2-8R-NNNN.xyz	1-25
Pd ⁺ Z ⁺ H ⁺ Z ⁻	pd1-8R-NNNN.xyz	1-26
(NO)Pd ⁺ Z ⁺ H ⁺ Z ⁻	pd1-no-8R-NNNN.xyz	1-28
(CO)Pd ⁺ Z ⁺ H ⁺ Z ⁻	pd1-co-8R-NNNN.xyz	1-28

Table S3.5: 8-ring - NNNNN Al pair

structure		filename	QM atoms
Pd^{2+}Z^-		pd2-8R-NNNNN.xyz	1-25
$\text{Pd}^+\text{Z}^-\text{H}^+\text{Z}^-$		pd1-8R-NNNNN.xyz	1-26
$(\text{NO})\text{Pd}^+\text{Z}^-\text{H}^+\text{Z}^-$		pd1-no-8R-NNNNN.xyz	1-28
$(\text{CO})\text{Pd}^+\text{Z}^-\text{H}^+\text{Z}^-$		pd1-co-8R-NNNNN.xyz	1-28

4 Investigation on the Impact of Ethene on the NO Adsorption Abilities of Pd/H-CHA

4.1 Abstract

Exhaust gas contains a variety of compounds that have been proven to be detrimental to the environment. NO, for example, is known for causing chemical smog and acid rain. To counteract these concerns, passive NO_x adsorbers or PNAs are installed downstream of the engine to capture escaping NO that is not transformed by catalytic converters at lower temperatures. The development of PNAs must also consider the presence of other components in the exhaust gas, such as water, CO, and hydrocarbons. The latter two have been studied in an effort to take advantage of their interactions with Pd: the previous chapter has shown that CO can be used to improve NO storage on Pd for PNA applications. Similar hypotheses have been proposed for the role of hydrocarbons such as C₂H₄, which can partially reduce Pd²⁺ to Pd⁺ cations that are capable of binding NO more strongly. Temperature-programmed desorption experiments have demonstrated that ethene does not have a positive effect on NO adsorption. Instead, ethene is found to take up Pd adsorption sites and to desorb in the form of CO, due to oxidation by traces of O₂ in the feed and by steam reforming. Consequently, NO storage significantly decreases compared to feeds free of ethene. In the co-feed experiments, NO enhances the ethene oxidation capabilities of Pd, producing large amounts of CO and CO₂. In addition, exposure to ethene at higher temperatures results in the formation of coke on the catalyst, blocking adsorption sites and preventing NO uptake in subsequent cycles.

4.2 Introduction

Pd/H-CHA is a popular PNA catalyst chosen for its strong hydrothermal stability and its high adsorption capacity compared to other supports.^{23,26,31} The adsorption reaction mechanism is heavily debated in the literature because of the lack of Pd⁺ reference material and as a result has numerous theories surrounding the formation and stability of the Pd adsorption site that will adsorb NO up to high temperatures (>573 K).^{19,20,23,60} However, additional insight on the adsorption reaction can be interpreted by studying the effects of other co-adsorbates. CO has been used to investigate the high temperature adsorption site in Pd/H-CHA. CO has been proposed to improve NO_x storage by forming a co-adsorbed complex with NO or producing an isocyanate complex.^{42,85} Another hypothesis is that it produces additional Pd⁺ cations that allow for more high temperature NO storage, and CO co-adsorption has been used to support this hypothesis.^{47,89} As a result, there is interest in looking into other co-adsorbates to glean additional support for the Pd⁺ cation. These co-adsorbates are also essential to study due to the hopes that automobile manufacturers will be able to take advantage of their presence in exhaust gas to bolster the adsorption efficiency of the catalyst.

Of the various co-adsorbates typically found in exhaust gas, HCs such as ethene and propylene. Propene has been reported to decrease the total NO_x storage, but shift more of the distribution of desorbing NO to higher temperatures. Malamis et al suggest that propene outcompetes NO for Brønsted acid sites reduces total NO storage.⁵² On the other hand, Liu et al report increased NO uptake when co-feeding propene and NO. They also hypothesize that propylene both partially reduces Pd²⁺ to Pd⁺ and reacts with NO to form a co-adsorbed complex that desorbs at higher temperatures.⁴⁸ Between these two experiments, the feed conditions differ significantly: Liu et al include water in their feed and use a higher concentration in O₂ compared

to that used by Malamis et al. As mentioned earlier, the difference in feed compositions in the literature significantly changes the results and the interpretations that follow.

Similarly to propene, ethene has been reported to outcompete NO for Brønsted acid sites and increase the amount of NO desorbing at higher temperatures.^{47,79} However, there is still a debate about how ethene aids NO storage. Ambast et al. have reported that ethene behaves similarly to CO by partially reducing Pd²⁺ to Pd⁺, and point to the formation of acetaldehyde as evidence of this process.⁴⁷ However, the authors also note that ethene can undergo oligomerization which produces byproducts that make it difficult to decipher the adsorption reaction.⁵⁴ Zelinsky et al. has also observed ethene oligomerization in their TPD experiments, noting that the amount of ethene uptake was four times the amount of available Pd sites.⁹⁰ Another interesting factor observed upon addition of ethene into the NO adsorption cycle is the impact of steric hindrance: Theis et al have reported that ethene improves NO adsorption on samples with few Al pairs.⁴⁹ This idea contradicts the understanding that more Al pairs allows for more Pd exchange and thus greater NO storage.^{1,49,91} The effect of ethene on the durability of the catalyst over repeated cycles is also debated. Theis et al have also suggested that ethene co-adsorption reduces the total NO_x storage over repeated tests, but this effect can be mitigated by the inclusion of H₂.^{44,49}

In this study, the effect of ethene on the NO adsorption capabilities of Pd/H-CHA was investigated. TPD and IR experiments were carried out on Pd/H-CHA using a mix of feed compositions that includes NO and ethene. The goals were to determine if ethene improves NO storage, whether it produces Pd⁺, and whether there is a combination of gases that can both improve storage without sacrificing the durability of the catalyst.

4.3 Experimental Methods

4.3.1 Adsorbent synthesis

The NH₄-CHA zeolite was provided by BASF. Palladium-exchanged CHA was prepared by incipient wetness impregnation. De-ionized water (18.2 MΩ) was added drop-wise to the NH₄-form zeolite while stirring until the total pore volume reached saturation, evidenced by a transformation of the mixture from a powder-like substance to a slurry. Assuming the same mass uptake as water, a Pd(NH₃)₄(NO₃)₂ solution (10 wt%, Sigma-Aldrich) was dissolved in de-ionized water (18.2 MΩ) to achieve a desired Pd loading. The Pd-exchanged CHA form was then dried overnight at room temperature (~298 K).

4.3.2 Temperature-programmed desorption studies

All TPD studies were conducted in a quartz reactor. Typically, 100 mg of adsorbent was loaded into the reactor. A quartz wool plug placed below the bed prevented the adsorbent from entering the effluent gas line. Before adsorption, the adsorbent underwent hydrothermal aging (HTA) in a stream of air containing 5% water heated from 348 K to 773 K at 2 K/min. The temperature was held at 773 K for 5 h in air and water vapor, and then cooled to 348 K in the absence of water vapor.

For adsorption, a feed stream containing the adsorbate was flowed over the adsorbent at 348 K until the adsorbent was saturated. The feed typically consisted of about 400 ppm of NO in a He balance flowing at 250 mL/min. 1000 ppm CH₄ was added to the NO/He stream as an inert tracer. For experiments using C₂H₄, about 300 ppm of C₂H₄ was added to the He stream. He (purity of 99.999% from Praxair) was dried by passage through moisture trap (Restek Moisture Trap, <10 ppb water) and NO (1.03% NO in He balance from Praxair) was purified by passage through traps to remove moisture and NO₂ (Alltech Gas Drier, <1 ppm NO₂ and H₂O). The air carrier gas was

provided by Praxair and was rated as extra dry (<10 ppm H₂O). The adsorption was monitored using an MKS 2030 Multigas analyzer, a non-dispersive infrared (NDIR) instrument. The concentration of adsorbate in the effluent was measured, and the adsorbate and CH₄ were shut off once the effluent concentration of adsorbate had reached the inlet value. The adsorbent was then purged with He until the concentration of adsorbate had returned to the level observed before the start of the adsorption step. A purge stream of He (250 mL/min) was fed to the reactor immediately after adsorption to remove any weakly bound adsorbates. The adsorbed adsorbate was then desorbed as the adsorbent was heated from 348 K to 773 K at 10 K/min, and subsequently held at 773 K for 20 min. Throughout this period the concentrations of adsorbates in the effluent were monitored by non-dispersive IR spectroscopy. Following a TPD experiment, the adsorbent was treated in one of several ways in order to prepare it for the next adsorption cycle. This typically involved cooling the adsorbent from 773 K back to 348 K in a defined gas mixture (e.g., He, air, air plus water vapor). This last step is referred to as a pretreatment, and for future discussion, pretreatment refers to the steps performed before an adsorption measurement when the adsorbent undergoes several adsorption/desorption cycles.

4.3.3 IR spectroscopy

The procedure for the initial treatment of Pd/H-CHA and pretreatment between NO adsorption experiments is similar to that used for the TPD experiments. About 30 mg of adsorbent was compressed into a pellet that was placed into a Harrick High Temperature cell with CaF₂ windows. The cell was heated resistively and the temperature was monitored with a thermocouple. The adsorbent was exposed to NO and/or C₂H₄ for 15 min, after which the NO flow was stopped and the TPD ramp was started. In-situ transmission IR experiments were conducted using a Nicolet 6700 spectrometer operated at 4 cm⁻¹ resolution. Each spectrum was obtained by averaging 256 scans. Background spectra of Pd/H-CHA, taken at the same temperatures as spectra recorded during a TPD IR experiment, were subtracted from the spectra of NO adsorbed on Pd-CHA.

4.4 Results and Discussion

4.4.1 NO and C₂H₄ storage on H-CHA

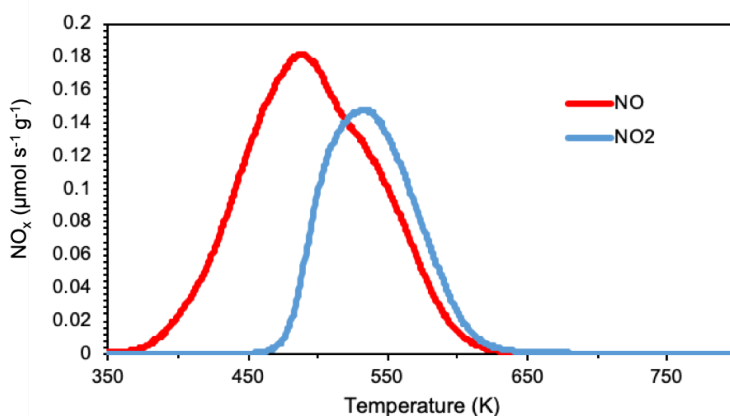


Figure 4.1. NO and NO₂ TPD profiles for NO adsorbed on H-CHA. H-CHA was de-greened in air and NO was adsorbed in He balance.

H-CHA was heated in air from 348 K to 773 K at 2 K/min and held at 773 K for 1 h. The sample was then cooled in air from 773 K to 348 K. Adsorption was from a flow of He containing 400 ppm of NO at 348 K. During TPD, the temperature was ramped from 348 K to 773 K at 10 K/min and then held at 773 K for 20 min in He. Similar to previously reported results, H-CHA adsorbs NO and releases it in the lower temperature range (<573 K) as NO and NO₂. In the absence of water in the pretreatment step, H-CHA is able to store 325 μmol of NO_x per gram catalyst. NO stores primarily as NO⁺ and some smaller amounts of nitrates according to IR spectroscopy studies.^{53,80} As shown in Chapter 2 of the manuscript, Pd is necessary to achieve high-temperature NO desorption. NO release at this temperature is not ideal for PNA applications.

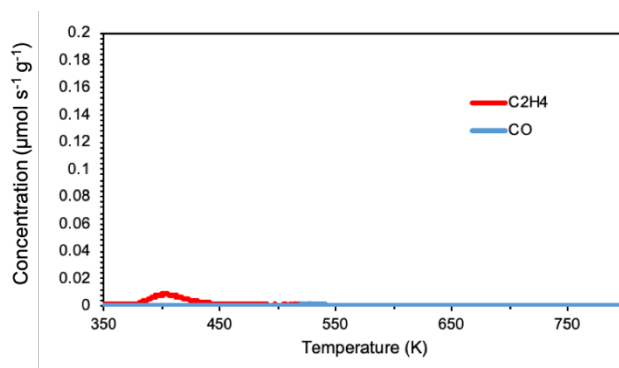


Figure 4.2: CO and C₂H₄ TPD profiles for C₂H₄ adsorbed on H-CHA. H-CHA was de-greened in He and C₂H₄ was adsorbed in He balance.

As seen in Fig. 4.2, H-CHA is unable to adsorb significant amounts of ethene at 428 K. The lack of additional byproducts, such as CO, ethane, and CO₂, also points to the fact that the BAS are incapable of catalyzing oligomerization and other reactions at the feed conditions. These findings are consistent with those reported by by Ryu et al., who tested C₂H₄ adsorption capacities of various H-zeolites.⁹² Therefore, it is concluded that BAS do not play a significant role on the influence of ethene on NO storage.

4.4.2 NO and C₂H₄ storage on Pd/H-CHA

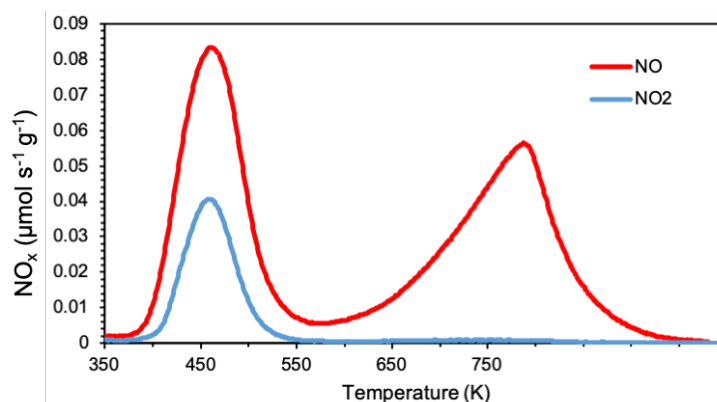


Figure 4.3: NO and NO₂ TPD profiles for NO adsorbed on Pd/H-CHA. Pd/H-CHA was de-greened in air and NO was adsorbed in He balance.

The effect of C₂H₄ on NO adsorption was tested. First, the NO adsorption capacity of Pd/H-CHA (Si/Al = 11, Pd weight % = 0.94) was measured. For these experiments, Pd/H-CHA was first de-

greened in a feed of air and 5% H₂O by heating the sample to 773 K at 2 K/min and held there for about 5 h. Then the sample was cooled back to 348 K in air. A feed of about 400 ppm NO in He balance was fed to the reactor until it was saturated with NO. The sample was purged of weakly adsorbed NO using a stream of He, and then heated at 10 K/min. As seen in earlier chapters, Pd/H-CHA adsorbs NO and produces two desorption peaks during TPD centered around 430 K and 750 K. As discussed in earlier chapters, the high-temperature peak in the TPD spectrum corresponds to NO desorbing from Pd⁺, and the low-temperature desorption peak corresponds to NO released from Pd²⁺ sites.^{19,84} Pd/H-CHA stored about 97 μmol of NO per gram catalyst, corresponding to about 1.10 NO/Pd. One NO/Pd is considered the limit due to NO expected to adsorb on a single Pd cation at most, assuming 100% ion-exchanged Pd. The additional NO is likely due to NO stored on BAS that were not completely blocked by the inclusion of water in the pretreatment or degreening step. This additional NO also explains the appearance of the NO₂ in the TPD spectrum, which forms alongside NO upon desorption on BAS.⁵³

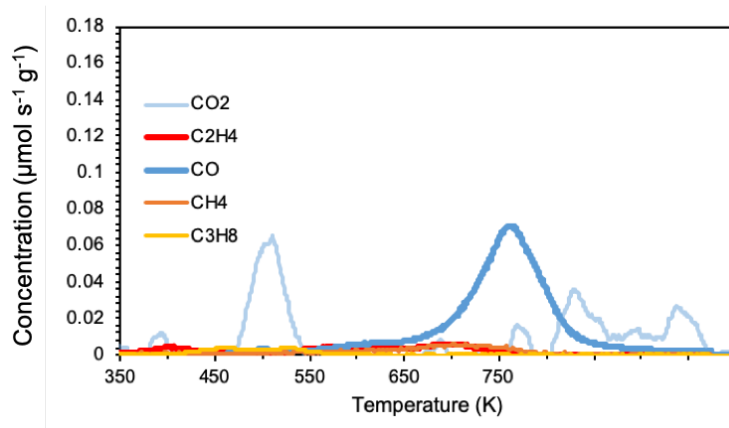


Figure 4.4: TPD profiles for C₂H₄ adsorbed on Pd/H-CHA. Pd/H-CHA was first pretreated in He, and C₂H₄ was adsorbed in He balance.

Next, the ethene adsorption capacity of Pd/H-CHA was investigated. The sample was pretreated in He from 773 K to 348 K, and then fed about 300 ppm of ethene in He balance at 348 K. It was found that the Pd/H-CHA does store significant amounts of ethene. A small amount of ethene desorbs at lower temperatures (~400 K), but the majority of any adsorbed ethene desorbs as CO₂ (16 μmol per gram catalyst) at low temperatures (500 K) and CO (47 μmol per gram catalyst) at higher temperatures (~730 K). Both of these TPD peaks, indicating the oxidation of ethene by Pd or precious group metals, have previously been reported.^{93,94} The CO_x appears despite the absence of O atoms in the feed. For the He only pretreatment, it is likely that the trace amounts of O₂, documented as an issue in Chapter 3, are involved in reacting with the ethene to produce CO. To investigate this possibility further, a temperature-programmed reduction (TPR) experiment was conducted.

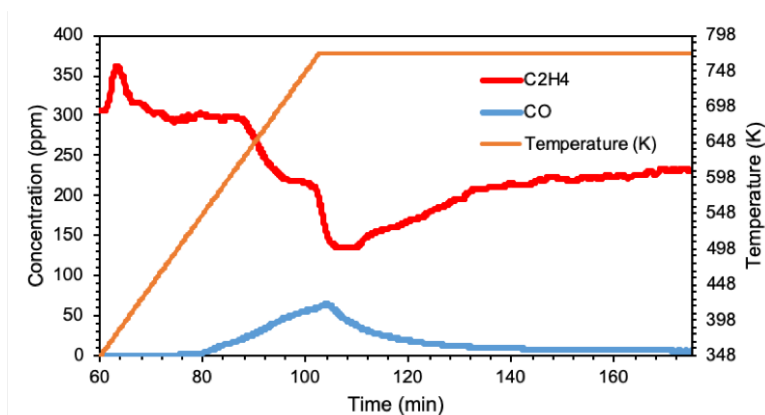


Figure 4.5: C_2H_4 and CO TPR profiles for Pd/H-CHA (left axis) and the temperature (right axis). Samples were cooled in He from 773 K to 348 K, and then C_2H_4 was fed in He balance while increasing the temperature at 10 K/min to 773 K. It was held at 773 K for an hour. At high temperatures, CO begins to be produced before falling to a steady ~ 4 ppm, while C_2H_4 fell with the peak of CO before returning and holding at around 250 ppm.

In this experiment (See Fig. 4.5), Pd/H-CHA was pretreated in He and cooled from 773 K to 348 K. Then about 300 ppm of ethene was flowed in He balance at 348 K. Once the catalyst was saturated, the temperature was ramped at 10 K/min to 773 K, still in a feed of ethene in He. There is a peak of ethene released upon the onset of the temperature ramp. This is likely ethene that was weakly adsorbed to Pd/H-CHA, which would have normally been released during the purge step between adsorption and TPD in previous experiments. Ethene holds is retained up to 600 K, where ethene concentration decreases as CO begins to rise. At higher temperatures, the Pd can catalyze the reaction of ethene to CO, resulting in a peak of CO.⁹⁵ However, due to the limited amount of O_2 in the feed, the CO signal peaks and then falls to about concentrations of 8 ppm, while the ethene signal increases again. This corresponds to an O_2 concentration in the feed of about 4 ppm. The large desorption peak of CO observed in Fig. 4.4 when C_2H_4 is adsorbed alone on Pd/H-CHA could be the result of trace O_2 reacting with ethene and storing as CO or an unknown $C_xH_yO_z$ complex. Alternatively, the O atoms could also come from PdO present in the catalyst alongside ion-exchanged Pd cations.⁹³ However, repeated ethene cycles in the absence of O atom sources in the feed have shown that this CO desorption peak persists, which would not happen if there was a limited supply of PdO. After several hours at 773 K, the ethene signal returns to feed level concentrations.

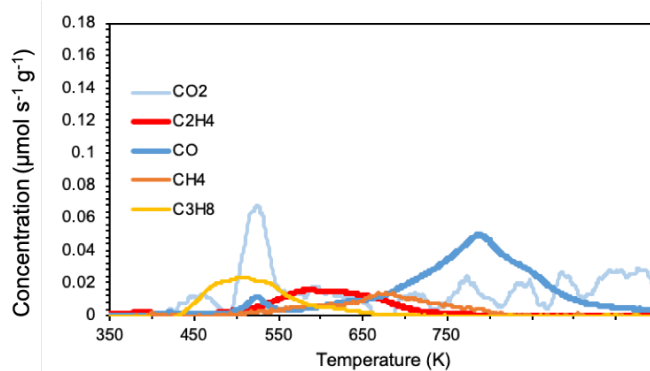


Figure 4.6: TPD profiles for C_2H_4 adsorbed on Pd/H-CHA. Pd/H-CHA was first pretreated in He and 5% H_2O , and C_2H_4 was adsorbed in He balance.

For comparison, ethene adsorption after adsorbent pretreatment in He and H₂O was investigated, both to serve as a comparison to Fig. 4.4 and to assess the previously reported beneficial impact of water on oxidation of HCs.^{92,96} In Fig. 4.6, there are additional products observed that were not present in the absence of H₂O, such as propane and methane. Compared to the He only pretreated sample (see Fig. 4.4), there is more CO_x desorption (57 μmol CO per gram catalyst and 11 μmol CO₂ per gram catalyst) and there are additional byproducts including CH₄ and C₃H₈. The total amount of C moles desorbing from Pd/H-CHA is greater for the cycle with water present during the pretreatment (165 μmol of C per gram catalyst) than the cycle without water in the pretreatment step (95 μmol of C per gram catalyst). Ryu et al. have reported that while water and C₂H₄ compete over Pd adsorption sites on other zeolites, this behavior is actually reversed for Pd/H-CHA, where the inclusion of water in the feed actually doubled the ethene adsorption capacity. These authors also observed that in wet conditions, Pd/H-CHA converted more of the ethene into other hydrocarbons.⁹² However, comparable amounts of CO_x were formed even without water. From these results, it is evident that water assists the storage of ethene, but is not the largest contributor to the formation of CO_x when water is absent from the feed.⁹² Therefore, It is likely that trace amounts of O₂ present in feed stream are responsible for ethene oxidation.

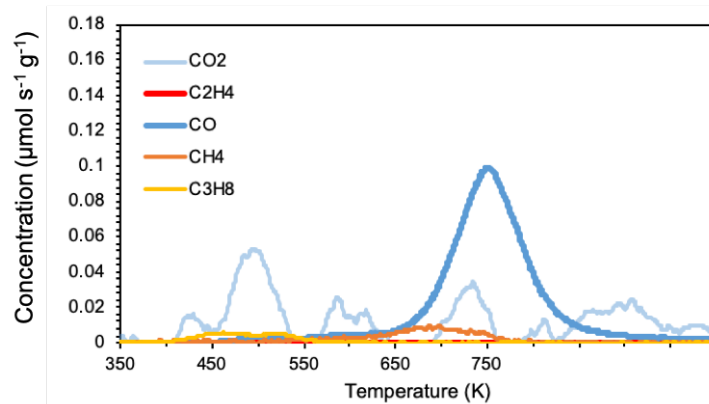


Figure 4.7: TPD profiles for C₂H₄ adsorbed on Pd/H-CHA. Pd/H-CHA was first pretreated in He, and then saturated with air for 20 min. After stopping air flow and purging for 1 h in He, C₂H₄ was adsorbed in He balance.

A sequential adsorption experiment was conducted in order to gauge the role of O₂ in the formation of CO_x from ethene adsorption. In this experiment, Pd/H-CHA, following a pretreatment in He, is exposed to a flow of air containing 20% O₂ for about 20 min. The air flow was then stopped, and the feed switched to He. The sample was purged of weakly adsorbed O₂ with the He stream for an hour. Then, 300 ppm of ethene in He balance was fed to the catalyst for about 20 min. After which, the ethene flow was ceased, and after purging any weakly adsorbed species, TPD was started. By exposing the Pd/H-CHA to air prior to the introduction of ethene, it is expected that a small portion of the O₂ will store on the sample and be available to help oxidize ethene. No notable products were observed in the effluent when flowing in air alone and during the He stream purge. The TPD shown in Fig. 4.7 reveals a spectrum similar to that seen in Fig. 4.4. However, there is a small increase in the of total moles of C desorbed: 119 μmoles of C per gram catalyst compared to the 95 μmoles of C per gram catalyst in Fig. 4.4. All of the products in the TPD increase to a small degree relative to those observed in Fig. 4.4. This experiment provides additional support for the hypothesis that O₂ is responsible for the adsorption and conversion of ethene into CO_x and HCs.

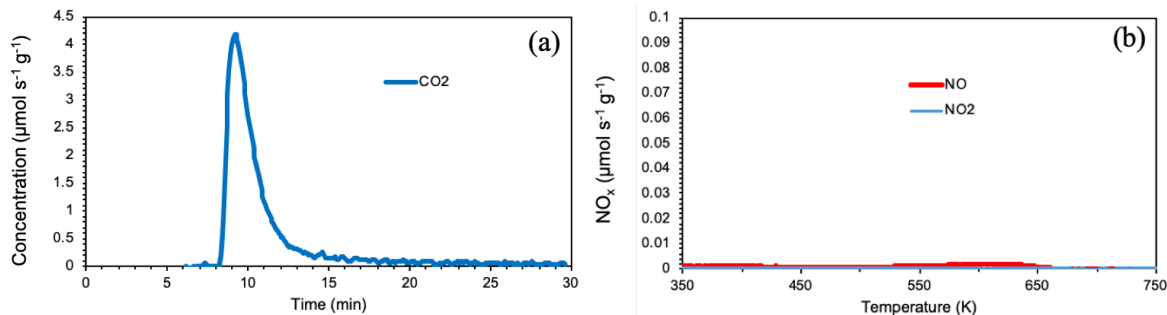


Figure 4.8: In Fig. 4.8a, the CO₂ profile is shown during a high-temperature air treatment for a Pd/H-CHA sample that recently underwent C₂H₄ TPR. Exposure to C₂H₄ at high temperatures results in buildup of coke on the sample: the Pd/H-CHA was then exposed to a feed of air at 773 K for about 20-30 min to burn off coke. As a result, a peak of CO₂ is observed. In Fig. 4.8b, the NO_x TPD profile is shown for a sample that did not undergo a high-temperature air treatment. Without this air treatment, the coke leftover from C₂H₄ TPR will remain and block NO adsorption from occurring in subsequent cycles.

The ethene TPR experiments also raised the issue of coke on the catalyst. Evidence of coke can be found when flowing air at high temperatures (773 K) through the catalyst (following ethene TPR), upon which a peak of CO₂ is observed indicating combustion of carbon from the catalyst (See Fig. 4.8a). This coking also causes issues in subsequent cycles, where the coke blocks NO from adsorbing on both Pd²⁺ and Pd⁺ sites, even after pretreatments involving water. It has been previously demonstrated that Pd is more prone to deactivation resulting from high-temperature reactions with ethene compared to other precious metals such as Pt and Rh.⁹⁵ To illustrate this point, Fig. 4.8b shows the TPR CO₂ profile observed during a high-temperature air treatment of a Pd/H-CHA sample that had recently undergone C₂H₄ TPR. During the subsequent NO adsorption cycle, no NO adsorption could be observed. To regenerate the catalyst for NO storage, a high-temperature air treatment, such as heating the catalyst at 773 K in a feed of air for 20-30 min, was necessary to burn off the accumulated coke. Afterwards, the NO storage capacity of Pd/H-CHA returned, and the TPD spectra look similar to that shown in Fig. 4.3.

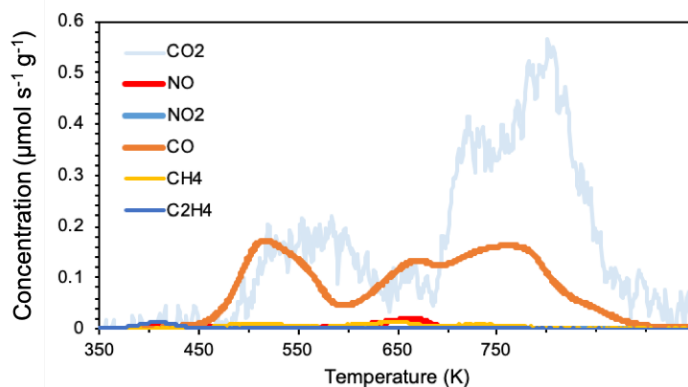


Figure 4.9: TPD spectra for NO and C₂H₄ adsorption on Pd/H-CHA. Pd/H-CHA was pretreated in air and H₂O and NO and C₂H₄ were adsorbed in He balance. NO and C₂H₄ react with one another resulting in additional byproducts like CO and small amounts of CH₄.

NO and ethene co-adsorption was investigated to see if ethene could improve total NO storage or promote additional NO storage at high-temperature adsorption sites. The adsorption protocol was similar as the previous TPD experiments (pretreated in air and H₂O), but now the

feed consisted of both 400 ppm NO and about 300 ppm of ethene in He balance. Fig 4.8 shows the formation of a myriad of products, including NO, CO, and other hydrocarbons. However, the beneficial effects on NO are not observed: although NO is desorbed by 700 K, the total storage is significantly lower than what is observed when NO is adsorbed alone (only about 10 μmol NO per gram catalyst compared to 97 from Fig. 4.3). Instead, there is a large amount of CO_x that is released during the TPD (807 μmol CO_x per gram catalyst). Gupta et al. have suggested that NO acts as a promoter to help oxidize ethene.²³ This promotional effect from NO could explain why the CO desorption is so much higher compared to ethene only adsorption. In addition, there are no notable C-based products that are produced during the adsorption step to suggest that C_2H_4 reacts with Pd^{2+} to partially reduce it to Pd^+ . In these co-feed experiments, ethene has been hypothesized to react with Pd to produce $\text{C}_2\text{H}_4\text{O}$ and Pd^+ , but $\text{C}_2\text{H}_4\text{O}$ was not observed.^{47,54,90} Similar to the effects observed when conducting ethene TPR studies on Pd/H-CHA, co-feeding NO and ethene also results in a loss of high-temperature NO desorption sites in subsequent cycles. Unlike the consequence of ethene TPR, the low-temperature NO_x desorption peaks are still observed (See Fig. 4.10), suggesting that exposure to ethene at higher temperatures may be necessary to completely block all Pd sites. However, the Pd/H-CHA is still unable to reach the same level of storage as reported in Fig. 4.3 (97 μmol NO per gram catalyst), only storing a total of 32 μmol NO per gram catalyst. Another high-temperature air treatment is needed to regenerate the high-temperature adsorption sites.

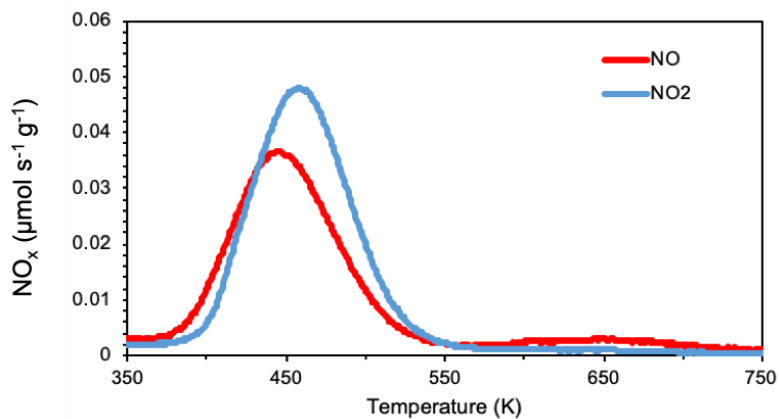


Figure 4.10: NO and NO_2 TPD profiles for Pd/H-CHA after adsorbing NO in He balance. First, Pd/H-CHA pretreated in air and H_2O was exposed to NO and C_2H_4 in He balance. Then, a TPD experiment was conducted, resulting in the desorption profiles seen in Fig. 4.6. Afterwards, the sample was then pretreated in He and H_2O from 773 K to 348 K. The sample was exposed to NO in He balance, and then TPD was conducted again, resulting in the TPD profile above. Due to the ethene exposure in the previous cycle, high-temperature NO desorption sites were blocked.

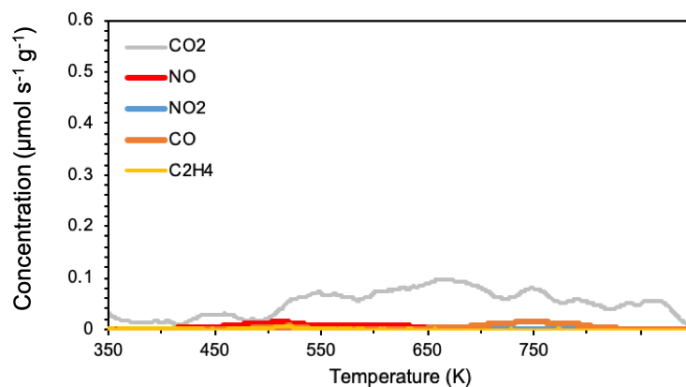


Figure 4.11: TPD spectra for C₂H₄ then NO adsorption on Pd/H-CHA. Pd/H-CHA was pretreated in air and H₂O. The catalyst was first saturated with C₂H₄ in He balance for about 20 min, then the C₂H₄ flow was stopped, and the sample was exposed to NO in He balance.

In addition to co-adsorption, ethene and NO can be sequentially adsorbed to tease out additional insight into the adsorption mechanisms of the two adsorbates. In sequential adsorptions (See Fig. 4.11), the Pd/H-CHA, following a pretreatment in air and H₂O, is exposed to 300 ppm of ethene in He balance for about 20 min. The ethene flow is then shut off, and the any weakly adsorbed species are purged. Then, Pd/H-CHA is exposed to 400 ppm NO in He balance. Once the adsorbent is saturated, the NO flow is ceased, and after purging any weakly adsorbed species, TPD is started. This technique was used in Chapter 3 to examine the impact of CO on the NO storage abilities of Pd/H-CHA. Unlike CO though, ethene does not enhance NO storage, and in fact the sequential adsorption experiment stores less NO_x and CO_x than the co-adsorption experiment: there is significantly less CO_x desorbed at intermediate and high temperatures (only desorbing 123 μmol of C per gram catalyst compared to 814 μmol of C per gram catalyst from Fig. 4.9). This is likely due to the absence of NO to react with C₂H₄ and provide additional sources of O atoms to produce CO. Combined with the lack of high-temperature NO desorption, it can be concluded that under these conditions, ethene does not assist NO storage on Pd/H-CHA, but the reverse statement is true.

4.4.3 IR spectroscopy of NO and C₂H₄ on Pd/H-CHA

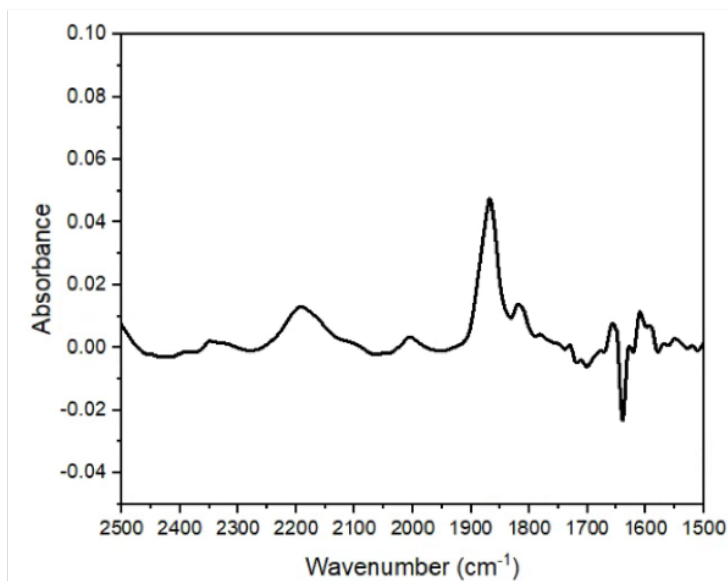


Figure 4.12: TPD IR spectrum for NO adsorbed on Pd/H-CHA taken at 348 K. A reference spectrum was taken of Pd/H-CHA before NO adsorption, and then subtracted from the spectrum taken after NO adsorption.

IR spectroscopy was conducted to identify the adsorbed NO and ethene species that desorb during TPD. Pd/H-CHA was de-greened by heating in air and 5% H₂O from 348 K to 773 K at 2 K/min and holding at 773 K for 5 h. The sample was then cooled to 348 K in air. NO adsorption was from a flow of He (250 mL/min) containing 400 ppm of NO at 348 K. During TPD, the temperature was ramped from 348 K to 773 K at 10 K/min and then held at 773 K for 20 min in He. Fig. 4.12 depicts the IR spectrum taken at 348 K after saturating the sample with NO. There are two distinct NO-Pd bands, corresponding to NO bound on Pd²⁺ and Pd⁺, at 1860 cm⁻¹ and 1810 cm⁻¹. There's also a smaller band around 2160 cm⁻¹, likely due to remaining NO⁺ species that were not completely blocked by water: this explains the observed NO₂ desorption feature in the TPD results (see Fig. 4.3), which is not normally observed after pretreatments including water.

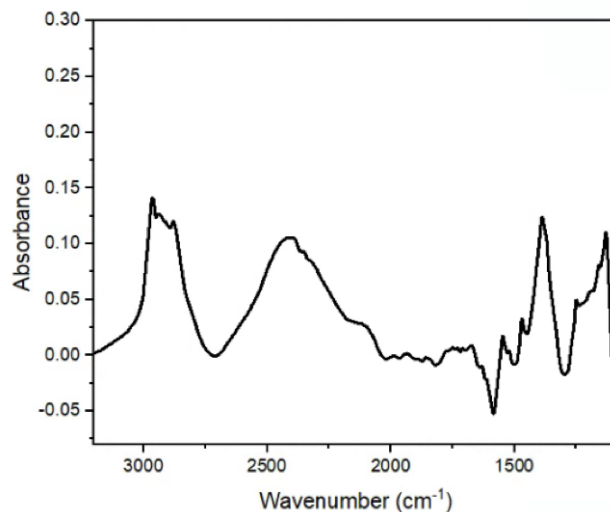


Figure 4.13: TPD IR spectrum for C_2H_4 adsorbed on Pd/H-CHA taken at 348 K. A reference spectrum was taken of Pd/H-CHA before C_2H_4 adsorption, and then subtracted from the spectrum taken after C_2H_4 adsorption.

For comparison, the IR spectrum was taken for C_2H_4 adsorption on Pd/H-CHA in Fig. 4.13. There are numerous bands that have been attributed to evidence of ethene adsorption on the zeolite and Pd. The bands ranging from 2700 to 3000 cm^{-1} have been assigned to interactions between the exchanged metal and ethene.^{77,97,98} Other significant bands include a band at 1130 cm^{-1} and 1380 cm^{-1} , which have been proposed to be methoxy and formate species respectively (involving C-H or COO stretches).⁹⁸ These species could be the precursors to CO_x species observed during TPD. There is an absence of a band around 1680 cm^{-1} , which has been attributed to the interactions between ethene and BAS, supporting the results observed in Fig. 4.2 where no NO adsorption was observed on H-CHA.²³ There are some broader bands at around 2300-2700 cm^{-1} that have been attributed to water, specifically O-H vibrations, as previously seen in Section 2.4.1 covering H_2O on H-CHA and Pd/H-CHA.^{76,78} In the TPD experiment in Fig. 4.4, all of the ethene comes off in the form of CO. However, there are no CO-Pd bands in the 2000-2300 cm^{-1} range, indicating that CO produced in the experiment shown in Fig. 4.4 likely originates from ethene or the aforementioned methoxy/formate species, and then reacts with water or trace O_2 to produce CO.^{23,90}

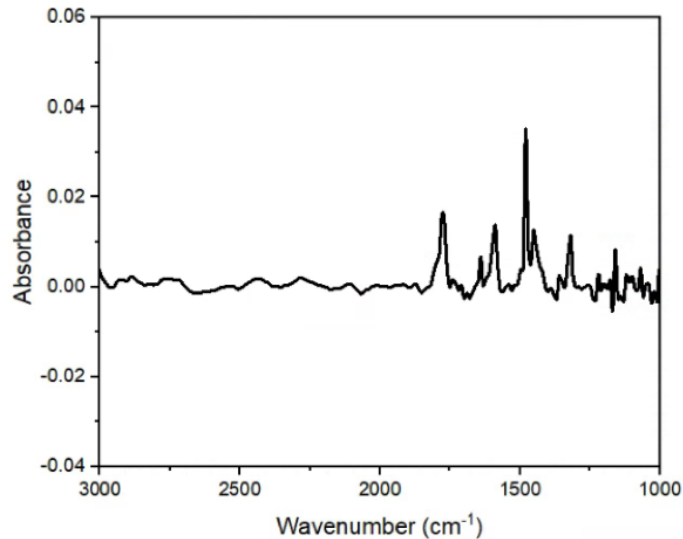


Figure 4.14: TPD IR spectrum for NO and C₂H₄ adsorbed on Pd/H-CHA taken at 348 K. A reference spectrum was taken of Pd/H-CHA before NO and C₂H₄ adsorption, and then subtracted from the spectrum taken after NO and C₂H₄ adsorption.

To identify the adsorbed species in Fig. 4.7 and 4.9, the IR spectrum was also obtained for NO and C₂H₄ co-adsorption in He balance. As seen in Fig 4.14, there are a few new notable IR bands not previously observed when NO is adsorbed alone. There are no characteristic NO-Pd bands in the 1800-1900 cm⁻¹ range, clearly showing that ethene does not improve NO adsorption on Pd at the typical adsorption sites. Instead, there is a feature at around 1770 cm⁻¹, which has previously been reported as a NO and hydrocarbon co-adsorbed complex: Khivantsev et al. have attributed this feature to a NO and C₂H₄ complex, while Hamid et al. assign this band to a NO and C₃H₆ complex instead.^{17,99} The band at 1600 cm⁻¹ has also been claimed to be a result of NO and ethene co-adsorption.⁴⁷ Unfortunately, the exact composition of this co-adsorbed complex has yet to be identified, and the rest of the literature has loosely labeled the species as Pd(II)(NO)(C₂H₄). There are additional bands at 1480 and 1300 cm⁻¹ have been attributed to ethene or some C-H signal, such as CH₂ scissoring or CH₃ bending.^{47,99} More interestingly, there is an absence of any bands (2000-2300 cm⁻¹) that indicate the adsorption of CO on Pd sites, despite most of the ethene in the TPD experiment coming off in the form of CO.^{17,40} Though it is difficult to ascertain the exact exchanged species, there is enough evidence to demonstrate that NO does form a co-adsorbed complex with ethene.

4.4.4 Effect of NO on C₂H₄ oxidation on Pd/H-CHA

The TPD spectra show a much larger amount of CO_x desorbing when NO and ethene co-adsorbing compared to ethene adsorption on its own. Because of the absence of CO bands, it is hypothesized that CO does not adsorb on Pd, but instead reacts with water or NO during the pretreatment step to produce the CO and CO₂ observed during TPD. Pd-based zeolites have found usage in HC trapping before, and are capable of catalyzing the oxidation of ethene, even without an excess amount of air in the exhaust gas.^{54,90,92,100} Ambast et al. have also proposed that Pd is capable of both adsorbing excess ethene and catalyzing the oxidation of ethene; O₂ can react with ethene adsorbed on Pd to produce CO_x.⁴⁷ The most likely case is that a combination of processes

causes the production of CO_x catalyzed by Pd. Ethene adsorbs on the Pd, and upon desorption, alongside with the water or NO, at elevated temperatures results in the production of CO, while at lower temperatures Pd can catalyze the formation of CO_2 via a steam reforming or water-gas shift reaction. Although acetaldehyde was not observed during the adsorption step in our experiments, the difference in feed conditions (Ambast et al. also fed air and water together with NO and ethene) likely affected the results.⁴⁷ Ryu et al. reported that Pd allows for H-zeolites to store ethene, though the exact mechanism is difficult to ascertain between π electron donation from the C=C to the unoccupied Pd^{2+} orbitals vs. π -back donation of d orbital Pd^{2+} electrons to the antibonding orbitals of ethene. In addition, they directly note that increasing the Pd^{2+} population in their Pd-zeolites led to a significant increase in the oxidation of ethene to CO_2 .⁹² Zelinsky et al. also found that hydrothermal aging treatments, used to convert more non-reducible Pd^{2+} into $[\text{Pd}(\text{OH})]^+$, hurt ethylene oxidation activity: though we have disproved the formation of $[\text{Pd}(\text{OH})]^+$ in our experimental conditions, our equivalent reduced Pd species, Pd^+ , could also be expected to have reduced ethylene activity.⁹⁰ Limited high-temperature desorption of NO may stem from the suppression of Pd^+ formation in favor of Pd^{2+} reacting with ethene. These results suggest that Pd/H-CHA functions as a strong HC trap, but still requires some form of a regeneration step to prevent coke from blocking adsorption sites. Future work should take additional steps to better identify the sources of O for ethene oxidation by utilizing isotopically labeled O_2 and H_2O in conjunction with mass spectroscopy.

4.5 Conclusions

The role of ethene on the NO adsorption abilities of Pd/H-CHA was investigated. H-CHA is unable to adsorb ethene, meaning all adsorption of ethene on Pd/H-CHA is due to Pd. Pd/H-CHA adsorbs ethene and releases it during TPD as CO at high temperatures (750 K) and some CO_2 at lower temperatures (500 K). IR spectroscopy was used to observe various C-H and COO vibrations, suggesting ethene binds on Pd as methoxy/formate species. There is also an absence of CO-Pd bands in the 2000-2300 cm^{-1} range; this suggests CO_x is instead produced upon desorption of adsorbed ethene. In the absence of O_2 in the feed, this CO_x likely comes from trace amounts of air that reacts with ethene. Water, when included in the pretreatment, can also react with adsorbed ethene, undergo steam reformation to produce CO_x , and produce additional HCs like methane and propane. Experiments involving ethene (including co-adsorption, sequential adsorption, and ethene TPR) result in the formation of coke on the catalyst surface that blocks NO adsorption on Pd/H-CHA in cycles immediately following the ethene exposure. High-temperature air treatment (773 K) is necessary to burn off the coke, producing CO_2 and allowing Pd/H-CHA to adsorb NO again. Previous studies have claimed ethene behaves similarly to CO, and reduces Pd^{2+} to Pd^+ to improve total NO storage, citing the production of acetaldehyde in the adsorption step as evidence for this reduction. However, no notable byproducts were found during the adsorption step. Instead, it was determined that the Pd^{2+} acts as both the ethene adsorption site and catalyst for ethene oxidation. Rather than improving NO storage, the NO acts as a facilitator for ethene oxidation. Experiments involving ethene and NO in He balance primarily result in oxidation of ethene to CO and CO_2 . Pd/H-CHA possesses a large capacity for HC trapping, but will require a regenerative, high-temperature air treatment to deal with the dangers of coking.

4.6 Acknowledgements

This material is based upon work supported by the U.S. Department of Energy's Office of Energy Efficiency and Renewable Energy (EERE) under the Vehicle Technologies Program Award Number DE-EE0008213.

5 Conclusions

This dissertation has utilized TPD and IR spectroscopy together with DFT analysis to uncover the nature of NO adsorption on Pd/H-CHA. Pd cations exchanged into CHA are found to be present exclusively as Pd²⁺ cations. These species adsorb NO but desorb it at low temperatures (350-550 K). Pd⁺ cations are formed by reduction of Pd²⁺ cations. It is shown that Pd⁺ cations can be formed during NO adsorption via reaction of NO and H₂O that had adsorbed on the zeolite during pretreatment of Pd/H-CHA in H₂O in He. This process can be described by the reaction $1.5 \text{ NO} + \text{Pd}^{2+}\text{Z}^-\text{Z}^- + 0.5 (\text{H}_2\text{O})\text{H}^+\text{Z}^- \rightarrow (\text{NO})\text{Pd}^+\text{Z}^-\text{H}^+\text{Z}^- + 0.5 \text{ NO}_2 + 0.5 \text{ H}^+\text{Z}^-$. DFT calculations confirmed that the free energy of this process is favorable for Pd²⁺ cations located various pairs of cation exchange sites. The validity of this reaction is also supported by the observation that the amount of NO₂ formed during NO adsorption at 348 K, is equivalent to amount of Pd⁺ sites formed. Adsorption of NO on Pd⁺ sites is stronger than on Pd²⁺ sites, as shown by DFT calculations, and correspondingly, the temperature for desorption of NO from these sites is high (750 K). IR spectroscopy was used to assess whether NO adsorbed on Pd²⁺ and Pd⁺ could be identified with specific bands, as had been suggested by the literature. A notable finding is that NO adsorbed on both oxidation states of Pd exhibit bands at 1810 cm⁻¹ and 1860 cm⁻¹, a finding supported by DFT estimates of the N-O vibrational frequencies for adsorbed NO. Therefore, an important conclusion of this study is that IR spectroscopy cannot be used to determine the presence of NO adsorbed on Pd²⁺ and Pd⁺ unambiguously.

Attempts were made to identify the presence of Pd⁺ by EPR. However, it was not possible to obtain definitive evidence for these cations by EPR. One possibility is that Pd⁺ cations are oxidized to Pd²⁺ cations due to exposure to trace amounts of O₂ prior to measurement of the EPR spectrum. This possibility is supported by theoretical calculations showing that even trace amounts (ppm concentrations) of O₂ are sufficient to transform Pd⁺ back into Pd²⁺. Another reason is the sensitivity of the Pd oxidation state to temperature, which may cause the produced Pd⁺ to transform to an EPR-silent species when conducting experiments at very low temperatures. In addition, experiments that have successfully observed Pd⁺ in EPR have done so in different conditions than those employed in cold start. Future work could expand upon the theoretical work to determine the stability of Pd⁺ under these colder temperatures (10-20 K) or could attempt to increase the Pd weight loading to increase the EPR signal.

Prior studies of NO adsorption on Pd/H-CHA have suggested that the co-adsorption of CO strengthens the adsorption of NO. No evidence for CO and NO co-adsorption was observed by either IR or TPD. In fact, NO was found to quantitatively displace any CO previously adsorbed onto Pd/H-CHA, a result that was supported by DFT calculations. Pd⁺ sites can also be formed by the adsorption of CO prior to or together with the adsorption of NO. In this case, the reduction of Pd²⁺ sites occurs via the reaction $1.5 \text{ CO} + \text{Pd}^{2+}\text{Z}^-\text{Z}^- + 0.5 (\text{H}_2\text{O})\text{H}^+\text{Z}^- \rightarrow (\text{CO})\text{Pd}^+\text{Z}^-\text{H}^+\text{Z}^- + 0.5 \text{ CO}_2 + 0.5 \text{ H}^+\text{Z}^-$. Here too, the proposed reduction process is supported by DFT calculations and by the observation that the amount of CO₂ formed is equivalent to the amount of Pd⁺ sites formed. Thus, the only effect of CO adsorption was the reduction of Pd²⁺ to Pd⁺ cations.

Another finding of the present work concerns the influence of ethene co-adsorption on NO adsorption on Pd/H-CHA. Ethene on its own is capable of adsorbing on Pd/H-CHA, and is released primarily in the form of CO and CO₂. Although prior literature has hypothesized ethene also strengthens NO adsorption, it was determined that ethene reduces total NO storage on Pd/H-CHA. Instead, NO was the co-adsorbate that increased the amount of ethene oxidized and stored on Pd/H-CHA. IR spectroscopy revealed a lack of CO-Pd bands in the 2000-2300 cm⁻¹ range, but did observe bands associated with co-adsorbed NO and ethene complexes (at 1770 cm⁻¹) as well as

bands associated with formate/methoxy species (1300 and 1480 cm^{-1}). The Pd/H-CHA is unfortunately vulnerable to coke formation at higher temperatures when flowing ethene, resulting in the blockage of NO adsorption sites. This weakness makes Pd/H-CHA unsuited for exhaust gases featuring a large amount of HCs without the aid of high-temperature air treatments in between cycles.

6 References

- (1) Lardinois, T. M.; Bates, J. S.; Lippie, H. H.; Russell, C. K.; Miller, J. T.; Meyer III, H. M.; Unocic, K. A.; Prikhodko, V.; Wei, X.; Lambert, C. K. Structural Interconversion between Agglomerated Palladium Domains and Mononuclear Pd (II) Cations in Chabazite Zeolites. *Chem. Mater.* **2021**, *33* (5), 1698–1713.
- (2) Ryou, Y.; Lee, J.; Cho, S. J.; Lee, H.; Kim, C. H.; Kim, D. H. Activation of Pd/SSZ-13 Catalyst by Hydrothermal Aging Treatment in Passive NO Adsorption Performance at Low Temperature for Cold Start Application. *Appl. Catal. B Environ.* **2017**, *212*, 140–149.
- (3) Team, T. A. C. and E. C. (ACEC) T. *US DRIVE Advanced Combustion and Emission Control Roadmap*; 2018.
- (4) Burch, S. D.; Potter, T. F.; Keyser, M. A.; Brady, M. J.; Michaels, K. F. Reducing Cold-Start Emissions by Catalytic Converter Thermal Management. *SAE Trans.* **1995**, 348–353.
- (5) Kim, B.-S.; Kim, P. S.; Bae, J.; Jeong, H.; Kim, C. H.; Lee, H. Synergistic Effect of Cu/CeO₂ and Pt–BaO/CeO₂ Catalysts for a Low-Temperature Lean NO_x Trap. *Environ. Sci. Technol.* **2019**, *53*, 2900–2907.
- (6) Yan, L.; Gu, Y.; Han, L.; Wang, P.; Li, H.; Yan, T.; Kuboon, S.; Shi, L.; Zhang, D. Dual Promotional Effects of TiO₂-Decorated Acid-Treated MnO_x Octahedral Molecular Sieve Catalysts for Alkaline-Resistant Reduction of NO_x. *ACS Appl. Mater. Interfaces* **2019**, *11* (12), 11507–11517.
- (7) Serrano-Lotina, A.; Monte, M.; Iglesias-Juez, A.; Pavón-Cadierno, P.; Portela, R.; Ávila, P. MnO_x-Support Interactions in Catalytic Bodies for Selective Reduction of NO with NH₃. *Appl. Catal. B Environ.* **2019**, *256*, 117821.
- (8) Choi, Y.; Jung, H.; Kim, S.; Han, J. W.; Lee, K. B. Structural Changes of Hydrotalcite-Based Co-Containing Mixed Oxides with Calcination Temperature and Their Effects on NO_x Adsorption: A Combined Experimental and DFT Study. *Chem. Eng. J.* **2022**, *437*, 135209.
- (9) Khatri, P.; Bhatia, D. Effect of Gas Composition on the NO_x Adsorption and Reduction Activity of a Dual-Function Ag/MgO/γ-Al₂O₃ Catalyst. *Appl. Catal. A Gen.* **2021**, *618*, 118114.
- (10) Moliner, M.; Corma, A. From Metal-Supported Oxides to Well-Defined Metal Site Zeolites: The next Generation of Passive NO_x Adsorbers for Low-Temperature Control of Emissions from Diesel Engines. *React. Chem. Eng.* **2019**, *4* (2), 223–234.
- (11) Ji, Y.; Xu, D.; Bai, S.; Graham, U.; Crocker, M.; Chen, B.; Shi, C.; Harris, D.; Scapens, D.; Darab, J. Pt-and Pd-Promoted CeO₂–ZrO₂ for Passive NO_x Adsorber Applications. *Ind. Eng. Chem. Res.* **2016**, *56* (1), 111–125.
- (12) Murata, Y.; Morita, T.; Wada, K.; Ohno, H. NO_x Trap Three-Way Catalyst (N-TWC) Concept: TWC with NO_x Adsorption Properties at Low Temperatures for Cold-Start Emission Control. *SAE Int. J. Fuels Lubr.* **2015**, *8* (2), 454–459.
- (13) Lobree, L. J.; Aylor, A. W.; Reimer, J. A.; Bell, A. T. NO Reduction by CH₄ in the Presence of O₂ over Pd-H-ZSM-5. *J. Catal.* **1999**, *181* (2), 189–204.
- (14) Khivantsev, K.; Jaegers, N.; Kovarik, L.; Hu, J. Z.; Wang, Y.; Gao, F.; Szanyi, J. Palladium/Zeolite Low Temperature Passive NO_x Adsorbers (PNA): Structure-Adsorption Property Relationships for Hydrothermally Aged PNA Materials. *Emiss. Control Sci. Technol.* **2019**, *6* (2), 126–138.
- (15) Ryou, Y.; Lee, J.; Lee, H.; Kim, C. H.; Kim, D. H. Effect of Various Activation Conditions

- on the Low Temperature NO Adsorption Performance of Pd/SSZ-13 Passive NO_x Adsorber. *Catal. Today* **2019**, *320*, 175–180.
- (16) Ryou, Y.; Lee, J.; Kim, Y.; Hwang, S.; Lee, H.; Kim, C. H.; Kim, D. H. Effect of Reduction Treatments (H₂ vs. CO) on the NO Adsorption Ability and the Physicochemical Properties of Pd/SSZ-13 Passive NO_x Adsorber for Cold Start Application. *Appl. Catal. A Gen.* **2019**, *569*, 28–34.
 - (17) Khivantsev, K.; Jaegers, N. R.; Koleva, I. Z.; Aleksandrov, H. A.; Kovarik, L.; Engelhard, M. H.; Gao, F.; Wang, Y.; Vayssilov, G. N.; Szanyi, J. Stabilization of Super Electrophilic Pd⁺² Cations in Small-Pore SSZ-13 Zeolite. *J. Phys. Chem. C* **2019**, *124* (1), 309–321.
 - (18) Zheng, Y.; Kovarik, L.; Engelhard, M. H.; Wang, Y.; Wang, Y.; Gao, F.; Szanyi, J. Low-Temperature Pd/Zeolite Passive NO_x Adsorbers: Structure, Performance, and Adsorption Chemistry. *J. Phys. Chem. C* **2017**, *121* (29), 15793–15803.
 - (19) Van der Mynsbrugge, J.; Head-Gordon, M.; Bell, A. T. Computational Modeling Predicts the Stability of Both Pd⁺ and Pd²⁺ Ion-Exchanged into H-CHA. *J. Mater. Chem. A* **2020**, *9* (4), 2161–2174.
 - (20) Mandal, K.; Gu, Y.; Westendorff, K. S.; Li, S.; Pihl, J. A.; Grabow, L. C.; Epling, W. S.; Paolucci, C. Condition-Dependent Pd Speciation and NO Adsorption in Pd/Zeolites. *ACS Catal.* **2020**, *10* (21), 12801–12818.
 - (21) Zhao, H.; Hill, A. J.; Ma, L.; Bhat, A.; Jing, G.; Schwank, J. W. Progress and Future Challenges in Passive NO Adsorption over Pd/Zeolite Catalysts. *Catal. Sci. Technol.* **2021**.
 - (22) Descorme, C.; Gélin, P.; Primet, M.; Lécuyer, C. Infrared Study of Nitrogen Monoxide Adsorption on Palladium Ion-Exchanged ZSM-5 Catalysts. *Catal. Letters* **1996**, *41* (3–4), 133–138.
 - (23) Gupta, A.; Kang, S. B.; Harold, M. P. NO_x Uptake and Release on Pd/SSZ-13: Impact Of Feed Composition and Temperature. *Catal. Today* **2020**, *360*, 411–425.
 - (24) Stokes, L. S.; Murphy, D. M.; Farley, R. D.; Rowlands, C. C.; Bailey, S. EPR Investigation of Pd I Species in Palladium-Exchanged ZSM-5 and Beta Zeolites. *Phys. Chem. Chem. Phys.* **1999**, *1* (4), 621–628.
 - (25) Taarit, Y. Ben; Vedrine, J. C.; Dutel, J. F.; Naccache, C. EPR Investigation of the Structure and Reactivity of Pd (I) Species Generated in Synthetic Mordenite-Type Zeolite. *J. Magn. Reson.* **1978**, *31* (2), 251–257.
 - (26) Khivantsev, K.; Jaegers, N. R.; Kovarik, L.; Wang, M.; Hu, J. Z.; Wang, Y.; Derewinski, M. A.; Szanyi, J. The Superior Hydrothermal Stability of Pd/SSZ-39 in Low Temperature Passive NO_x Adsorption (PNA) and Methane Combustion. *Appl. Catal. B Environ.* **2020**, *280*, 119449.
 - (27) Farneth, W. E.; Gorte, R. J. Methods for Characterizing Zeolite Acidity. *Chem. Rev.* **1995**, *95* (3), 615–635.
 - (28) Liu, S.; Feng, X.; Liu, J.; Lin, Q.; Xiong, L.; Wang, Y.; Xu, H.; Wang, J.; Chen, Y. Investigation of the Selective Catalytic Reduction of NO with NH₃ over the WO₃/Ce_{0.68}Zr_{0.32} O₂ Catalyst: The Role of H₂O in SO₂ Inhibition. *New J. Chem.* **2019**, *43* (5), 2258–2268.
 - (29) McKenna, F.-M. NO_x Trap Composition. Google Patents 2015.
 - (30) Sazama, P.; Mokrzycki, L.; Wichterlova, B.; Vondrova, A.; Pilar, R.; Dedecek, J.; Sklenak, S.; Tabor, E. Unprecedented Propane–SCR–NO_x Activity over Template-Free Synthesized Al-Rich Co-BEA* Zeolite. *J. Catal.* **2015**, *332*, 201–211.
 - (31) Bian, C.; Li, D.; Liu, Q.; Zhang, S.; Pang, L.; Luo, Z.; Guo, Y.; Chen, Z.; Li, T. Recent

- Progress of Pd/Zeolite as Passive NO_x Adsorber: Adsorption Chemistry, Structure-Performance Relationships, Challenges and Prospects. *Chinese Chem. Lett.* **2021**.
- (32) Bates, S. A.; Verma, A. A.; Paolucci, C.; Parekh, A. A.; Anggara, T.; Yezerets, A.; Schneider, W. F.; Miller, J. T.; Delgass, W. N.; Ribeiro, F. H. Identification of the Active Cu Site in Standard Selective Catalytic Reduction with Ammonia on Cu-SSZ-13. *J. Catal.* **2014**, *312*, 87–97.
- (33) Gui, R.; Yan, Q.; Xue, T.; Gao, Y.; Li, Y.; Zhu, T.; Wang, Q. The Promoting/Inhibiting Effect of Water Vapor on the Selective Catalytic Reduction of NO_x. *J. Hazard. Mater.* **2022**, 129665.
- (34) Khivantsev, K.; Jaegers, N. R.; Kovarik, L.; Hanson, J. C.; Tao, F.; Tang, Y.; Zhang, X.; Koleva, I. Z.; Aleksandrov, H. A.; Vayssilov, G. N. Achieving Atomic Dispersion of Highly Loaded Transition Metals in Small-Pore Zeolite SSZ-13: High-Capacity and High-Efficiency Low-Temperature CO and Passive NO_x Adsorbers. *Angew. Chemie* **2018**, *130* (51), 16914–16919.
- (35) Li, D.; Yang, G.; Chen, M.; Pang, L.; Guo, Y.; Yu, J.; Li, T. Na Co-Cations Promoted Stability and Activity of Pd/SSZ-13 for Low-Temperature NO Adsorption. *Appl. Catal. B Environ.* **2022**, *309*, 121266.
- (36) Khivantsev, K.; Jaegers, N. R.; Kovarik, L.; Proding, S.; Derewinski, M. A.; Wang, Y.; Gao, F.; Szanyi, J. Palladium/Beta Zeolite Passive NO_x Adsorbers (PNA): Clarification of PNA Chemistry and the Effects of CO and Zeolite Crystallite Size on PNA Performance. *Appl. Catal. A Gen.* **2019**, *569*, 141–148.
- (37) Yasumura, S.; Ide, H.; Ueda, T.; Jing, Y.; Liu, C.; Kon, K.; Toyao, T.; Maeno, Z.; Shimizu, K. Transformation of Bulk Pd to Pd Cations in Small-Pore CHA Zeolites Facilitated by NO. *JACS Au* **2021**, *1* (2), 201–211.
- (38) Usui, T.; Liu, Z.; Igarashi, H.; Sasaki, Y.; Shiramata, Y.; Yamada, H.; Ohara, K.; Kusamoto, T.; Wakihara, T. Identifying the Factors Governing the Early-Stage Degradation of Cu-Chabazite Zeolite for NH₃-SCR. *ACS omega* **2019**, *4* (2), 3653–3659.
- (39) Wang, J.; Gao, F.; Dang, P.; Tang, X.; Lu, M.; Du, Y.; Zhou, Y.; Yi, H.; Duan, E. Recent Advances in NO Reduction with CO over Copper-Based Catalysts: Optimization Strategies, Reaction Mechanisms, and Anti-Inactivation Measures. *Chem. Eng. J.* **2022**, 137374.
- (40) Pace, R. B.; Lardinois, T. M.; Ji, Y.; Gounder, R.; Heintz, O.; Crocker, M. Effects of Treatment Conditions on Pd Speciation in CHA and Beta Zeolites for Passive NO_x Adsorption. *ACS omega* **2021**, *6* (44), 29471–29482.
- (41) Gilot, P.; Guyon, M.; Stanmore, B. R. A Review of NO_x Reduction on Zeolitic Catalysts under Diesel Exhaust Conditions. *Fuel* **1997**, *76* (6), 507–515.
- (42) Khivantsev, K.; Gao, F.; Kovarik, L.; Wang, Y.; Szanyi, J. Molecular Level Understanding of How Oxygen and Carbon Monoxide Improve NO_x Storage in Palladium/SSZ-13 Passive NO_x Adsorbers: The Role of NO⁺ and Pd (II)(CO)(NO) Species. *J. Phys. Chem. C* **2018**, *122* (20), 10820–10827.
- (43) Chen, H.-Y.; Collier, J. E.; Liu, D.; Mantarosie, L.; Durán-Martín, D.; Novák, V.; Rajaram, R. R.; Thompsett, D. Low Temperature NO Storage of Zeolite Supported Pd for Low Temperature Diesel Engine Emission Control. *Catal. Letters* **2016**, *146* (9), 1706–1711.
- (44) Theis, J. R.; Ura, J. A. Assessment of Zeolite-Based Low Temperature NO_x Adsorbers: Effect of Reductants During Multiple Sequential Cold Starts. *Catal. Today* **2021**, *360*, 340–349.
- (45) Feng, Z.; Liu, X.; Wang, Y.; Meng, C. Recent Advances on Gallium-Modified ZSM-5 for

- Conversion of Light Hydrocarbons. *Molecules* **2021**, *26*, 2234.
- (46) Villamaina, R.; Iacobone, U.; Nova, I.; Tronconi, E.; Ruggeri, M. P.; Mantarosie, L.; Collier, J.; Thompsett, D. Mechanistic Insight in NO Trapping on Pd/Chabazite Systems for the Low-Temperature NO_x Removal from Diesel Exhausts. *Appl. Catal. B Environ.* **284**, 119724.
- (47) Ambast, M.; Gupta, A.; Rahman, B. M. M.; Grabow, L. C.; Harold, M. P. NO_x Adsorption with CO and C₂H₄ on Pd/SSZ-13: Experiments and Modeling. *Appl. Catal. B Environ.* **2021**, *286*, 119871.
- (48) Liu, C.; Wang, J.; Chen, Z.; Wang, J.; Shen, M. Improvement of NO_x Uptake/Release over Pd/Beta by Propylene: Shielding Effect of Intermediates on Adsorbed NO_x Species. *Phys. Chem. Chem. Phys.* **2021**, *23* (9), 5261–5269.
- (49) Theis, J. R.; Ura, J.; Getsoian, A. B.; Prikhodko, V. Y.; Thomas, C. R.; Pihl, J. A.; Lardinois, T. M.; Gounder, R.; Wei, X.; Ji, Y. Effect of Framework Al Pairing on NO Storage Properties of Pd-CHA Passive NO_x Adsorbers. *Appl. Catal. B Environ.* **2023**, *322*, 122074.
- (50) Kyriakidou, E. A.; Lee, J.; Choi, J.-S.; Lance, M.; Toops, T. J. A Comparative Study of Silver-and Palladium-Exchanged Zeolites in Propylene and Nitrogen Oxide Adsorption and Desorption for Cold-Start Applications. *Catal. Today* **2020**, *360*, 220–233.
- (51) Pashkova, V.; Sklenak, S.; Klein, P.; Urbanova, M.; Dědeček, J. Location of Framework Al Atoms in the Channels of ZSM-5: Effect of the (Hydrothermal) Synthesis. *Chem. - A Eur. J.* **2016**, *22*, 3937–3941.
- (52) Malamis, S. A.; Harold, M. P.; Epling, W. S. Coupled NO and C₃H₆ Trapping, Release and Conversion on Pd/BEA: Evaluation of the Lean Hydrocarbon NO_x Trap. *Ind. Eng. Chem. Res.* **2019**, *58* (51), 22912–22923.
- (53) Hadjiivanov, K.; Saussey, J.; Freysz, J. L.; Lavalley, J. C. FT-IR Study of NO+O₂ Co-Adsorption on H-ZSM-5: Re-Assignment of the 2133 cm⁻¹ Band to NO⁺ Species. *Catal. Letters* **1998**, *52* (1–2), 103–108.
- (54) Gupta, A.; Ambast, M.; Harold, M. P. NO_x and Hydrocarbon Trapping and Conversion in a Sequential Three-Zone Monolith: Spatiotemporal Features. *ACS Eng. Au* **2022**.
- (55) Zhang, N.; Xin, Y.; Li, R.; Han, D.; Jia, J.; Li, Q.; Wang, J.; Zhang, Z. Pd/SAPO-34 Passive NO_x Adsorbers: Stable Pd Ion Adsorption Sites in Six-Member Rings. *Mater. Res. Express* **2021**, *8* (3), 35505.
- (56) Chakarova, K.; Ivanova, E.; Hadjiivanov, K.; Klissurski, D.; Knözinger, H. Co-Ordination Chemistry of Palladium Cations in Pd-H-ZSM-5 as Revealed by FTIR Spectra of Adsorbed and Co-Adsorbed Probe Molecules (CO and NO). *Phys. Chem. Chem. Phys.* **2004**, *6* (013), 3702–3709.
- (57) Cui, Y.; Zhu Chen, J.; Peng, B.; Kovarik, L.; Devaraj, A.; Li, Z.; Ma, T.; Wang, Y.; Szanyi, J.; Miller, J. T. Onset of High Methane Combustion Rates over Supported Palladium Catalysts: From Isolated Pd Cations to PdO Nanoparticles. *JACS Au* **2021**, *1* (4), 396–408.
- (58) Zhang, B.; Shen, M.; Wang, J.; Wang, J.; Wang, J. Investigation of Various Pd Species in Pd/BEA for Cold Start Application. *Catalysts* **2019**, *9* (3), 247.
- (59) Wang, A.; Lindgren, K.; Di, M.; Bernin, D.; Carlsson, P.-A.; Thuvander, M.; Olsson, L. Insight into Hydrothermal Aging Effect on Pd Sites over Pd/LTA and Pd/SSZ-13 as PNA and CO Oxidation Monolith Catalysts. *Appl. Catal. B Environ.* **2020**, *278*, 119315.
- (60) Khivantsev, K.; Jaegers, N. R.; Kovarik, L.; Hu, J. Z.; Gao, F.; Wang, Y.; Szanyi, J. Palladium/Zeolite Low Temperature Passive NO_x Adsorbers (PNA): Structure-Adsorption Property Relationships for Hydrothermally Aged PNA Materials. *Emiss. Control Sci.*

- Technol.* **2019**, *6* (2), 126–138.
- (61) Pommier, B.; Gelin, P. Infrared and Volumetric Study of NO Adsorption on Pd-H-ZSM-5. *Phys. Chem. Chem. Phys.* **2001**, *3* (6), 1138–1143.
- (62) Homeyer, S.; Sachtler, W. M. H. Oxidative Redispersion of Palladium and Formation of PdO Particles in NaY: An Application of High Precision TPR. *Appl. Catal.* **1989**, *54* (1), 189–202.
- (63) Jacquemin, J.; Siffert, S.; Lamonier, J.-F.; Zhilinskaya, E.; Aboukais, A. Catalytic Properties of Beta Zeolite Exchanged with Pd and Fe for Toluene Total Oxidation. In *Studies in Surface Science and Catalysis*; Elsevier, 2002; Vol. 142, pp 699–706.
- (64) Loiland, J. A.; Lobo, R. F. Oxidation of Zeolite Acid Sites in NO/O₂ Mixtures and the Catalytic Properties of the New Site in NO Oxidation. *J. Catal.* **2015**, *325*, 68–78.
- (65) *Database of Zeolite Structures*. <http://www.iza-structure.org/databases/>.
- (66) Mansoor, E.; Van der Mynsbrugge, J.; Head-Gordon, M.; Bell, A. T. Impact of Long-Range Electrostatic and Dispersive Interactions on Theoretical Predictions of Adsorption and Catalysis in Zeolites. *Catal. Today* **2018**, *312*, 51–65.
- (67) Chai, J.-D.; Head-Gordon, M. Long-Range Corrected Double-Hybrid Density Functionals. *J. Chem. Phys.* **2009**, *131* (17), 174105.
- (68) Chai, J.-D.; Head-Gordon, M. Long-Range Corrected Hybrid Density Functionals with Damped Atom–Atom Dispersion Corrections. *Phys. Chem. Chem. Phys.* **2008**, *10* (44), 6615–6620.
- (69) Zimmerman, P. M.; Head-Gordon, M.; Bell, A. T. Selection and Validation of Charge and Lennard-Jones Parameters for QM/MM Simulations of Hydrocarbon Interactions with Zeolites. *J. Chem. Theory Comput.* **2011**, *7* (6), 1695–1703.
- (70) Li, Y.-P.; Gomes, J.; Mallikarjun Sharada, S.; Bell, A. T.; Head-Gordon, M. Improved Force-Field Parameters for QM/MM Simulations of the Energies of Adsorption for Molecules in Zeolites and a Free Rotor Correction to the Rigid Rotor Harmonic Oscillator Model for Adsorption Enthalpies. *J. Phys. Chem. C* **2015**, *119* (4), 1840–1850.
- (71) Verstraelen, T.; Van Speybroeck, V.; Waroquier, M. ZEOBUILDER: A GUI Toolkit for the Construction of Complex Molecular Structures on the Nanoscale with Building Blocks. ACS Publications 2008.
- (72) Mardirossian, N.; Head-Gordon, M. Thirty Years of Density Functional Theory in Computational Chemistry: An Overview and Extensive Assessment of 200 Density Functionals. *Mol. Phys.* **2017**, *115* (19), 2315–2372.
- (73) Shao, Y.; Gan, Z.; Epifanovsky, E.; Gilbert, A. T. B.; Wormit, M.; Kussmann, J.; Lange, A. W.; Behn, A.; Deng, J.; Feng, X. Advances in Molecular Quantum Chemistry Contained in the Q-Chem 4 Program Package. *Mol. Phys.* **2015**, *113* (2), 184–215.
- (74) Grimme, S. Supramolecular Binding Thermodynamics by Dispersion-corrected Density Functional Theory. *Chem. Eur. J.* **2012**, *18* (32), 9955–9964.
- (75) Yasumura, S.; Liu, C.; Toyao, T.; Maeno, Z.; Shimizu, K. Lean NO_x Capture and Reduction by NH₃ via NO⁺ Intermediates over H-CHA at Room Temperature. *J. Phys. Chem. C* **2021**, *125* (3), 1913–1922.
- (76) Bordiga, S.; Regli, L.; Lamberti, C.; Zecchina, A.; Bjørgen, M.; Lillerud, K. P. FTIR Adsorption Studies of H₂O and CH₃OH in the Isostructural H-SSZ-13 and H-SAPO-34: Formation of H-Bonded Adducts and Protonated Clusters. *J. Phys. Chem. B* **2005**, *109* (16), 7724–7732.
- (77) Sedlmair, C.; Gil, B.; Seshan, K.; Jentys, A.; Lercher, J. A. An in Situ IR Study of the NO_x

- Adsorption/Reduction Mechanism on Modified Y Zeolites. *Phys. Chem. Chem. Phys.* **2003**, *5* (9), 1897–1905.
- (78) Lónyi, F.; Solt, H. E.; Valyon, J.; Decolatti, H.; Gutierrez, L. B.; Miró, E. An Operando DRIFTS Study of the Active Sites and the Active Intermediates of the NO-SCR Reaction by Methane over In, H-and In, Pd, H-Zeolite Catalysts. *Appl. Catal. B Environ.* **2010**, *100* (1–2), 133–142.
- (79) Kvasničková, A.; Kočí, P.; Ji, Y.; Crocker, M. Effective Model of NO_x Adsorption and Desorption on PtPd/CeO₂-ZrO₂ Passive NO_x Adsorber. *Catal. Letters* **2020**, *150* (11), 3223–3233.
- (80) Hadjiivanov, K. I. Identification of Neutral and Charged N_xO_y Surface Species by IR Spectroscopy. *Catal. Rev.* **2000**, *42* (1–2), 71–144.
- (81) Aljama, H.; Head-Gordon, M.; Bell, A. Assessing the Stability of Pd-Exchanged Sites in Zeolites with the Aid of a High Throughput Quantum Chemistry Workflow. *Nat. Commun.* **2021**, *13*, 1–9. <https://doi.org/10.21203/rs.3.rs-396201/v1>.
- (82) Di Iorio, J. R.; Gounder, R. Controlling the Isolation and Pairing of Aluminum in Chabazite Zeolites Using Mixtures of Organic and Inorganic Structure-Directing Agents. *Chem. Mater.* **2016**, *28* (7), 2236–2247.
- (83) Korin, E.; Reshef, R.; Tshernichovesky, D.; Sher, E. Reducing Cold-Start Emission from Internal Combustion Engines by Means of a Catalytic Converter Embedded in a Phase-Change Material. *Proc. Inst. Mech. Eng. Part D J. Automob. Eng.* **1999**, *213* (6), 575–583.
- (84) Kim, P.; Van der Mynsbrugge, J.; Aljama, H.; Lardinois, T. M.; Gounder, R.; Head-Gordon, M.; Bell, A. T. Investigation of the Modes of NO Adsorption in Pd/H-CHA. *Appl. Catal. B Environ.* **2022**, *304*, 120992.
- (85) Theis, J. R.; Lambert, C. K. Mechanistic Assessment of Low Temperature NO_x Adsorbers for Cold Start NO_x Control on Diesel Engines. *Catal. Today* **2019**, *320*, 181–195.
- (86) Feher, G.; Kip, A. F. Electron Spin Resonance Absorption in Metals. I. Experimental. *Phys. Rev.* **1955**, *98* (2), 337.
- (87) Hunger, M. Multinuclear Solid-State NMR Studies of Acidic and Non-Acidic Hydroxyl Protons in Zeolites. *Solid State Nucl. Magn. Reson.* **1996**, *6*, 1–29.
- (88) Stathi, P.; Belles, L.; Deligiannakis, Y. Multipotent Atomic Palladium Species Pd¹⁺, Pd²⁺–O²⁻, and Pd³⁺ Formed at the Interface of Pd/TiO₂ Nanoparticles: Electron Paramagnetic Resonance Study. *J. Phys. Chem. C* **2022**, *126* (33), 14125–14137.
- (89) Kim, P.; Van der Mynsbrugge, J.; Head-Gordon, M.; Bell, A. T. Experimental and Theoretical Studies of Pd Cation Reduction and Oxidation During NO Adsorption on and Desorption from Pd/H-CHA. *J. Phys. Chem. C* **2022**.
- (90) Zelinsky, R. P.; Dean, D. P.; Breckner, C. J.; Marino, S.; Miller, J. T.; Epling, W. S. Pd/BEA Hydrocarbon Traps: Effect of Hydrothermal Aging on Trapping Properties and Pd Speciation. *Appl. Catal. B Environ.* **2023**, *320*, 121938.
- (91) Khivantsev, K.; Derewinski, M. A.; Jaegers, N. R.; Boglajenko, D.; Hernandez, X. I. P.; Pearce, C.; Wang, Y.; Szanyi, J. Increasing Al-Pair Abundance in SSZ-13 Zeolite via Zeolite Synthesis in the Presence of Alkaline Earth Metal Hydroxide Produces Hydrothermally Stable Co-, Cu- and Pd-SSZ-13 Materials. **2022**.
- (92) Ryu, T.; Jeong, J.; Byun, S. W.; Kweon, S.; Park, J.; Bae, W. Bin; Kim, Y. J.; Park, M. B.; Kang, S. B. Ethylene Trapping of Palladium-Impregnated Zeolites for Cold-Start Emission Control. *Chem. Eng. J.* **2022**, *442*, 136197.
- (93) Lupescu, J.; Xu, L.; Jen, H.-W.; Harwell, A.; Nunan, J.; Alltizer, C.; Denison, G. A New

- Catalyzed HC Trap Technology That Enhances the Conversion of Gasoline Fuel Cold-Start Emissions. *SAE Int. J. Fuels Lubr.* **2018**, *11* (4), 411–426.
- (94) Xu, L.; Lupescu, J.; Cavataio, G.; Guo, K.; Jen, H. The Impacts of Pd in BEA Zeolite on Decreasing Cold-Start NMOG Emission of an E85 Fuel Vehicle. *SAE Int. J. Fuels Lubr.* **2018**, *11* (3), 239–246.
- (95) Graf, P. O.; Mojet, B. L.; van Ommen, J. G.; Lefferts, L. Comparative Study of Steam Reforming of Methane, Ethane and Ethylene on Pt, Rh and Pd Supported on Yttrium-Stabilized Zirconia. *Appl. Catal. A Gen.* **2007**, *332* (2), 310–317.
- (96) Caporali, R.; Chansai, S.; Burch, R.; Delgado, J. J.; Goguet, A.; Hardacre, C.; Mantarosie, L.; Thompsett, D. Critical Role of Water in the Direct Oxidation of CO and Hydrocarbons in Diesel Exhaust after Treatment Catalysis. *Appl. Catal. B Environ.* **2014**, *147*, 764–769.
- (97) Abreu, N. J.; Valdés, H.; Zaror, C. A.; Azzolina-Jury, F.; Meléndrez, M. F. Ethylene Adsorption onto Natural and Transition Metal Modified Chilean Zeolite: An Operando DRIFTS Approach. *Microporous Mesoporous Mater.* **2019**, *274*, 138–148.
- (98) Wang, S.; Zhang, L.; Wang, P.; Jiao, W.; Qin, Z.; Dong, M.; Wang, J.; Olsbye, U.; Fan, W. Highly Selective Hydrogenation of CO₂ to Propane over GaZrO_x/H-SSZ-13 Composite. *Nat. Catal.* **2022**, 1–13.
- (99) Hamid, Y.; Matarrese, R.; Morandi, S.; Castoldi, L.; Lietti, L. Pd-Doped SSZ-13 for Low-T NO_x Adsorption: An Operando FT-IR Spectroscopy Study. *Top. Catal.* **2022**, 1–11.
- (100) Xu, L.; Lupescu, J.; Ura, J.; Harwell, A.; Paxton, W.; Nunan, J.; Alltizer, C. Benefits of Pd Doped Zeolites for Cold Start HC/NO_x Emission Reductions for Gasoline and E85 Fueled Vehicles. *SAE Int. J. Fuels Lubr.* **2018**, *11* (4), 301–318.